5-2016

POLY (ADP) RIBOSE POLYMERASE INHIBITORS FOR THE TREATMENT OF MALIGNANT PERIPHERAL NERVE SHEATH TUMOR

Christine M. Kivlin

POLY (ADP) RIBOSE POLYMERASE INHIBITORS FOR THE TREATMENT OF MALIGNANT PERIPHERAL NERVE SHEATH TUMOR

by

Christine Michelle Kivlin, BS

APPROVED:

_____

Keila E. Torres, MD, PhD
Advisory Professor

_____

Robert C. Bast Jr., MD

_____

David J. McConkey, PhD

_____

Rosemarie E. Schmandt, PhD

_____

Subrata Sen, PhD

APPROVED:

_____

Dean, Graduate School of Biomedical Sciences
The University of Texas Health Science Center at Houston

POLY (ADP) RIBOSE POLYMERASE INHIBITORS FOR THE TREATMENT OF MALIGNANT PERIPHERAL NERVE SHEATH TUMOR

A

DISSERTATION

Presented to the Faculty of

The University of Texas

Health Science Center at Houston

and

The University of Texas

MD Anderson Cancer Center

Graduate School of Biomedical Sciences

in Partial Fulfillment

of the Requirements

for the Degree of

DOCTOR OF PHILOSOPHY

by

Christine Michelle Kivlin B.S.

Houston, Texas

May, 2016

Dedication

To my family and friends- your encouragement, support, and love mean more to me than I could ever truly express.

Acknowledgements

Thank you to Dr. Keila Torres for her support during my doctoral training. Thank you for emphasizing independence and allowing me to run my project.

To the past and present members of the sarcoma research lab, thank you for all of your help over the years. I appreciate all of your guidance and patience. It has made me a better researcher.

To Dr. Dina Lev and Dr. Raphael Pollock, thank you for all of your advice and encouragement. I appreciate all of the confidence you had in me early in my academic career and for supporting me while I developed my project.

To my advisory committee members, Dr. Robert Bast, Dr. David McConkey, Dr. Subrata Sen, and Dr. Rosemarie Schmandt, thank you for your direction and advice concerning my dissertation project and for your interest in my career development as a young scientist.

Thank you to my collaborators for your advice and assistance. Brian Menegaz and Salah Lamhamedi for their advice and support. Dr Jian Gu and YiLei Gong for their assistance with the gamma phosphorylation histone 2A variant X (gamma H2AX) assay. Dr. Naoto Ueno and Angie Torres Adorno for use of their Neon Transfection system and training. Dr. Steven Ullrich for use of his FS40 machine and training. Karen Ramirez and Ryan Jewell for their trouble-shooting and support with flow cytometry analysis.

I appreciate the support of the Children's Tumor Foundation and thank them for recognizing me with their Young Investigator Award. It means the world to me to have received your support early in my career. I would also like to thank the Amschwand Sarcoma Cancer Foundation and the Sally M. Kingsbury Sarcoma Cancer Research Foundation for their financial support during my graduate training.

To my parents who always told me I could do anything I wanted if I tried my best. Thank you for your continued support and encouragement while I achieved this dream.

To my sister. Not only did you believe in me that I could survive graduate school, you led the way, and showed me by example. Thank you for always showing me the way and helping me.

To my Houston friends and family, thank you for sticking with me day in and day out when I was tired, frustrated, and ready to quit. A special thank you to Caitlin May, Davis Ingram, and Kelsey Watson-Schertz. Your support and friendship is what got me through the last six years and I really could not have done it without you.

And last but certainly not least, thank you to James Christopher Farrell. Your constant positivity and strength is what motivated me to continue to fight for this dream. I appreciate your unconditional love and support more than I could ever really say and I'm so blessed to be able to spend the rest of my life with you.

POLY (ADP) RIBOSE POLYMERASE INHIBITORS FOR THE TREATMENT OF MALIGNANT PERIPHERAL NERVE SHEATH TUMOR

Christine Michelle Kivlin, BS

Advisory Professor: Keila E. Torres, MD, PhD

Malignant peripheral nerve sheath tumor (MPNST) is a rare subtype of soft tissue sarcoma. Surgical excision has remained the standard of care for this highly aggressive malignancy for over a decade. Conventional chemotherapy and radiotherapy have shown limited efficacy in MPNST; therefore, it is imperative that targeted treatment be identified to improve the outcome for MPNST patients. Poly (ADP) ribose polymerase (PARP) inhibitors were first reported over a decade ago to have substantial anti-tumorigenic effects in malignancies with defective DNA repair, specifically those with *BRCA1/2* (breast cancer, early onset 1/2) mutations. Further evaluation of these inhibitors has shown multiple mechanisms of sensitivity, all of which are associated with the DNA damage response and DNA repair. While no specific defects in DNA repair machinery have been reported in MPNST, sensitivity to PARP inhibition may be predicted by its complex karyotype and inherent genomic instability. We show increased PARP1 and PARP2 expression in MPNST patient tumor samples and increased PARP activity in cell lines. We also demonstrate the anti-MPNST effect of the PARP inhibitor AZD2281 *in vitro* and *in vivo*. Specifically, decreased cell proliferation and induction of apoptosis were observed in MPNST cell lines at AZD2281 doses and time points similar to, or less than, those used in cells lines with known DNA repair defects. In addition, AZD2281 treatment suppressed MPNST subcutaneous xenograft growth and lung metastasis progression, and increased survival times of mice with metastatic disease. Upon investigation of a potential mechanism of sensitivity, we found decreased efficacy of homologous recombination (HR) and increased

activity of non-homologous end joining (NHEJ) in MPNST cell lines, suggesting a potential mechanism of sensitivity to PARP inhibition due to increased genomic instability. We also observed decreased expression of Cockayne syndrome B (CSB), a pivotal member of the transcription coupled repair (TCR) pathway. Subsequent overexpression of CSB decreased the sensitivity of a subset of MPNST cell lines to AZD2281 treatment. Our results suggest that PARP is a valuable anti-MPNST target and that sensitivity could be due to defective DNA repair pathways. Moreover, AZD2281 should be evaluated for its efficacy as a therapeutic agent for MPNST patients.

Table of Contents

List of Illustrations

List of Tables

Abbreviations

ATM: ataxia telangiectasia mutated

ATR: ataxia telangiectasia and Rad3-related protein

BARD1: BRCA1 associated RING domain 1

BER: base excision repair

BRCA1/2: breast cancer 1/2, early onset

CC3: cleaved caspase 3

CDK12: cyclin dependent kinase 12

CDKN1B: cyclin dependent kinase inhibitor 1B

CETN2: centrin, EF-hand protein, 2

CHK1/2: checkpoint kinase1/2

CKIT: v-kit hardy-zuckerman 4 feline sarcoma viral oncogene

CMV: cytomegalovirus

CPDs: cyclobutane pyrimidine dimers

CS: Cockayne syndrome

CSA: Cockayne syndrome A

CSB: Cockayne syndrome B

CSBOE: Cockayne syndrome B overexpression

CtIP: CtBP interacting protein

DDB1: damage-specific DNA binding protein 1

DMC1: DNA meiotic recombinase 1

DMEM: Dulbecco's modified Eagle's medium

DMEM/F12: Dulbecco's modified Eagle medium:nutrient mixture F-12

DMSO: dimethyl sulfoxide

DNA: deoxyribonucleic acid

DNAPKcs: protein kinase, DNA-activated, catalytic polypeptide

DSB: double strand DNA break

EC50: half-maximal effective concentration

ELISA: enzyme-linked immunosorbent assay

ERCC1: excision repair cross-complementation group 1

ERCC5: excision repair cross-complementation group 5

ERCC6: excision repair cross-complementation group 6

EWS-FLI1: EWS RNA-binding pritein 1- fli-1 proto-oncogene, ETS transcription factor

EXO1: exonuclease 1

FACS: fluorescence-activated cell sorting

FBS: fetal bovine serum

FC: fold change

FITC: fluorescein isothiocyanate

GEN1: GEN1 Holliday junction 5' flap endonuclease

GFP: green fluorescent protein

GGR: global genome repair

GIST: gastrointestinal stromal tumor

Gamma-H2AX: gamma phosphorylated histone 2A variant X

H&E: hematoxylin-eosin

HGF: hepatocyte growth factor

HHRAD23B: human homolog of RAD23B

HJ: Holliday junction

HPCD: hydroxypropyl-β-cyclodextrin

HMGN1: high mobility group nucleosome binding domain 1

HR: homologous recombination

IACUC: *Institutional Animal Care and Use Committee*

IHC: immunohistochemistry

IP: intraperitoneal injection

Ku70/Ku80: Ku autoantigen p70 subunit/ Ku autoantigen p80 subunit

LOH: loss of heterozygosity

MAPK: mitogen-activated protein kinase

MRE11: meiotic recombination 11

MPNST: malignant peripheral nerve sheath tumor

MSH4: MutS homolog 4

MTS: 3-(4,5-dimethyl-2-yl)-5-(3-carboxymethoxyphenyl)-2-(4-sulfophenyl)-2H-tetrazolium, inner salt

NAD: nicotinamide adenine dinucleotide

NBS1: Nijmegen breakage syndrome 1

NER: nucleotide excision repair

***NF1*:** neurofibromin 1

NF1: neurofibromatosis type 1

NHEJ: non-homologous end joining

NHEJ1: non-homologous end-joining factor 1

NSCs: normal Schwann cells

PAR: poly (ADP) ribose

PARG: poly (ADP) ribose glycohydrolase

PARP: poly (ADP) ribose polymerase

PARP-HSA: PARP enzyme-high specific activity

PARPi: PARP inhibitor

PBS: phosphate buffered saline

PCNA: proliferating cell nuclear antigen

PDGFRA: platelet-derived growth factor receptor, alpha polypeptide

PDGFRB: platelet-derived growth factor receptor, beta polypeptide

PER1: period circadian clock 1

PET: positron emission tomography

PGBD3: PiggyBac transposable element derived 3

PMSF: phenylmethylsulfonyl fluoride

PI: propidium iodide

PTCH1: patched 1

PTEN: phosphatase and tensin homolog

Rad50: RAD50 homolog

Rad51: RAD51 recombinase

RE: restriction enzyme

RFC: replication factor c

RPA: replication protein a

ROS: reactive oxygen species

RNA: ribonucleic acid

RNAPI: RNA polymerase 1

RNAPII: RNA polymerase 2

RNAseq: RNA sequencing

SCID: severe combined immunodeficiency

SDSA: synthesis- dependent strand annealing

SEM: standard error of the mean

SLX1-4: SLX1-4 structure-specific endonuclease subunit

SOLO1/2: study of olaparib in ovarian cancer

SSB: single strand break

STR: short tandem repeat

STS: soft tissue sarcoma

TCR: transcription coupled repair

TFIIH: transcription factor II human

TFIIS: transcriptional elongation factor

TP53: tumor protein p53

TMA: tissue microarray

UPS: undifferentiated pleomorphic sarcoma

USP7: ubiquitin specific peptidase 7

UVSSA: UV-stimulated scaffold protein A

XAB2: XPA binding protein 2

XRCC1: X-ray repair complementing defective repair in Chinese hamster cells 1

XRCC4 X-ray repair complementing defective repair in Chinese hamster cells 4

XP: xeroderma pigmentosum

XPA: xeroderma pigmentosum, complementation group A

XPB: xeroderma pigmentosum, complementation group B

XPC: xeroderma pigmentosum, complementation group C

XPD: xeroderma pigmentosum, complementation group D

XPE: xeroderma pigmentosum, complementation group E

XPF-ERCC1: xeroderma pigmentosum, complementation group F-excision repair cross-complementation group 1

XPG: xeroderma pigmentosum, complementation group G

Chapter 1

Introduction

1.1 Soft tissue sarcoma

Soft tissue sarcoma (STS) is a relatively rare malignancy, accounting for less than 1% of adult cancers diagnosed in 2015. (1) These tumors can arise in muscle, fat, blood vessels, and nerves and occur in any area of the body, with the majority arising in the extremities. (2) There are over 80 distinct histological subtypes of STS which are classified and named according to their cell of origin. (3) While the incidence of STS is rare with approximately 12,000 new cases diagnosed in the United States annually, 41% of patients are expected to succumb to their disease. (1) Overall, the five-year survival rate for STS is 83% for localized disease and substantially decreases with more advanced disease to 16% for patients with distant spread. (1)

STS can be categorized into two groups based on the type and extent of the molecular alterations characteristic of histological subtypes. Several STSs, such as Ewing's sarcoma, well-differentiated liposarcoma, have a "simple karyotype", with defined recurring chromosomal translocations and copy number changes that are linked to tumorigenesis. (4) Within this category are also those STSs with specific genetic mutations that drive tumor formation such as the v-kit hardy-zuckerman 4 feline sarcoma viral oncogene (*cKIT*) or platelet-derived growth factor receptor, beta polypeptide (*PDGFRB*) mutation in gastrointestinal stromal tumor. (5) However, the majority of STSs has complex karyotypes associated with substantial chromosomal aberrations and high levels of genomic instability. (6) One example of a karyotypically complex STS is malignant peripheral nerve sheath tumor (MPNST).

1.2 Malignant peripheral nerve sheath tumor

Incidence and clinical features

MPNST accounts for 2-5% of all STS diagnoses, accounting for approximately 238 new cases in the United States annually (Figure 1). (3,7) MPNST can arise in three settings: sporadic, neurofibromatosis type 1-associated (NF1-associated), and radiation-associated. Sporadic MPNST accounts for 40% of cases, while NF1-associated MPNST accounts for 50% of cases. Radiation-associated MPNST occurs in a field of prior therapeutic radiation and accounts for 10% of cases. (7-9)

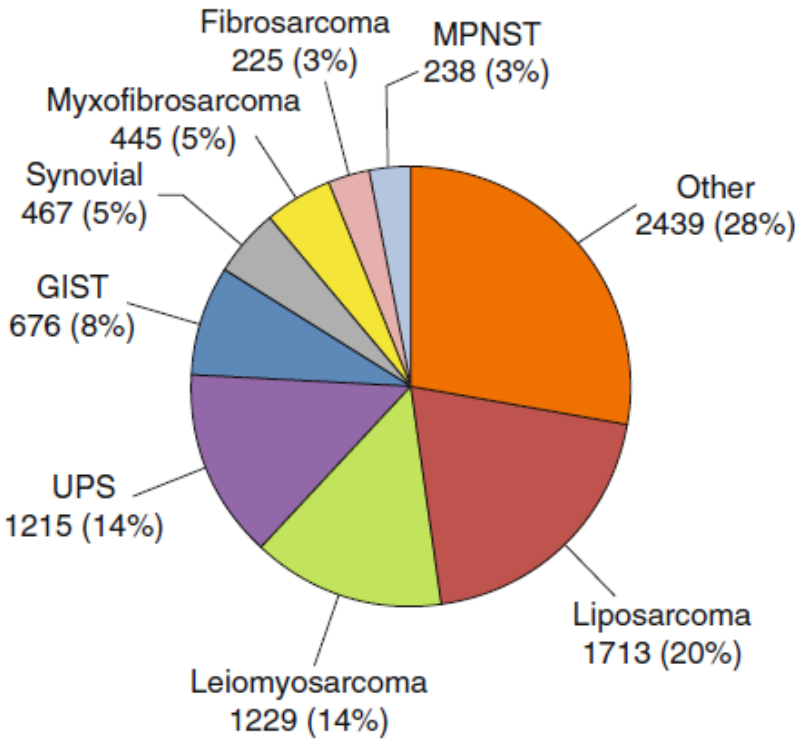

Figure 1. Soft tissue sarcoma subtypes. Distribution by histology for adult patients with soft tissue sarcoma, all sites. MSKCC 7/1/1982-6/30/2010. GIST: gastrointestinal stromal tumor; UPS: undifferentiated pleomorphic sarcoma; MPNST: malignant peripheral nerve sheath tumor

In general, MPNST is a highly aggressive tumor that often occurs in the upper or lower extremities involving large nerve bundles such as the sciatic nerve or the brachial plexus. (7) Due to the rapidly growing nature of the disease, patients will present with pain, motor weakness, or paresthesia; additionally, up to 50% of patients will present with systemic disease. (7)

Neurofibromatosis type 1-associated malignant peripheral nerve sheath tumor

Neurofibromatosis type 1 (NF1) is the most common hereditary disease affecting approximately 1 in 3000 individuals. NF1 is typified by several clinical features, most commonly café-au-lait spots, skinfold freckling, cognitive impairment, and cutaneous neurofibromas (Figure 2). (10) In NF1 patients, a mutation of one allele of the neurofibromin 1 (*NF1*) gene is inherited in an autosomal dominant fashion, or occurs *de novo,* and is defective in all cells, resulting in a loss of heterozygosity. A second acquired mutation then occurs in Schwann cells resulting in the formation of neurofibromas. According to the human gene mutation database, almost 1500 mutations of *NF1* have been reported and are associated with the disease phenotype. Approximately 5-10% of NF1 patients will have a large deletion of *NF1* accompanied by a deletion in the surrounding chromosomal area, which is associated with a severe phenotype; or microdeletions either 1.4Mb in size encompassing 14 genes or 1.3Mb in size encompassing 13 genes. (11) However, the majority of patients (approximately 90%) will have a *NF1* intragenic mutation, where no clear phenotype-genotype correlation has been established. (11,12)

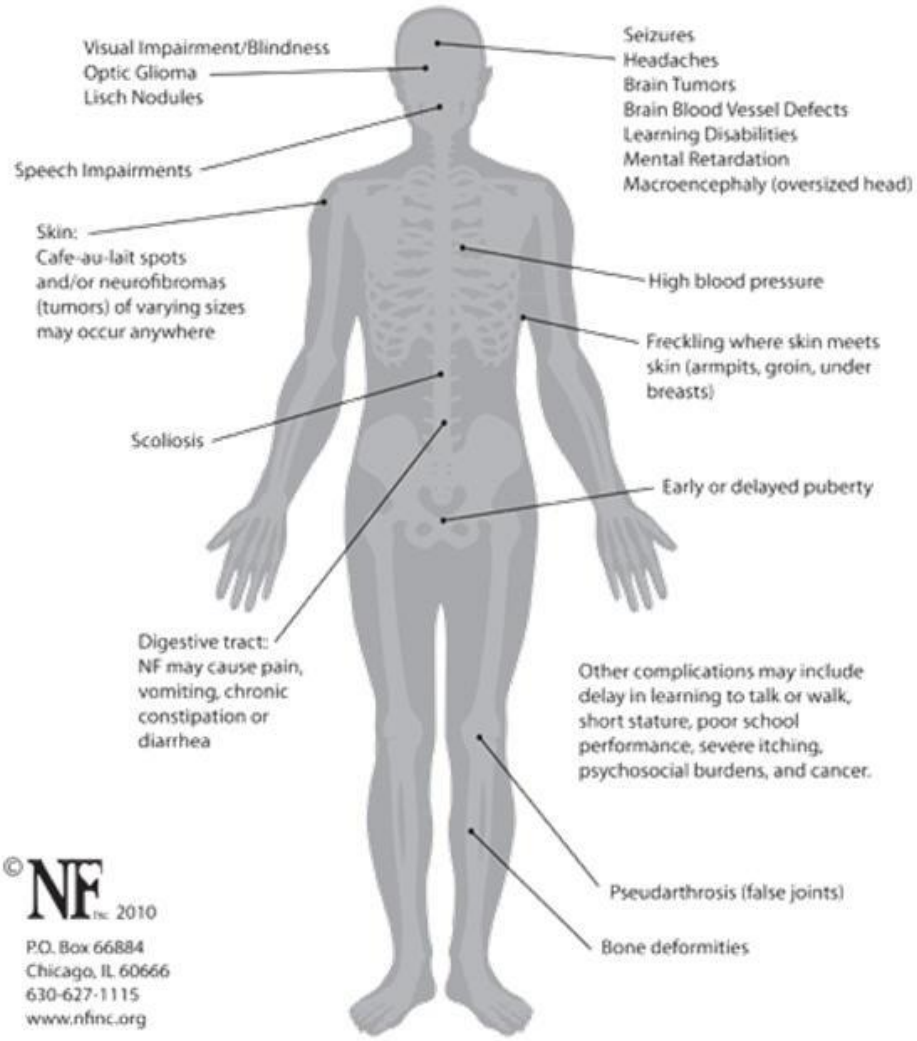

Figure 2. Clinical manifestations of neurofibromatosis type I (NF1).

Reprinted with permission from the neurofibromatosis network.

Neurofibromas manifest as superficial cutaneous neurofibromas (localized nodules on or beneath the skin found in almost all adult NF1 patients) and/or as diffuse or plexiform neurofibromas (deep-seated tumors that growth along the length of large nerve bundles which occur in approximately 30-40% of patients). (13) Only deep neurofibromas can undergo malignant transformation to become MPNSTs, which is the main cause of morbidity and mortality of NF1 patients. (14) Malignant transformation in NF1 patients peaks at adolescence with an increased risk remaining through adulthood. (15) There is an estimated 8–13% lifetime risk of MPNST development in NF1 patients (Figure 3). (13)

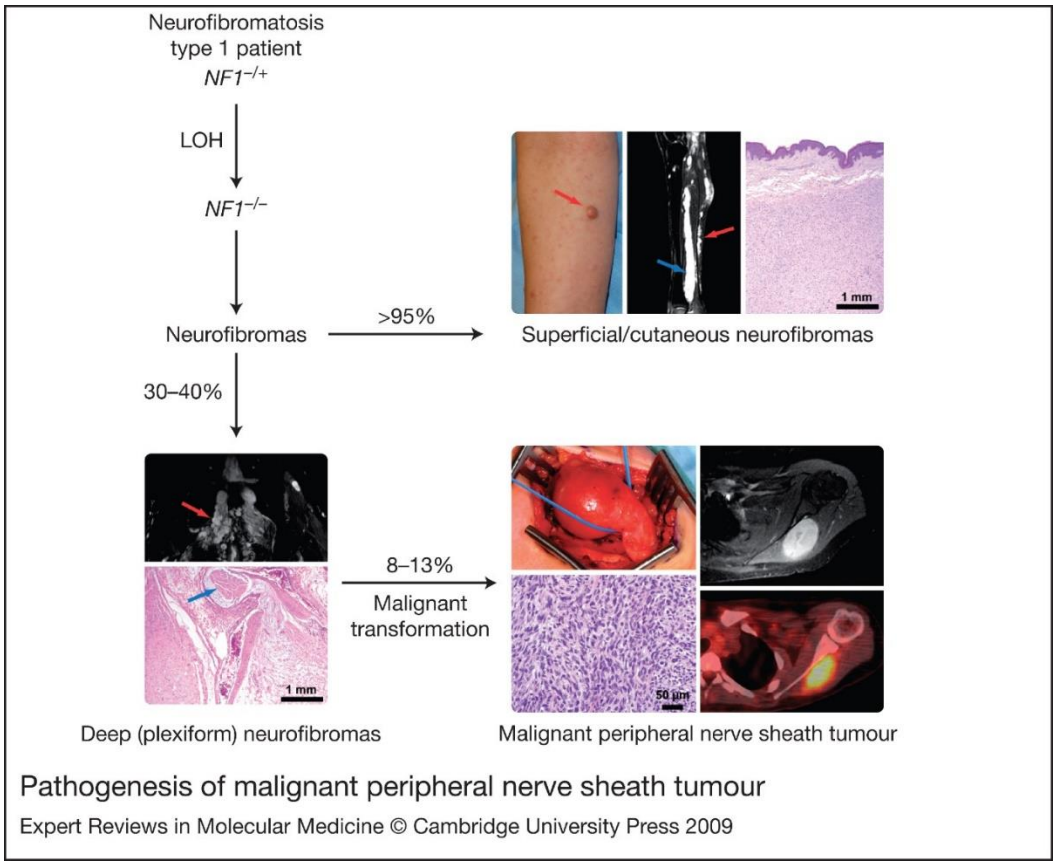

Figure 3. Neurofibromatosis type I molecular pathogenesis. Neurofibromatosis 1 (NF1) is a neurogenetic disorder caused by loss of function of the NF1 gene. Neurofibromas are the most common benign peripheral nerve sheath lesions in NF1 and manifest as superficial

cutaneous neurofibromas (nonplexiform) in virtually all patients and/or as deep (often plexiform) neurofibromas. Only deep neurofibromas have the significant propensity to undergo malignant transformation to MPNSTs, with an estimated 8–13% lifetime risk in a patient. Most MPNSTs are believed to arise in association with deep neurofibromas, but they may arise outside of this context as well. In the superficial cutaneous neurofibroma panel, a clinical photograph depicts a cutaneous neurofibroma (red arrow), and a radiograph from a different patient shows both superficial (red arrow) and deep (blue arrow) neurofibromas involving the lower extremity. The haematoxylin and eosin (H&E) photomicrograph shows a dermal neurofibroma. The deep neurofibroma panel features a radiograph of lobular, plexiform neurofibroma (red arrow) deep in the pelvis and an H&E image of a plexiform neurofibroma associated with a nerve (blue arrow). Additional molecular events must accumulate for malignant transformation. In the MPNST panel, an intraoperative photograph shows an MPNST in an NF1 patient involving the sciatic nerve with a histological photomicrograph of an MPNST below. The images to the right show a radiograph of an MPNST near the scapula and a PET (positron emission tomography) image showing avid glucose uptake consistent with intense metabolic activity in the same case directly below. Clinical and radiographic images were kindly provided by John Madewell, John Slopis and Ian McCutcheon of M.D. Anderson Cancer Center, Houston, TX, USA. Abbreviations: LOH, loss of heterozygosity; MPNST, malignant peripheral nerve sheath tumour; NF1, neurofibromin gene.

Molecular characteristics

The *NF1* gene encodes the protein neurofibromin which functions as a Ras GTPase-activating protein, a key negative regulator of the mitogen-activated protein kinase (MAPK) pathway. Mutated *NF1* effects the expression and/or function of neurofibromin. Loss of neurofibromin function results in dysregulated Ras activity and hyperactive MAPK signaling, leading to constitutive activation of downstream pathways and increased cell proliferation. (10) Association with a genetic cancer predisposition disorder makes MPNST unique from other STS subtypes.

Available treatment options

MPNST is largely unresponsive to chemotherapy or radiotherapy; however, neoadjuvant chemotherapy has been shown to provide disease stabilization, and external beam radiation therapy may offer improved local control. (16) Therefore, the mainstay of treatment for MPNST is surgical resection, though this is often difficult due to the location and size of these tumors. (17,18) Recent studies have identified several recurring genetics aberrations in MPNST (occurring in *NF1*, *TP53*, *CDKN1B*, *PDGFRA*, *HGF*, and others), as well as irregular receptor tyrosine kinase activity that could be exploited for treatment or highlight other targetable molecular dysregulations. (19-21) However, clinical trials evaluating targeted agents such as erlotinib (targeting EGFR), sorafenib (targeting VEGF and RAS), and imatinib (targeting KIT) reported minimal observed responses in STS patients, including those with MPNST. (7,22)

Patient outcome

Even with surgical resection of primary disease, studies show MPNSTs have a high propensity to recur (40%-65%) and metastasize (41%). (13,23) Metastasis typically occurs to the lung (67%) with the liver and brain being less common sites (36%). (23) Additionally, in the MD Anderson Cancer Center experience with MPNST cases, the five-year survival

rate for patients with NF1-associated MPNST is approximately 48%. The five-year survival rate decreases substantially in patients with radiation-associated MPNST (43%), while increasing slightly in patients with sporadic MPNST (63%) (Figure 4). (24)

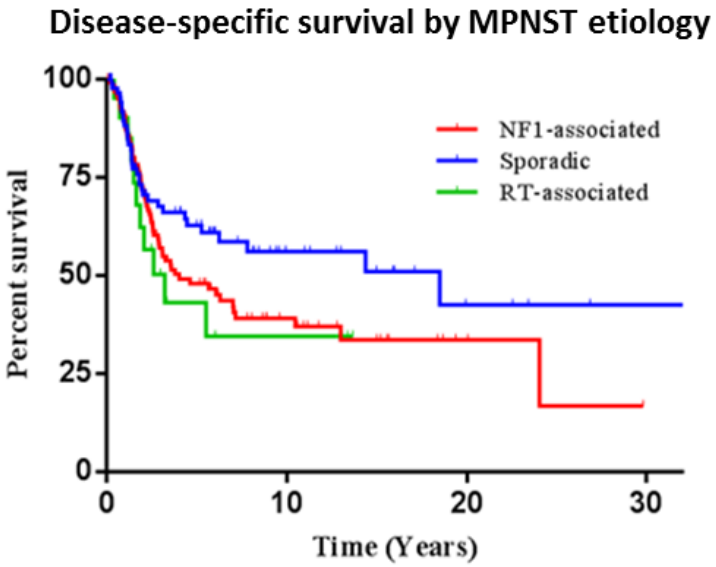

Figure 4. Disease-specific survival of MPNST patients by etiology.

Reprinted from Watson, K. L., Al Sannaa, G. A., Kivlin, C. M., Ingram, D. R., Landers, S. M., Roland, C. L., Cormier, J. N., Hunt, K. K., Feig, B. W., Guadagnolo, B. A., Bishop, A. J., Wang, W.-L., Slopis, J. M., McCutcheon, I. E., Lazar, A. J. & Torres, K. E. Patterns of recurrence and survival in sporadic, neurofibromatosis type 1-associated, and radiation-associated malignant peripheral nerve sheath tumors (MPNSTs). Journal of Neurosurgery, In Press. (2016). (24)

1.3 Poly (ADP) ribose polymerases

Family members and function in DNA repair

Poly (ADP) ribose polymerases (PARP) were first identified in 1966 with the discovery of PARP1. (25) Subsequent PARPs were characterized based on their sequence homology to the PARP domain/catalytic domain in PARP1, resulting in a PARP superfamily with 17 members, named sequentially PARP1- PARP 16. (26) PARPs contain several conserved domains: domain A is a deoxyribonucleic acid (DNA) binding domain containing two zinc fingers, domain B contains a nuclear localization sequence, domain D is an automodification domain, and domain F is the catalytic domain. (27,28) The enzymatic product of PARP is poly (ADP) ribose (PAR) which acts to post-translationally modify nuclear acceptor proteins. (28) Enzymatic activity has mainly been attributed to PARP1 (>90%) and PARP2 (5-10%). (25,29)

Upon stimulation by DNA single strand breaks, PARP catalytic activity increases approximately 500 fold and, via its DNA binding domain, binds to sites of DNA damage. (25) Using the ADP ribosyl moiety of NAD as a substrate, PARP generates long, often branched, chains of PAR of various sizes in successive transfer cycles onto nuclear acceptor proteins with the release of nicotinamide. (28) Poly (ADP) ribosylation (PARylation) domains frequently overlap with the functional domains of acceptor proteins, thereby altering their function. (30) Additionally, PAR is highly negatively charged, therefore PAR can also alter its acceptor protein's functions, including protein-protein interactions, protein-nucleic acid interactions, enzymatic activity, and/or subcellular localization, via charge effects or by acting as a steric block due to its large size. (31) This is a well-balanced process which leads to a rapid turnover of PAR. Poly (ADP) ribose glycohydrolase (PARG) splits the ribose-ribose linkages of PAR, creating free ADP-ribose and de-PARylating the acceptor protein (Figure 5). (28)

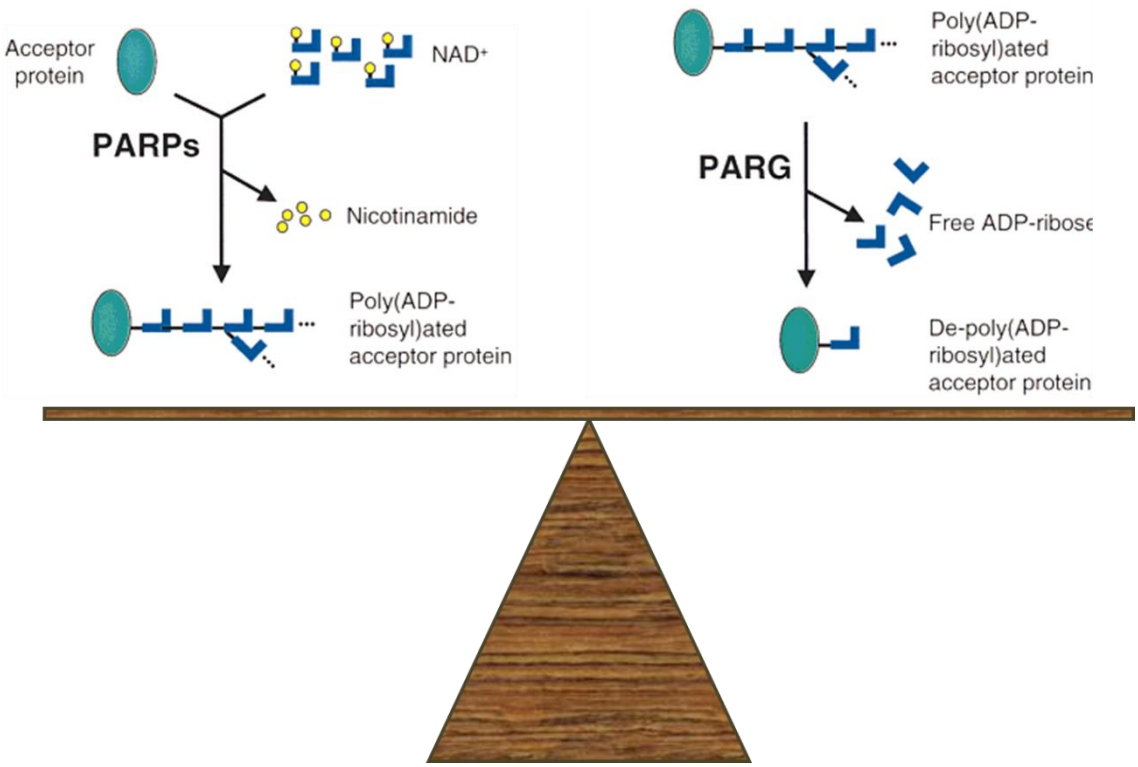

Figure 5. Poly (ADP) ribose polymerase function. Poly (ADP- ribose) polymerases (PARPs) use the ADP-ribosyl moiety (L- shaped symbols in blue) for NAD+ to covalently modify acceptor proteins in successive transfer cycles thus creating branched chains of poly (ADP-ribose), with stoichiometric release of nicotinamide. Poly (ADP-ribose) glycohydrolase (PARG) splits the ribose- ribose linkages between ADP- ribosyl units of the polymer, thus creating free ADP- ribose.

Modified and reprinted with permission from John Wiley and Sons: [Bioessays] (28), Copyright 2001.

The classic role of PARP is in DNA damage repair through the base excision repair (BER) pathway. Upon single strand DNA damage, PARP signals the extent of injury and relaxes the chromatin, by PARylating histones, for increased access to DNA breaks; additionally, a large portion of PAR is bound to PARP itself in an automodification reaction. PARP activity recruits other repair proteins either directly by PARylation or indirectly through interaction with other PARylated proteins, such as the scaffold protein x-ray repair complementing defective repair in Chinese hamster cells 1 (XRCC1), that assemble and activate BER. PARylation of PARP1 causes its release from damaged DNA which suppresses further PAR synthesis and provides access for other repair proteins to fully repair the DNA insult (Figure 6). (32,33) The BER process begins with the recognition and removal of the damaged base by DNA glycosylase, which creates an abasic site (AP site). (34) The DNA backbone is then cut on the 5' side by an AP endonuclease, such as apurinic-apyrimidinic endonuclease 1 (APEX1), which is subsequently removed by a DNA phosphodiesterase. DNA polymerase 1 then replaces the missing base alone (short patch BER) or along with several bases downstream by first removing them with its 5' to 3' exonuclease activity, then replacing them with its polymerase activity (long patch BER). (35-37) Long patch BER also requires the activities of PCNA to assist DNA polymerase in displacement and synthesis of DNA longer than one base. (37) This process creates a flap that is incompatible with ligation. (37) Therefore, flap endonuclease 1 cleaves the resulting flap so the gaps can be ligated. (37) DNA ligase 3 (short patch BER) or DNA ligase 1 (long patch BER) completes the repair by annealing the gap. (34,36) PARP1 has been shown to be able to bind to approximately 90% of genes transcribed by RNA polymerase II; additionally PARP2 is a positive cofactor for transcription of approximately 600-1000 genes. (33) PARylation acceptor proteins also include those involved in transcription, replication, cell cycle, chromatin structure, and cell death, therefore PARPs have non-DNA damage function as well. (38)

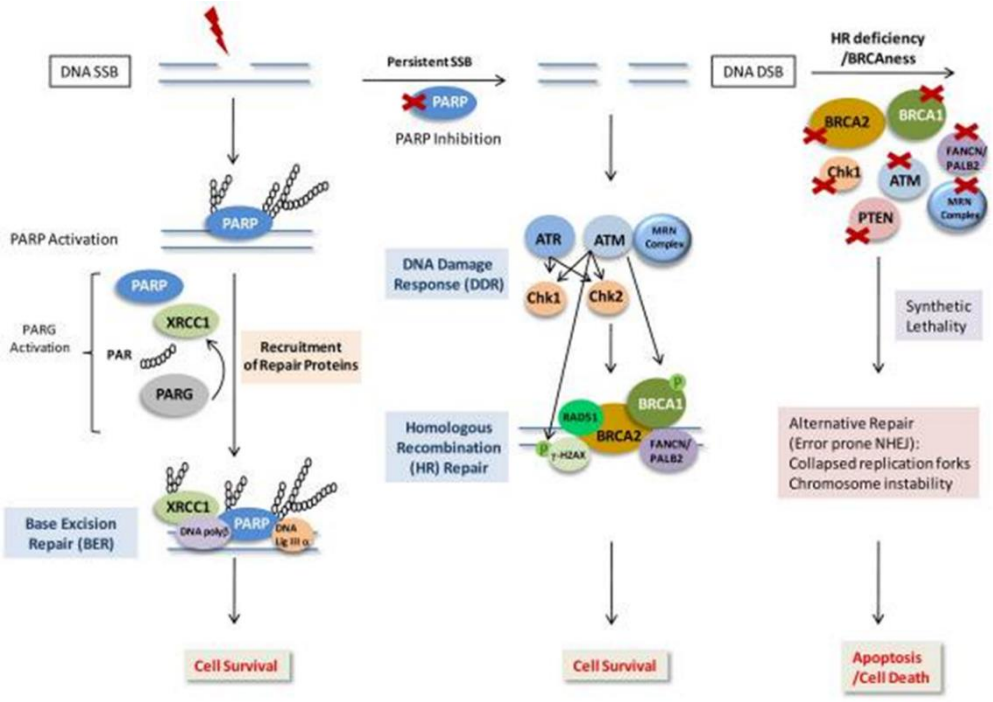

Figure 6. Effect of Poly (ADP) Ribose Polymerase function and inhibition on DNA repair. PARP is activated in response to DNA SSB by detecting and binding SSB to initiate the process of BER. Its catalytic activity results in poly(ADP-ribosyl)ation on itself and other key BER proteins such as XRCC1. Activated PARP then recruits other DNA repair proteins via poly(ADP-ribosyl)ation and direct interactions to facilitate DNA repair. The cellular levels of PAR are regulated by the opposing actions of PARP and PARG. Degradation of PAR polymer by PARG leads to release of modified proteins from damaged DNA. PARP inhibition causes an increase in persistent SSBs in DNA that are converted into DSBs. Both HR and DDR proteins are involved in the repair of DSBs. However, HR deficient cells or cells with BRCAness are unable to repair the accumulated DSBs caused by PARP inhibition, resulting in collapsed replication forks, chromosome instability and cell death.

Reprinted from Wang X, Weaver DT. The ups and downs of DNA repair biomarkers for PARP inhibitor therapies. American Journal of Cancer Research. 2011;1(3):301-327. (32)

Poly (ADP) ribose polymerase inhibition

Nicotinamide was the first PARP inhibitor to be established and was evaluated almost thirty years ago. (39) Second generation PARP inhibitors were then discovered through screening of chemical libraries, thus enhancing the potency and structure-specific activity of these inhibitors. (40) The current third generation inhibitors act as a competitive inhibitor of NAD, the substrate of PAR. (41,42)

There are two approaches for the clinical development of PARP inhibitors: (1) exploit a defect in the targeted cell so the cell dies when PARP activity is lost (synthetic lethality) or (2) use a PARP inhibitor as a chemosensitizer, in combination with traditional chemotherapy or radiotherapy. Synthetic lethality is the principle that either of two mutations has no effect, but the combination of mutations is lethal. This idea was applied to cancer therapeutics in 1997. (43) For example, the addition of a PARP inhibitor would compromise the efficacy of BER and lead to the conversion of single strand breaks to double strand breaks. If the cell has intact DNA double strand break repair machinery, the damage can be repaired and the cell would survive. However, if PARP inhibition is applied to a cell with a deficiency in homologous recombination (HR), the error-free pathway of DNA double strand break (DSB) repair, the cell will be unable to fix the damage and the replication fork will collapse, leading to chromosomal instability and cell death due to mitotic catastrophe (Figure 6). (32,44)

Most notably, PARP inhibition in tumors with a breast cancer 1/2, early onset (*BRCA1/2*) mutation or a *BRCA*-deficient phenotype without a germline *BRCA* mutation (termed "*BRCA*ness") was shown to cause synthetic lethality. (45,46) The majority of preclinical and subsequent clinical studies with PARP inhibitors have been performed in *BRCA*-mutated breast and ovarian carcinomas with significant anti-tumor effects reported. (47) Over 100 clinical trials have been performed with an array of PARP inhibitors alone and in combination with conventional chemotherapies.

The PARP inhibitor AZD2281 (Olarparib) is arguably the most well-characterized PARP inhibitor clinically available, and has been shown to have significant single-agent efficacy in *BRCA*-mutant cells and synergizes with DNA-damaging platinum drugs in preclinical studies. (48,49) In clinical trials, AZD2281 has been shown to be generally well-tolerated and produced an objective response in 47% of 19 patients with *BRCA*-mutant breast, ovarian, or prostate cancer, in addition to a 63% disease control rate. (50,51) Currently, AZD2281 is in several phase 3 clinical trials including study of olaparib in ovarian cancer (SOLO1 and SOLO2) for *BRCA*-mutated ovarian cancer.

However, recent studies have revealed that due to the nature of *BRCA* mutations, drug-resistant populations can form, due to secondary mutations that restore wildtype function of BRCA, increased expression and function of hypomorphic *BRCA1/2*, or increased drug efflux. (52) Because this population seems to develop over a period of time, a heterogeneous tumor population may exist prior to treatment. Continued exposure to a PARP inhibitor results in the selection of the drug resistant population, which becomes the predominate population, therefore PARP inhibition is no longer an effective therapy. (52)

Almost ten years ago, studies showed that cancer cells with defective DNA repair proteins such as ataxia telangiectasia and Rad3 related (ATR), ataxia telangiectasia mutated (ATM), and checkpoint kinase 1/2 (CHK1/2) are profoundly sensitive to PARP inhibitors and may represent biomarkers for patient selection and PARP efficacy. (46,53) In addition, the presence of the EWS-FLI1 fusion protein, resulting from the EWS RNA-binding protein 1-Fli-1 proto-oncogene, ETS transcription factor translocation in Ewing's sarcoma, has been shown to elicit PARP inhibitor sensitivity. (54) This preclinical observation has led to a current clinical trial for Ewing's sarcoma patients that have failed traditional chemotherapies. Lord and Ashworth have also proposed other predictive biomarkers of PARP inhibitor sensitivity including loss of function mutations of cyclin-dependent kinase 12 (CDK12), often found in serous ovarian cancer, and loss of expression of excision repair cross-complementation

group 1 (ERCC1), seen in non-small cell lung cancer. (51) These findings expand the use of PARP inhibitors beyond *BRCA*-mutant cancer types and could lead to larger clinical trials where patients are included based on genetic screenings of their tumors.

1.4 Nucleotide excision repair

Function in DNA repair

The nucleotide excision repair (NER) pathway repairs bulky DNA lesions that cause a distortion of the DNA; the two major types of photoproducts that result in this type of distortion are cyclobutane pyrimidine dimers (CPDs) and [6,4]-pyrimidine dimers. (55,56) This type of DNA adduct can be caused by exogenous (UV) or endogenous (reactive oxygen species) sources. (57) The pathway is divided into two sub-pathways: repair of the actively transcribed pathway (transcription coupled repair), and the non-transcribed region (global genome repair). (58) During transcription coupled repair (TCR), DNA damage is detected through the arrest of RNA polymerase. (59) Cockayne syndrome A and B then allow access to the DNA damage site by inducing dissociation of RNA polymerase as well as recruiting several TCR-specific proteins involved in chromatin remodeling for rapid repair of the lesion, including UV-stimulated scaffold protein A (UVSSA), ubiquitin-specific-processing protease 7 (USP7), XPA-binding protein 2 (XAB2), high mobility group nucleosome-binding domain-containing protein 1 (HMGN1), and the transcriptional elongation factor, TFIIS. (60,61) These factors help to facilitate chromatin remodeling and enable the resumption of transcription after the lesion is removed. (62) DNA damage in global genome repair is detected through the binding of xeroderma pigmentosum, complementation group C (XPC) (further stabilized by human homolog of RAD23B (HHRAD23B) and centrin 2 (CETN2)), and XPE which serves to further stimulate XPC binding to the lesion, and is thought to further distort the DNA structure. (61) Subsequent steps of DNA repair are identical between the two sub- pathways. (63) The general

transcription factor complex (TFIIH) binds the area of DNA damage through the interaction with either XPC or the arrested transcription machinery. (63) This complex is composed of ten subunits, most notably xeroderma pigmentosum, complementation group B (XPB) and xeroderma pigmentosum complementary group D (XPD). XPB and XPD are DNA helicases which unwind DNA from 5' to 3' or 3' to 5' respectively, near the damaged base. XPD also acts as a verification step and checks for distortion of the DNA strand, as well as, a damaged base to prevent unnecessary NER. (59,63) Once the DNA is unwound, replication protein A (RPA) is recruited and acts to protect the separated single strand. (60) Xeroderma pigmentosum, complementation group G (XPG), a structure specific nuclease, is also recruited at this time, whereas XPC is released, free to recognize other damaged sites to initiate a new round of NER. (64) The area around the damage is then cleaved by XPG/XPA, a 3' nuclease, and a 5' nuclease, xeroderma pigmentosum, complementation group F-excision repair cross-complementation group 1 (XPF-ERCC1). (60,65) The region containing the lesion is displaced, allowing for gap repair synthesis. DNA polymerase delta (along with replication factor C (RFC), and proliferating cell nuclear antigen (PCNA)), or DNA polymerase epsilon alone bind to the 3'-OH overhang created by the cut of XPF-ERCC1 and extend the DNA to span the gap, thus causing the displacement of the repair proteins. (59,65) The gap is finally ligated by DNA ligase I or by DNA ligase III in non-cycling cells (Figure 7). (58,61)

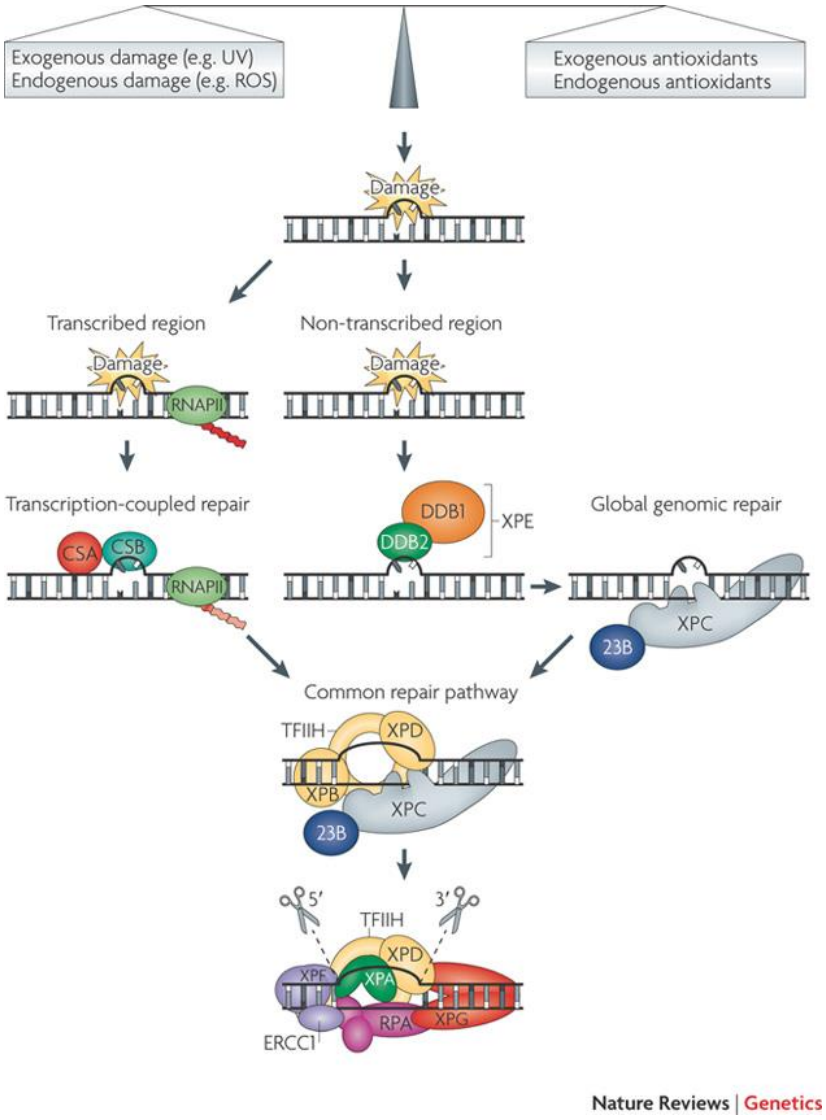

Figure 7. Nucleotide excision repair. The nucleotide excision repair (NER) system consists of a series of reactions by which DNA damage caused by, for example, ultraviolet radiation-induced photoproducts or similar chemically induced products is recognized and repaired. Damage can occur from external and endogenous sources (shown as a balance in the figure). Photoproducts include cyclobutane pyrimidine dimers (CPDs) and [6–4] photoproducts, which can both involve T and C pyrimidines. When repair of these photo- or chemical products is faulty owing to mutations in the NER system, replication errors lead to characteristic C to T mutations, especially CC to TT mutations, which are found in TP53, Patched 1 (PTCH1) and other oncogenes in sunlight-induced skin cancers of patients with

xeroderma- pigmentosum (XP) and others. The damage is endogenous in other systemic disorders and is thought to be caused mainly by reactive oxygen species (ROS). Depending on whether the damage occurs in a transcriptionally active or inactive domain, repair can occur by two pathways: global genomic repair (GGR) or transcription-coupled repair (TCR) (shown in the figure). Damage in transcriptionally active regions is detected through the arrest of transcription by RNA polymerase I (RNAPI; not shown) and RNA polymerase II (RNAPII). Transcription arrest is enhanced by mutations in the Cockayne syndrome A (CSA) and Cockayne syndrome B (CSB) proteins, and both are required for ubiquitylation of the carboxy-terminal domain of RNAPII. Cells with mutations in CSA (also known as ERCC8) and CSB (also known as ERCC6) do not show the increased rate of photoproduct repair in transcriptionally active regions that occurs in normal cells, and carry out GGR at normal rates. Arrested polyubiquitylated RNAPII is removed and degraded, leaving the active genes accessible for repair and the resumption of transcription. CSA is a WD40 protein that is part of the ubiquitin E3 ligase that acts on XPC and DNA damage-binding 2 (DDB2). Damage in transcriptionally inactive regions is detected by the DNA damage-binding protein XPC and complex Damage-Specific DNA Binding Protein 1 (XPE). Mutation of either of these can cause XP140. The individual DNA damage-binding proteins have weak affinities for their substrate, so the binding process can be viewed either as a sequential process in which one protein facilitates binding by another or as a grouping of weakly interacting partners that form transient pre-incision complexes that are locked in place by the XPB (also known as ERCC3) ATPase. The CPDs and [6–4] photoproducts make substantially different structural changes in DNA: CPDs are much less distorting and require more active participation of XPE. Damage recognition is followed by binding of the ten-component basal transcription factor TFIIH through interaction with either XPC or the arrested transcription apparatus. XPD (also known as ERCC2) is a component of TFIIH and is a DNA helicase that is involved in 5′ to 3′ unwinding of the DNA in the vicinity of a

damaged base. ATP hydrolysis by the XPB component of TFIIH facilitates binding of the NER complex to the damaged site. The amino terminus of XPB interacts with XPD and XPG (also known as ERCC5), whereas the carboxyl terminus is required for 5′ cleavage. XPD carries out a further damage recognition step when its migration along the helix is blocked by a photoproduct. The DNA around the damaged site is then cleaved by the XPG 3′ nuclease and the XPF–ERCC1 5′ nuclease. Recent evidence suggests that 5′ cleavage occurs first. XPG is bound through interaction with XPC and TFIIH. The nucleases are anchored by XPA–replication protein A (RPA), which defines the cleavage sites and strand specificity. Once the damaged oligonucleotide is removed, a patch is resynthesized by proliferating cell nuclear antigen, polymerases δ, ε or κ and a ligase. In quiescent cells, ligation involves X-ray repair cross-complementing protein 1 (XRCC1) and ligase III. In proliferating cells, ligation involves ligase I.

Mutations within the NER pathway can give rise to xeroderma pigmentosum (XP), caused by a mutation in XP (subtype A-G) genes, Cockayne syndrome (CS), caused by a mutation in *ERCC6/8*, or trichothiodystrophy, caused by a mutation in *ERCC2/3*. (65) Cells with a mutation in CSA or CSB do not show the increased rate of DNA repair in the transcriptionally active strand due to a loss of TCR, instead those cell carry out GGR at normal rates. (57,66) CS patients have light sensitivity, neurological, facial, and limb abnormalities, premature aging, dwarfism, and often early death due to neurodegeneration. (57,63,66) If the NER pathway is deficient, the replication fork may collapse and the single strand breaks can be converted into double strand DNA breaks. (67,68)

Possible implication with poly (ADP) ribose polymerase inhibitors

In addition to *BRCA*ness, other components of DNA repair may determine sensitivity to PARP inhibition. Lord and Ashworth demonstrated, via siRNA screen, that the nucleotide excision repair genes, XPA binding protein (XAB2) and damage-specific DNA binding protein (DDB1), were lethal targets when combined with PARP siRNA. (69) The authors hypothesized that TCR-deficient cells may stall the replication fork in response to DNA lesions, leading to cell cycle arrest until the fork can be restarted. This can lead to collapse of the replication fork and double strand DNA breaks beyond a threshold that is compatible with cell viability. Therefore a TCR deficiency can make cells sensitive to PARP inhibition.

1.5 Double strand DNA repair mechanisms

Homologous Recombination

Double strand DNA breaks are the most detrimental form of DNA damage. (70) Double strand DNA breaks can occur through multiple physical (ex: replication across a nick) or pathological (ex: ionizing radiation) means. (71) There are two main methods of double strand DNA break repair: homologous recombination (HR) and non-homologous end joining (NHEJ). HR is a high fidelity pathway that requires a homologous region of DNA

as a template to repair the damage and therefore occurs during S and G2 phases of the cell cycle. (70,72,73) HR is initiated when the meiotic recombination 11/ RAD50 homolog/ Nijmegen breakage syndrome 1 (MRE11/Rad50/NBS1 [MRN]) complex and CtBP interacting protein (CtIP) are recruited to sites of double strand DNA damage. (73) This leads to 5' to 3' end resection of the DNA by MRN and further resection by exonuclease 1 (EXO1) to produce long stretches of 3' single strand DNA, which is then coated by replication protein A (RPA) to prevent the formation of secondary structure. (58,73,74) Resection of the DNA ends commits the repair of the DSB to the HR pathway as opposed to NHEJ and is facilitated by BRCA1. (75,76) BRCA2, in a relatively not-well understood process, interacts with BRCA1, BRCA1 associated RING domain 1 (BARD1), and partner and localizer of BRCA2 (PALB2) to displace RPA, and enable the loading of RAD51 recombinase (Rad51) onto the 3' overhangs. (58,73,74,77) The Rad51-DNA filaments, referred to as the nucleofilament, further stabilized by Rad54 then invade the sister chromatid in search of a homologous sequence and form the synaptic complex, a three strand intermediate that allows the invading strand to anneal with the complementary strand and displace the third strand to form a structure known as the D loop. (58,72,74,78) The 3' end of the invading strand is then extended by DNA polymerases, in a process called strand extension. (73) If this newly synthesized strand dissociates from the template strand and reanneals with the other original ssDNA overhang, it will form a non-crossover product in a process termed synthesis-dependent strand annealing (SDSA). (72,74) Evidence suggests this is the main conclusion of DNA DSBs in somatic mammalian cells. (79) Otherwise the extension of the invading strand can cause the D loop to migrate until it reaches the second end of the double strand break where it can form two Holliday junctions (HJs), in a process called second end capture. (72) The bloom syndrome, recQ helicase-like-topoisomerase III-recQ mediated genome instability 1 (BLM-TOPOIII-RMI1) complex can then resolve the Holliday junctions to a non-crossover product. (58,72,74) Alternatively,

the Holliday junctions can be ameliorated by HJ resolvases such as MUS81 structure-specific endonuclease subunit- essential meiotic structure-specific endonuclease 1 (MUS81-EME1), GEN1 (Holliday junction 5' flap endonuclease), or SLX1 structure-specific endonuclease (SLX1-SLX4), which can lead to crossover or non-crossover products due to their symmetrical cleavage of the Holliday junctions (Figure 8). (58,74)

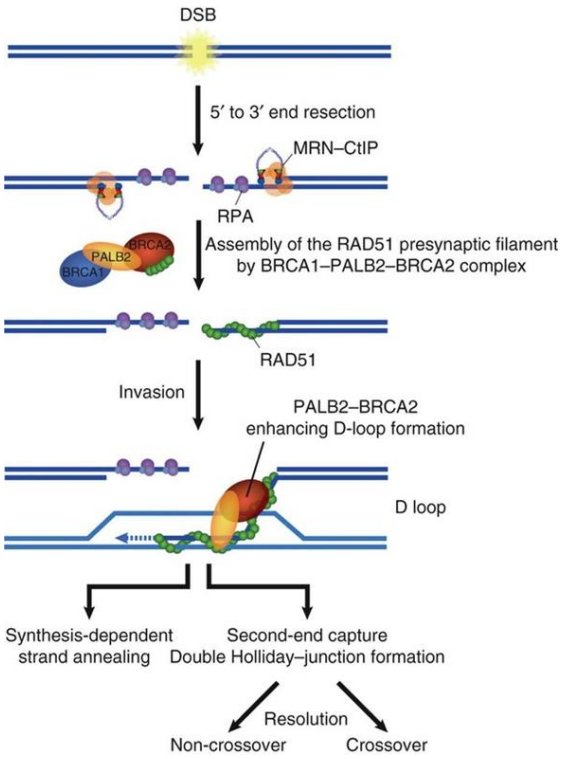

Figure 8. Homologous Recombination (HR). After DNA damage end resection by MRN and CtIP, PALB2–BRCA2 activates RAD51 to promote the invasion of an undamaged template, leading to synthesis-dependent strand annealing or second-end capture and double–Holliday junction formation to allow DSB repair.

Reprinted with permission from Nature Publishing Group: [Nature Structural and Molecular Biology] (77), Copyright 2010.

Implication with PARP inhibitors

PARP inhibitors are primarily used in malignancies with a deficiency in homologous recombination (HR) in order to enhance the conversion of single strand DNA breaks to double strand DNA breaks. The inability of the HR deficient cell to efficiently repair double strand DNA breaks translates into replication fork collapse and cell death. (80) However, there are currently no publications citing a homologous recombination pathway deficiency in MPNST.

Non-Homologous End Joining

Determining whether double strand DNA breaks will be repaired by HR or NHEJ is a complex question. If the damage occurs outside of the S or G2 phase where a sister chromatid or homologous chromosome is not available, HR cannot occur and NHEJ must be used to repair the damage. (71,73) In addition, tumor protein p53 binding protein 1 (53BP1) and its effector replication timing regulatory factor 1 (Rif1) act to antagonize BRCA1 and direct repair through NHEJ. (76) Upon DNA damage, the Ku autoantigen p70 subunit/Ku autoantigen p80 subunit (Ku70/Ku80) heterodimer binds to each side of the double strand break and prevents non-specific 5' end resection. (74,81) This protein has a high affinity for DNA ends and is ubiquitously expressed in the cell (approximately 500,000 molecules per cell); once bound it is referred to as a Ku:DNA complex. (71,74,81) These end complexes can recruit subsequent nuclease, polymerase, and ligase proteins in any order, causing a large number of outcomes that can possibly result from the same starting lesion in NHEJ. (58,82) DNA-dependent protein kinase catalytic subunit (DNA-PKcs) is recruited to the Ku:DNA complex and forms the DNA-PK holoenzyme. Artemis is recruited, phosphorylated, and therefore activated by DNA-PKcs, where it processes incompatible DNA ends due to its diverse nuclease activity. (82) DNA-PKcs also acts to tether the two ends of the DNA together, as well as protect the ends from degradation and prevent premature ligation. (58,70) If the DSB is highly complex, polymerase mu and lambda are

recruited by the Ku:DNA complex to synthesize and fill the gap. (71,73) Polymerase mu is highly adaptable, able to perform template-dependent synthesis but can also polymerize across a discontinuous template strand, making it well-suited for this flexible DNA repair mechanism. (81) Polymerase lambda has also been shown to have template-independent activity. (81) Finally, x-ray cross-complementation group 4 (XRCC4), nonhomologous end-joining factor 1 (NHEJ1), also known as XRCC4-like factor (XLF) and DNA ligase 4 seal the ends. (58,73,83) Compared to HR, NHEJ is a highly error-prone process and its resulting DNA product are highly mutagenic and inaccurate compared to the original sequence. (71,83,84) If the DNA ends have at least four nucleotides of sequence homology on DNA overhangs, XRCC4-DNA ligase 4 can simply ligate the ends of one single strand overhang while the other is filled by polymerases, without the activity of any of the members of the NHEJ pathway. (71,82) This scenario is the only form of NHEJ in which the original sequence of the DNA could be preserved (Figure 9). (71,82).

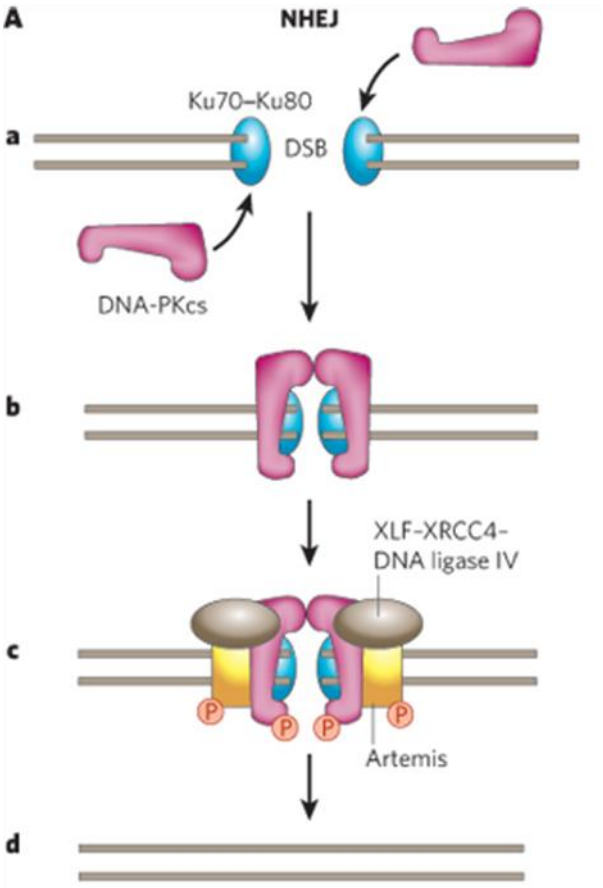

Figure 9. Non- Homologous End Joining (NHEJ). There are two main pathways of DNA repair: NHEJ and homologous recombination. **A,** NHEJ. **a,** A DSB is recognized by the Ku dimer (Ku70–Ku80) and DNA-PKcs. **b,** The two DNA ends are synapsed. **c,**DNA-PKcs and Artemis are phosphorylated, and the DNA ends are processed by a complex consisting of XLF (XRCC4-like complex; also known as NHEJ1), XRCC4 (X-ray-repair cross-complementing protein 4) and DNA ligase IV, and by Artemis. **d,** The DNA ends are ligated by DNA ligase IV, and the DNA-repair factors dissociate.

Modified and reprinted with permission from Nature Publishing Group: [Nature] (85), Copyright 2007.

Possible implication with PARP inhibitors

It has been shown recently that treatment with a PARP inhibitor enhanced the phosphorylation of DNK-PKcs and therefore aberrantly activate NHEJ in ovarian cancer cell lines. (86) The authors of this study hypothesize that the deregulated and highly mutagenic NHEJ further increases genomic instability and cytotoxicity associated with PARP inhibition. Therefore, in the setting of HR- deficiency, increased NHEJ activity contributes to synthetic lethality and may predict sensitivity to PARP inhibitors (Figure 10).

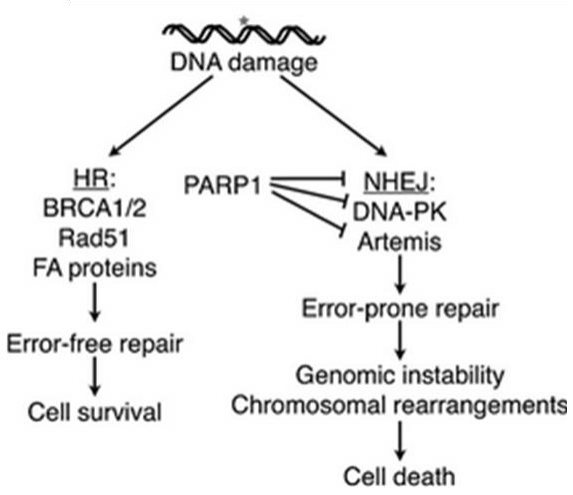

Figure 10. Role of HR and NHEJ in PARP inhibition. Current model explaining synthetic lethality of PARP inhibition and HR deficiency. PARP inhibition is thought to induce accumulation of SSBs, which are converted to DSBs by collisions with replication machinery. The inability of HR-deficient cells to adequately repair DSBs results in genomic instability and eventual cell death.

Reprinted from Patel, A. G., Sarkaria, J. N. & Kaufmann, S. H. Nonhomologous end joining drives poly(ADP-ribose) polymerase (PARP) inhibitor lethality in homologous recombination-deficient cells. Proceedings of the National Academy of Sciences of the United States of America 108, 3406-3411, doi:10.1073/pnas.1013715108 (2011). (86)

1.6 Hypothesis and specific aims

Although MPNSTs do not have a characterized defect in *BRCA1/2* or any DNA repair pathway deficiency, they have a karyotypically-complex phenotype that would suggest a deficiency in DNA damage repair and a high level of inherent DNA damage and genomic instability. (87,88) Therefore, I hypothesize that poly (ADP) ribose polymerase (PARP) inhibition is an effective therapeutic strategy in MPNST.

To pursue this hypothesis, I developed the following specific aims:

Aim 1: Evaluate the effects of PARP inhibition on MPNST *in vitro* and *in vivo.*

Aim 2: Identify potential mechanisms underlying MPNST sensitivity to PARP inhibitors.

Chapter 2

Materials and Methods

Clinically annotated tissue microarray

This study was approved by The University of Texas MD Anderson Cancer Center Institutional Review Board. A clinically annotated tissue microarray (TMA) containing samples of 115 human atypical and plexiform neurofibromas (n = 24) and MPNSTs (primary, n = 38; recurrent, n = 32; MPNST, n = 21) was used for immunohistochemical staining. TMAs were constructed as previously described. (89)

Cell lines

MPNST cell lines used in this study include three NF1-associated MPNST cell lines (S462 [provided by Dr. Brian Rubin, The Cleveland Clinic and The Cleveland Clinic Lerner College of Medicine, Case Western Reserve University, Cleveland, OH] and ST88 and MPNST92-417/T265 [provided by Dr. Jonathan Fletcher, Brigham and Women's Hospital, Boston, MA]), and two sporadic MPNST cell lines (STS26T [provided by Dr. Steven Porcelli, Albert Einstein College of Medicine, Bronx, NY] and MPNST724 [provided by Dr. Jonathan Fletcher]). Primary human adult normal Schwann cell (NSC) cultures were provided by Dr. Patrick Wood (University of Miami, Miami, FL) or purchased from ScienCell Research Laboratories. MDA-MB-231, MDA-MB-436, and T47D breast cancer cells were purchased from the MD Anderson Cancer Center characterized cell line core. MPNST cells were grown in Dulbecco's modified Eagle medium (DMEM) supplemented with 10% fetal bovine serum (FBS), 100U/ml penicillin, and 100µg/ml streptomycin. MPNST cell lines with Cockayne syndrome B overexpression (CSBOE) or CSB shRNA were grown in DMEM with 10% FBS, 100U/ml penicillin, and 100µg/ml streptomycin; positive transfectants were selected with 1 µg/ml puromycin then grown under selective pressure. Schwann cells were grown in Schwann cell media (#1701, ScienCell Research Laboratories) supplemented with 5% FBS,

100U/ml penicillin, 100µg/ml streptomycin, and 1% Schwann cell growth supplement (#1752, ScienCell Research Laboratories). MDA-MB-231 and MDA-MB-436 were grown in Dulbecco's modified Eagle medium:Nutrient mixture F-12 (DMEM F-12) supplemented with 10% FBS, 100U/ml penicillin, and 100µg/ml streptomycin. T47D cells were grown in RPMI-1640 media supplemented with 5% FBS, 100U/ml penicillin, and 100µg/ml streptomycin. DNA fingerprinting (short tandem repeat, STR) was conducted as previously described to verify the identity of all MPNST cell lines. (90)

Antibodies and reagents

The PARP inhibitors AZD2281 was purchased from ChemieTek (CT-A2281). For *in vitro* studies, the drugs were dissolved in dimethyl sulfoxide (DMSO) and stored at -80°C. For *in vivo* experiments, AZD2281 (50mg/kg/day) was dissolved in PBS, 10% DMSO, and 10% 2-hydroxypropyl-β-cyclodextrin (HPCD). The DNA-PK inhibitor NU7026 was purchased from Selleck Chemicals (S2893). For *in vitro* studies the drug was dissolved in dimethyl sulfoxide (DMSO) and stored at -80°C**.** Commercially available antibodies were used for western blot or immunohistochemical (IHC) detection of PARP1 (9542, Cell Signaling Technology), PARP2 (PA1-4280, ThermoFisher Scientific Pierce) and (SAB2500751, Sigma-Aldrich), PAR (4335-AMC-050, Trevigen Inc) and (ALX-084-220-R100, Enzo Life Sciences, Inc.), gamma-H2AX (2577, Cell Signaling Technology), CSB (10459, Santa Cruz Biotechnology), DNA-PKcs (4602, cell signaling), DNA-PKcs Ser2056 (124918, Abcam), Ki67 (CRM325, Biocare Medical), cleaved caspase 3 (CC3; CP229, Biocare Medical), cyclin B1 (752, Santa Cruz Biotechnology), and β-actin-HRP (47778-HRP, Santa Cruz Biotechnology). Terminal deoxynucleotidyl transferase dUTP nick end labeling (TUNEL) was performed using the TdT-FragEL™ DNA Fragmentation Detection Kit according to the manufacturer's instructions (QIA33, EMD Millipore). The pEGFP-Pem1 system HR and NHEJ plasmids were provided by Dr. Vera Gobunova (University of Rochester, Rochester, NY). The CSB OE plasmid (pLenti-GIII-CMV-hERCC6-HA; LV150273) and viral packaging vectors (LV053) were purchased

from Applied Biological Materials British Columbia, Canada. Viral packaging was performed by the MD Anderson Cancer Center shRNA and ORFeome Core. *ERCC6* shRNA (Individual Human SMARTvector 2.0 Lentiviral shRNA particles) were purchased from ThermoFisher Scientific (VSH6063). Polybrene (sc-134220, Santa Cruz Biotechnology) and puromycin (400-128P, Gemini Bio-Products) were used for shRNA transductions. Restriction enzymes, ISCE1 and HindIII, were purchased from New England Biolabs and used according to New England Biolabs established conditions and protocols.

ERCC6 shRNA transductions

Approximately $5x10^5$ MPNST cells were trypsinized, centrifuged, and resuspended in 1 mL of DMEM supplemented with 5% FBS. Polybrene (1µg/ml) was added to each cell suspension, which were subsequently plated into six well tissue culture plates. Approximately $5.0x10^6$ viral particles were added to each well and incubated at 37°C for 8 hours. The media was then changed to DMEM supplemented with 10% FBS and incubated at 37°C for an additional 64 hours. Cells were grown under selective pressure (1.0µg/ml puromycin) for subsequent experiments. Knockdown of CSB was confirmed by western blot.

MTS assays

CellTiter96 AQueous One Solution Cell Proliferation Assays [3-(4,5-dimethylthiazol-2-yl)-5-(3-carboxymethoxyphenyl)-2-(4-sulfophenyl)-2H-tetrazolium, inner salt; MTS] (G3580, Promega) were used to evaluate cell proliferation per the manufacturer's instructions. Briefly, cells were seeded in 96-well plates in 100µL of media. Attached cells were subsequently treated with AZD2281 and incubated with drug for 96 hours or 7 days (drug and media changed after 96 hours). MTS reagent was added to each well and incubated for 1-2 hours at 37°C. Absorbance was measured at a wavelength of 490nm. The absorbance values of treated cells were represented as a percentage of the absorbance of untreated cells. The

half-maximal effective concentration (EC50) of AZD2281 was determined using nonlinear regression log(inhibitor) vs. response (four parameters) curve fitting in GraphPad Prism version 6.05.

Clonogenic assay

Clonogenic assays were conducted by plating 100-500 MPNST cells in 6-well plates. Cells were then treated with DMSO or AZD2281 in DMEM for approximately 2 weeks. The media was removed, and the cells were washed twice with phosphate-buffered saline (PBS). The cells were fixed with 5% gluteraldehyde for 20 minutes and then washed and stained with 0.1% crystal violet in 20% methanol for at least 1 hour. The wells were washed with water and allowed to dry. Pictures were captured digitally and individual clones were counted manually. Clones of treated cells were represented relative to the untreated control.

Western blot analysis

Western blot analyses were conducted according to previously published standard methods. (91) Densitometry was assessed using the ImageJ Gel Analysis tool version 1.49 (NIH).

Flow cytometry

Cell cycle progression was measured by propidium iodide (PI) staining followed by fluorescence activated cell sorting (FACS) analysis. Cells were incubated with AZD2281 for 24 hours and subsequently fixed in 70% ethanol. Fixed cells were resuspended in a PI staining solution (75μg/mL PI and 10μg/mL RNAse A). For evaluation of apoptosis, cells were treated with AZD2281 for 96 hours. Apoptosis was measured via Annexin V-Fluorescein isothiocyanate (Annexin V-FITC)/PI staining and FACS analysis with the FITC Annexin V Apoptosis Detection Kit I (556547, BD Biosciences) per the manufacturer's recommendations. Cells reported as apoptotic include those in early and late phase apoptosis. Cell cycle and apoptosis samples were analyzed with the use of a Gallios flow

cytometer (Beckman Coulter Inc.) by the Flow Cytometry and Cellular Imaging Core at MD Anderson. Data from these experiments were analyzed with the use of the Multicycle program in FCS Express (De Novo Software).

PARP activity assay

PARP activity assays were performed by using the Trevigen Universal PARP Colormetric Assay Kit (4677-096-K, Trevigen Inc) according to the manufacturer's instructions with the following modifications. Cells were seeded in six-well plates at approximately 50% confluency. The cells were then treated with AZD2281 and incubated for 24 hours at 37° C. Endogenous PARP activity was established without AZD2281 pretreatment. Cellular protein was extracted by scraping using the Cell Extraction Buffer (1x PARP Buffer [20X PARP buffer provided in kit diluted in water], 0.4M NaCl, 0.9% Triton X-100, 0.4nM PMSF, cOmplete Protease Inhibitor Cocktail Tablets [11697498001, Roche]). The suspension was centrifuged at 4°C for 10 minutes at >10,000g; the supernatant was extracted and the protein concentration was measured.

Histone-coated strip wells were hydrated by using 1x PARP buffer for 30 minutes at room temperature; three wells per condition were used. The positive control wells contained diluted PARP-HSA enzyme (provided in kit), 1x PARP buffer, and 1x PARP cocktail (10x PARP cocktail provided in kit, 10x Activated DNA provided in kit, and 1x PARP buffer) at a final volume of 50µl. The negative control wells contained DMSO, 1x PARP buffer, and 1x PARP cocktail at a final volume of 50µl. The experimental wells included 10µg pretreated cell lysate in a total volume of 25µl, and 1x PARP cocktail at a final volume of 50µl. The wells were incubated for 1 hour at room temperature. The remainder of the experiment was performed according to the manufacturer's instructions. The absorbance values of three wells from each experiment were averaged and the absorbance values of treated cells were

represented as a percentage of the absorbance of untreated cells. The data were represented as the average of two experiments with the standard error of the mean (SEM).

RNA sequencing

Total RNA was prepared using the RNeasy Mini Kit (74104, Qiagen) according to the manufacturer's protocol. RNA sequencing was performed by the MD Anderson Cancer Center Sequencing and Microarray Facility with an Illumina HiSeq2000 sequencer. The raw reads were aligned to the human reference genome build hg19, using Tophat2 RNASeq alignment software. The mapping rate was 95.27% overall across all the samples in the dataset. HTseq-Count was used to quantify the gene expression counts from Tophat2 alignment files. Differential expression analysis was performed on the count data using R package DESeq2. P-values obtained after multiple binomial tests were adjusted using FDR (BH).

TaqMan PCR confirmation of RNAseq results

Total RNA was extracted from cell lines using the RNeasy Mini Kit according to the manufacturer's protocol. RNA was converted into cDNA using the iScript cDNA synthesis kit (1708890, Bio-Rad Laboratories) via the kit protocol. Excision repair cross-complementation group 6 (ERCC6) expression was confirmed using TaqMan PCR (Hs00972920_m1 primer: 4331182, ThermoFisher Scientific) according to the manufacturer's instructions.

pEGFP-Pem1 system transfection

The pEGFP-Pem1 plasmid system was a kind gift from the Vera Gorbunova laboratory (University of Rochester). (92,93) The HR plasmid of the pEGFP-Pem1 system was linearized by I-SceI digestion. 500ng of the linearized plasmid was transiently transfected into approximately $5x10^5$ cells using the Neon transfection system according to the manufacturer's instructions (ThermoFisher Scientific) along with the transfection control plasmid pDs-Red2 (100ng). The electroporation parameters were 1350V (pulse voltage), 20ms (pulse width), 2 pulses (pulse number) for cell lines. The cells were then plated in DMEM supplemented with

10% FBS. GFP was measured by flow cytometry 72 hours post transfection. The pEGFP-Pem1 system also contains a plasmid to measure NHEJ efficiency. DSBs were induced by I-SceI or Hind-III and the transfection proceeded similar to the HR plasmid. The data was reported as a ratio of green (indicating efficient HR in the cell) to red (indicating a transfected cell). Cells were analyzed with the use of a LSR Fortessa flow cytometer (BD Biosciences) located in the Flow Cytometry and Cellular Imaging Core at MD Anderson. Data from these experiments were analyzed with the use of the Multicycle program in FCS Express (De Novo Software).

Metaphase spread

Cell lines were treated with DMSO, 2.5μM AZD2281, 500nM NU7026, or combination treatment for 72 hours. Chromosome analysis was performed in duplicate at the UTMDACC Molecular Cytogenetics Facility (funded by the Center for Genetics and Genomics). Metaphase spreads from each sample were photographed using a Nikon 80i microscope equipped with karyotyping software from Applied Spectral Imaging (ASI) Inc.

The samples were scored for structural aberrations including chromosomal breaks, fusions, fragments, and radial structures. Thirty-five cells per plate and condition were evaluated.

CPD ELISA

MPNST cells were plated in 6 well dishes to approximately 50% confluency. Prior to UV exposure, the wells were washed with PBS and the media was replaced with 500μl PBS. The dishes were then exposed to 256J/m^2/min UVB using the FS40 lamp. (94) Immediately after exposure, the 0hr time point was harvested for cell lysates and pelleted for DNA extraction and use in the cyclobutane pyrimidine dimer (CPD) enzyme- linked immunosorbent assay (ELISA). The media in the remaining wells was replaced with DMEM supplemented with 10% fetal bovine serum, 100U/ml penicillin, and 100μg/ml streptomycin and harvested at the corresponding time points. DNA extraction was then performed using the QIAamp DNA Mini

Kit. The OxiSelect™ UV-Induced DNA Damage ELISA Kit (STA-322, Cell Biolabs) was then carried out according to the manufacturer's instructions.

In vivo *animal models*

All animal procedures and care were approved by The University of Texas MD Anderson Cancer Center Institutional Animal Care and Usage Committee (IACUC). Animals received humane care as per the Animal Welfare Act and the NIH "Guide for the Care and Use of Laboratory Animals." Animal models were utilized as previously described. (95,96) Trypan blue confirmed viable MPNST724 cells ($2x10^6$ in 0.1mL of PBS/mouse) or STS26T cells ($2x10^6$ in 0.1mL of PBS/mouse) were injected into the flank of 6–week-old female hairless severe combined immunodeficient (SCID) outbred mice (Crl:SHO-Prkdc^{scid}Hr^{hr}, Strain Code: 474) (474-SCID Hairless, Charles River Laboratories) (MPNST724: vehicle group n=9 and AZD2281 group n=8; STS26T: n=8/for each treatment group), and growth was measured twice weekly. When average tumor volumes reached 50 mm^3, the mice were assigned to two treatment groups: (a) control (vehicle only) and (b) AZD2281. AZD2281 (50mg/kg/daily, intraperitoneal injection [IP]) resuspended in PBS, 10% DMSO, and 10% 2-hydroxypropyl-β-cyclodextrin (Sigma-Aldrich, St. Louis, MO) was used. Mice were monitored for tumor size, body weight, and well-being, and were euthanized when control group tumors reached an approximate volume of 1500 mm^3. Tumors were resected, weighed, and fixed in formalin and paraffin-embedded for IHC studies.

An experimental lung metastasis MPNST model was used to evaluate metastatic growth. This model has been described previously. (96) Viable STS26T cells were injected as cell suspensions ($1x10^6$ in 0.1mL of PBS/mouse) into the tail vein of 6–week-old female hairless severe combined immunodeficient (SCID) outbred mice (Crl:SHO-Prkdc^{scid}Hr^{hr}, Strain Code: 474). Mice were monitored for 3 weeks (a time point by which 95%-100% of mice develop established lung metastases). (97) Mice were then assigned to the following treatment groups: (a) control (vehicle only) and (b) AZD2281 (50mg/kg/d, IP). AZD2281

resuspended in PBS, 10% DMSO, and 10% 2-hydroxypropyl-β-cyclodextrin was used. Mice were euthanized when physical signs of disease were present (weight loss >20% of baseline, difficulty of breathing, hunched posture, pallor, impaired ambulation, and lethargy). Lungs were resected, weighed, and examined for macroscopic lung metastases; these tissues were then fixed in formalin and paraffin-embedded for IHC studies. Survival studies proceeded as above; however, mice were sacrificed individually when euthanasia was required.

IHC analysis

PARP1 and PARP2 immunostaining was scored by two independent observers (AJL and GAA) for TMA analyses. Intensity scores were designated as negative (0), weak (1 and 2), or strong (3). The percentage of cells staining positive was evaluated on a scale of 0-100%. A combined score ranging from 0-300 was obtained from the product of the intensity and cells-positive scores. Xenograft-derived specimens were analyzed for markers of cell proliferation (Ki67), cell cycle arrest (cyclin B1), inhibitor specificity (PAR), and apoptosis (CC3 and TUNEL). Representative images of the TMA and xenograft- derived specimens were captured at 200x and 400x total magnification, respectively, using an Olympus microscope (BX41) and camera (DP72) with Olympus cellSens Standard v1.5 software.

Statistical analyses

Differences among expression of PARP1 and PARP2 between tumor types were evaluated using Mann-Whitney U tests. Univariate Cox proportional hazards models were used to assess the potential prognostic significance of PARP1 expression in primary and recurrent MPNST samples and further visualized utilizing univariate Kaplan-Meier curves. Two-sided *p*-values <0.05 were considered statistically significant. All analyses were performed using SPSS version 21.

Cellular assays were repeated at least two times; the mean and SEM were calculated for each assay. The mean and standard deviation were calculated for xenograft experiments.

Correlation analysis between the fold change expression of CSB and the EC50 value of AZD2281 was established using Spearman's correlation. Significance of findings was assessed using a two-tailed Student's *t*-test ($p<0.05$ = *; $p<0.001$ = ***).

Chapter 3

PARP inhibition *in vitro* and *in vivo*

This chapter is based upon the citation below and has been reprinted with permission from Taylor and Francis: [Cancer Biology and Therapy], copyright 2015.

Kivlin, C. M. et al. Poly (ADP) Ribose Polymerase Inhibition: A Potential Treatment of Malignant Peripheral Nerve Sheath Tumor. Cancer biology & therapy, 0, doi:10.1080/15384047.2015.1108486 (2015).

PARP1 and PARP2 are highly expressed in MPNST tissue samples.

To determine the expression of PARP1 and PARP2 in human tumor samples, we performed IHC on a clinically annotated TMA containing patient samples of neurofibroma, primary MPNST, recurrent MPNST, and metastatic MPNST (Figure 11). The overwhelming majority of MPNST samples were positive for PARP staining. Overall, moderate to high expression of PARP1 and PARP2 was observed (Table 1).

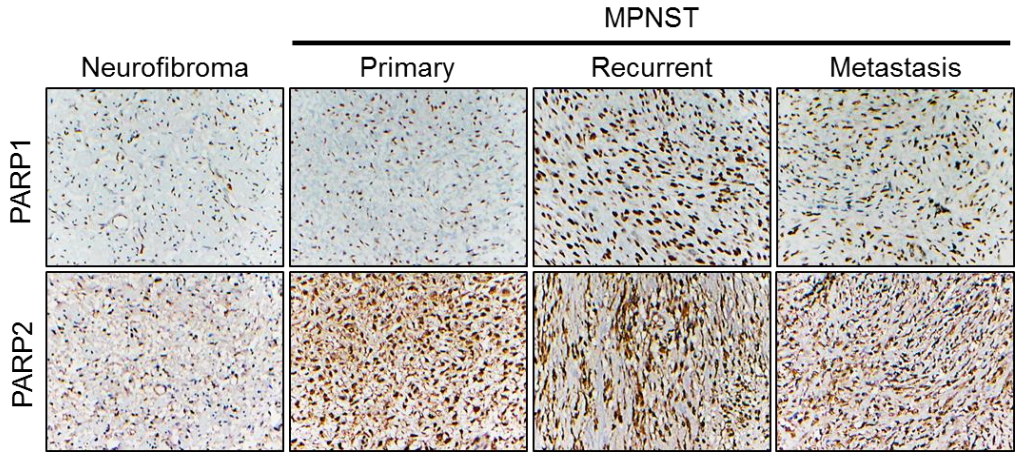

Figure 11. PARP1 and PARP2 are highly expressed in MPNST tissue compared to neurofibroma. MPNST TMA stained for PARP1 and PARP2. Images were captured at 200x magnification.

Reprinted with permission from Taylor and Francis: [Cancer Biology and Therapy] (98), copyright 2015.

Table 1. Mean Expression of PARP1 and PARP2 in 115 neurofibroma and MPNST tissues			
Mean IHC score (% tumors +)	Neurofibroma	MPNST	*P-value*
PARP1	232.5 (100%)	179.6 (90%)	0.017*
PARP2	117.1 (100%)	122.8 (100%)	0.287

Table 1. Mean expression of PARP1 and PARP2 combined score (0-300) and percentage of tumors with positive staining in neurofibroma and MPNST.

While there was differential expression of PARP1 and PARP2 between primary, recurrent, and metastatic MPNST samples with regard to percent positive cells, nuclear intensity, and combined score, the clinical relevance of these minor variations is negligible as the overall expression levels remain high (Table 2 and Table 3).

Table 2. Mean Expression of PARP1 and PARP2 in 115 neurofibroma and MPNST tissues

Mean IHC score	Neurofibroma	Primary MPNST	Recurrent MPNST	Metastatic MPNST
PARP1				
% Positive	79.6	79.4	79.3	64.0
Nuclear Intensity	2.9	2.7	2.4	1.5
Combined	232.5	210.3	193.9	104.3
PARP2				
% Positive	54.1	62.0	59.6	67.7
Nuclear Intensity	2.1	2.1	1.85	1.8
Combined	117.1	132.4	111.4	127.7

Table 2. Mean expression of PARP1 and PARP2 percentage of staining, nuclear intensity, and combined score in neurofibroma and MPNST disease states.

Table 3. Summary of p-values for PARP1 and PARP2 expression between neurofibroma and MPNST samples

Comparison	PARP1			PARP2		
	% Positive	NI	Combined	% Positive	NI	Combined
Neurofibroma versus primary MPNST	0.778	0.161	0.433	0.132	0.929	0.144
Neurofibroma versus recurrent MPNST	0.961	0.009*	0.098	0.280	0.021*	0.932
Neurofibroma versus metastatic MPNST	0.016*	<0.001*	<0.001*	0.028*	0.046*	0.175
Primary MPNST versus recurrent MPNST	0.754	0.116	0.431	0.582	0.009*	0.131
Primary MPNST versus metastatic MPNST	0.015*	<0.001*	<0.001*	0.272	0.030*	0.976
Recurrent MPNST versus metastatic MPNST	0.014*	0.003*	0.001*	0.094	0.977	0.197

*Statistically significant at level of p <0.05

Table 3. Summary of PARP1 and PARP2 distribution. PARP percentage of expression and nuclear intensity was scored from the MPNST TMA. The P value to determine the significance of distribution between disease states is shown.

In addition, we evaluated whether PARP1 expression correlated with the survival outcomes of MPNST patients. Although not statistically significant, a trend towards better survival was observed in patients with tumors expressing low levels of PARP1 when compared to patients that had tumors with moderate to high expression (p = 0.165; HR 0.51, 95% CI 0.19-1.32) (Figure 12; Table 4). PARP2 was not evaluated by log-rank comparison due to its homogenously uniform expression.

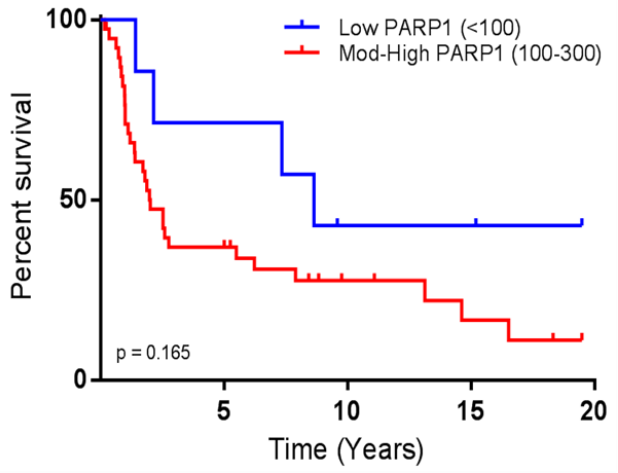

Figure 12. PARP1 staining correlated to patient outcomes. Kaplan-Meier curve depicting a trend toward decreased survival in patients with moderate-high levels of PARP1 staining compared to low PARP1 staining, as determined by IHC.

Reprinted with permission from Taylor and Francis: [Cancer Biology and Therapy] (98), copyright 2015.

Table 4. Overall and Disease-specific Survival Outcomes

	Overall Survival		Disease-specific Survival	
PARP1	P-value	HR (95% CI)	P-value	HR (95% CI)
% Cells Positive, score range 0-100 Low/Moderate (<69%) v high (>70%)	0.251	0.17 (0.69-4.2)	0.191	0.54 (0.23-1.36)
Nuclear Intensity, score range 0-3 No-low (0-1) v mod-high (2-3)	0.347	0.56 (0.17-1.86)	0.409	0.61 (0.18-1.99)
Combined Score, score range 0-300 Low (<100) v moderate-high (100-300)	0.165	0.51 (0.19-1.32)	0.229	0.55 (0.21-1.45)

Table 4. Overall and disease- specific survival outcomes for MPNST patients determined by PARP1 percentage of staining, nuclear intensity, or combined score.

Reprinted with permission from Taylor and Francis: [Cancer Biology and Therapy] (98), copyright 2015.

PARP1 is highly expressed in MPNST cell lines.

Based on the enhanced expression of PARP1 and PARP2 seen in our MPNST tissue samples, we assessed their expression in a panel of MPNST cell lines. An immunoblot of PARP1 and PARP2 suggested increased expression in MPNST cell lines versus the normal Schwann cell control (Figure 13).

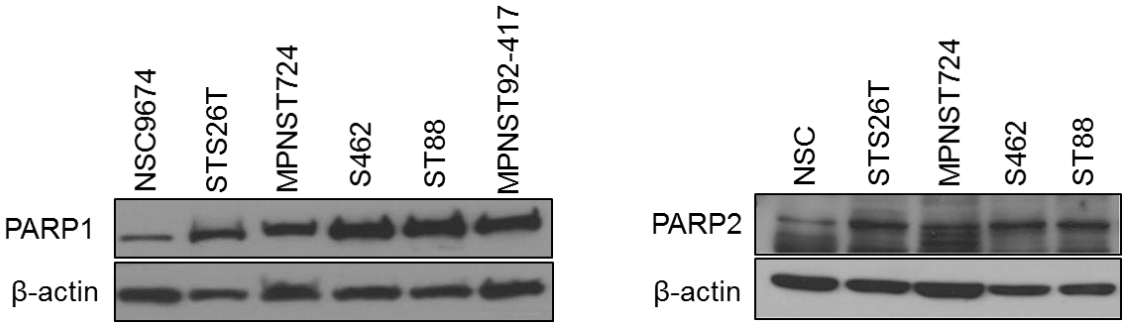

Figure 13. PARP1 and PARP2 are highly expressed in MPNST cell lines compared to normal Schwann cells. Immunoblot of PARP1 and PARP2 in a MPNST cell panel and normal Schwann cell control.

PARP activity is enhanced in MPNST cell lines.

PARP1 and PARP2 modify acceptor proteins through PARylation and thus influence their cellular function. Therefore, PAR expression can be used as a marker of PARP catalytic activity. We performed western blot analysis to interrogate a panel of MPNST cell lines (sporadic: MPNST724 and STS26T; NF1-associated: S462 and ST88) for endogenous PAR expression. MPNST cell lines have enhanced PAR expression, suggestive of increased PARP activity compared with normal Schwann cells (NSCs), with MPNST724 cells showing the lowest expression of the MPNST cell lines (Figure 14). Because PARP activity is stimulated by DNA damage, increased endogenous PAR expression could indicate the relatively high levels of endogenous DNA damage in MPNST cell lines.

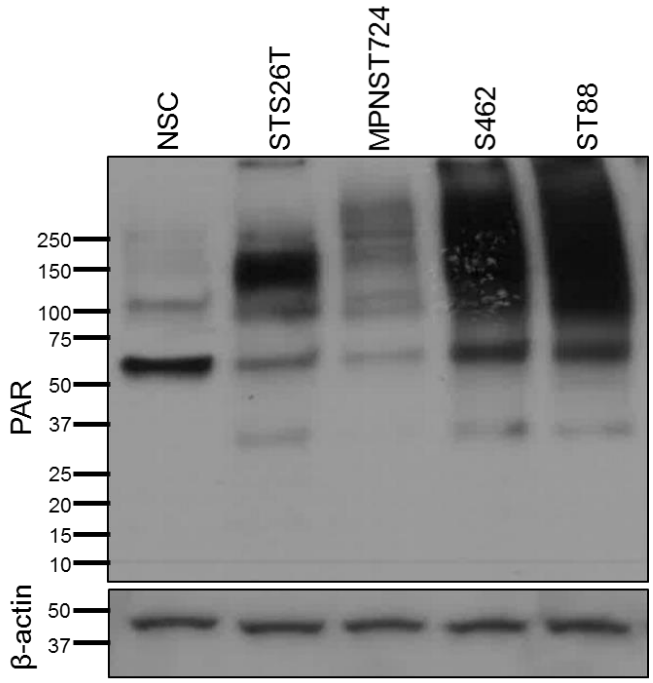

Figure 14. MPNST cell lines have enhanced PAR expression. PAR immunoblot of MPNST cell panel and normal Schwann cells.

Reprinted with permission from Taylor and Francis: [Cancer Biology and Therapy] (98), copyright 2015.

To validate that enhanced PARP expression is representative of endogenous PARP activity in MPNST cell lines, untreated MPNST cell lines and NSCs were used in a modified Universal PARP Colorimetric Assay. PARP activity was found to be more than three-fold higher in MPNST cell lines compared to NSCs in this cell-free system (Figure 15).

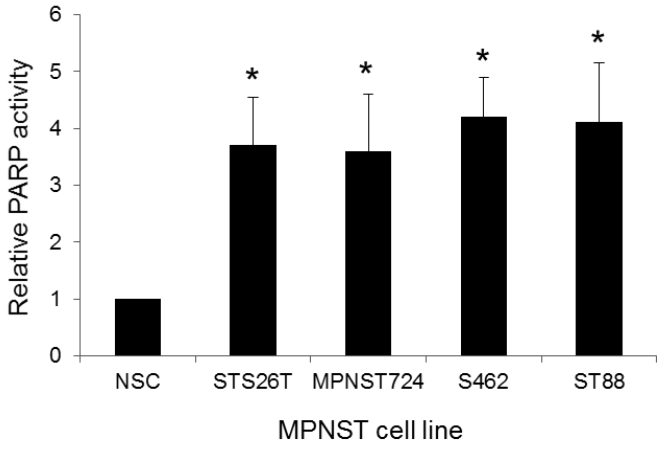

Figure 15. MPNST cell lines have increased PARP activity compared to NSCs. Endogenous PARP activity in untreated MPNST cells and normal Schwann cells (n=4). Error bars represent standard error of the mean; (*= p<0.05).

Reprinted with permission from Taylor and Francis: [Cancer Biology and Therapy] (98), copyright 2015.

AZD2281 is a highly effective single-agent inhibitor of MPNST *in vitro.*

Before assessing the effect of AZD2281 on MPNST tumorigenicity, we evaluated the efficacy of this inhibitor to block PARP activity. A panel of MPNST cell lines was treated with increasing doses of AZD2281 for 24 hours and evaluated by the modified Universal PARP Colorimetric Assay. AZD2281 treatment resulted in a dose-dependent decrease in PARP activity in all MPNST cell lines (Figure 16).

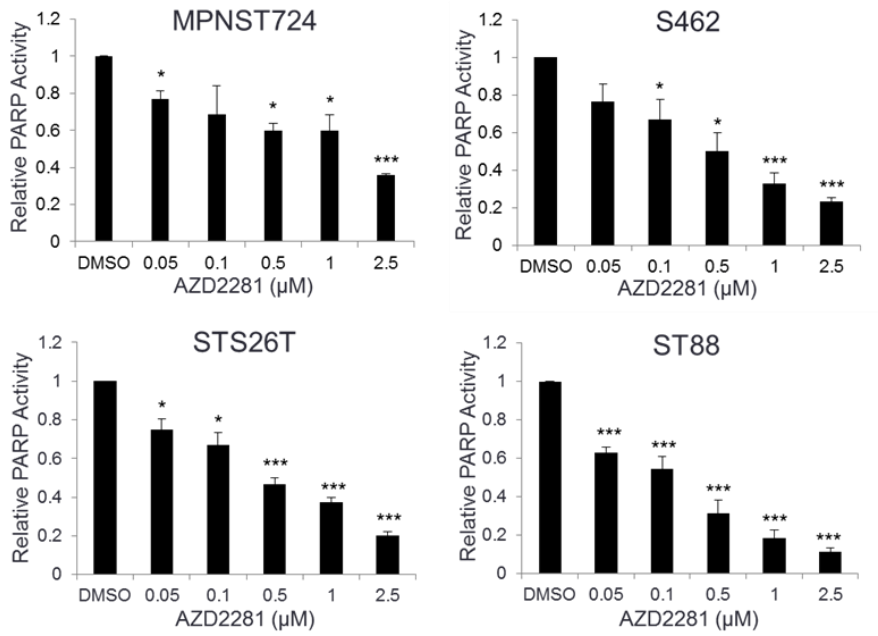

Figure 16. PARP inhibition decreases PARP activity in MPNST cell lines. A panel of MPNST cell lines were pretreated for 24 hours with AZD2281 and subjected to a modified PARP activity assay (26T, ST88, and 462 n=3; 724 n=2). Error bars represent standard error of the mean; * = $p<0.05$; *** = $p<0.001$.

Reprinted with permission from Taylor and Francis: [Cancer Biology and Therapy] (98), copyright 2015.

Treatment of MPNST cell lines with elevated concentrations of AZD2281 for 96 hours resulted in a proportional decrease in cell proliferation. All EC50 values for the MPNST cell panel were in the micromolar range (2.92 – 12 μM) with no variation in sensitivity between the sporadic and NF1-associated cell lines. In comparison, normal Schwann cell lines treated with the same dose of AZD2281 showed only a slight decrease in cell proliferation. EC50s ranged from 18μM to greater than 20μM, which was the highest treatment dose used (Figure 17). Compared to cell lines known to be sensitive or resistant to AZD2281 as determined by their AZD2281 EC50 values, the EC50s of MPNST cell lines more closely resemble those of the the known sensitive cell lines (Table 5). Additionally, AZD2281 decreased the clonogenic potential of MPNST cell lines in a dose-dependent manner (Figure 18).

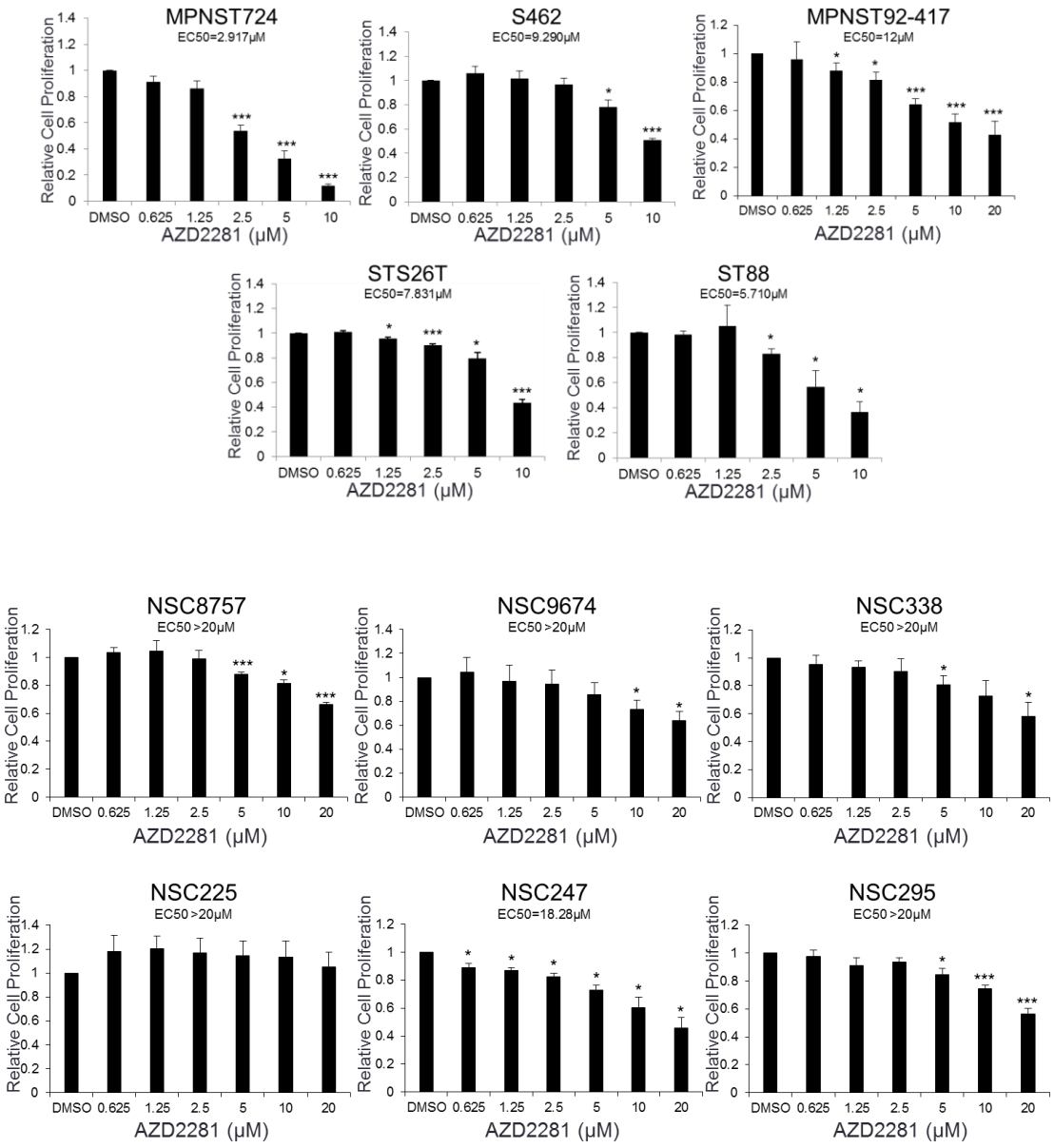

Figure 17. PARP inhibition significantly inhibits MPNST cell proliferation *in vitro* compared to normal Schwann cells. MPNST and NSC cell lines were treated for 96 hours with AZD2281 and cell proliferation was assessed by MTS assay (n=3; ST88 n=4). Error bars represent standard error of the mean; * = $p<0.05$; *** = $p<0.001$.

Reprinted with permission from Taylor and Francis: [Cancer Biology and Therapy] (98), copyright 2015.

Table 5. Cell line sensitivity to AZD2281		
Cell line	Reported PARPi sensitivity	EC50 (μM)
TC71	Sensitive	2.015
MPNST724	n/a	2.917
MDA-MB-436	Sensitive	3.254
MDA-MB-231	Resistant	EC50>10μM
MCF-7	Resistant	EC50>10μM
Lipo 224A	Resistant	EC50>10μM

Table 5. Cell line sensitivity to AZD2281. MPNST cell lines have AZD2281 EC50s more similar to known sensitive cell lines. Cells treated with AZD2281 for 96 hours and assessed by MTS assays to acquire EC50 values.

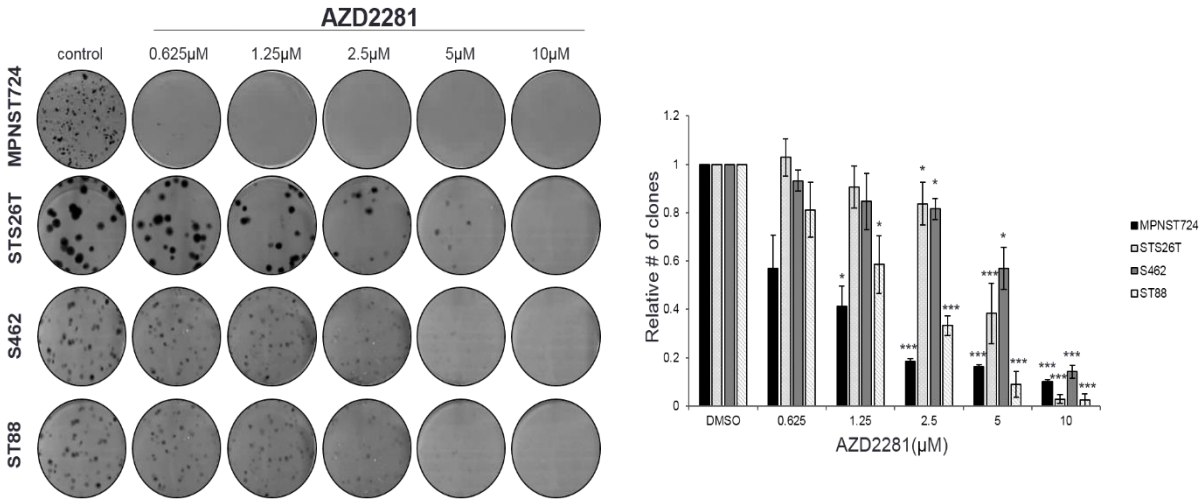

Figure 18. AZD2281 treatment decreases the clonogenic potential of MPNST cells. Representative images of clonogenic assays wells. Graph of replicate experiments with clones of treated cells represented relative to the untreated control (724 n=2; 462 and ST88 n=4; 26T n=5). Error bars represent standard error of the mean; (*=p<0.05; ***=p<0.001).

Reprinted with permission from Taylor and Francis: [Cancer Biology and Therapy] (98), copyright 2015.

Based on the reduced cell proliferation and clone-forming ability observed, we wanted to evaluate cell cycle distribution and apoptosis after AZD2281 treatment. A significant increase in the G2/M phase of the cell cycle was observed following a 24-hour treatment with AZD2281 (Figure 19).

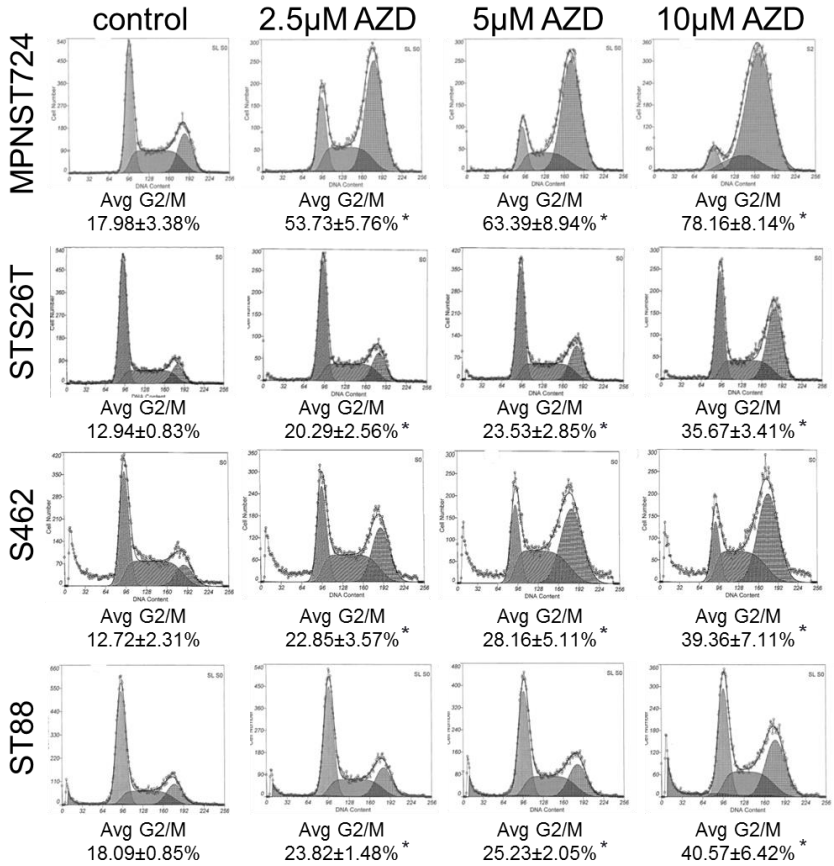

Figure 19. AZD2281 induces a dose-dependent cell cycle arrest. PI FACS analysis after 24 hour treatment with AZD2281 in MPNST cell lines (26T and ST88 n=3; 724 and 462 n=4). Error bars represent standard error of the mean; (*=p<0.05).

Reprinted with permission from Taylor and Francis: [Cancer Biology and Therapy] (98), copyright 2015.

This analysis also revealed that AZD2281 induced apoptosis in MPNST cells after 96 hours of treatment (Figure 20). These *in vitro* responses prompted us to evaluate the functional effects of PARP inhibition on MPNST tumor growth.

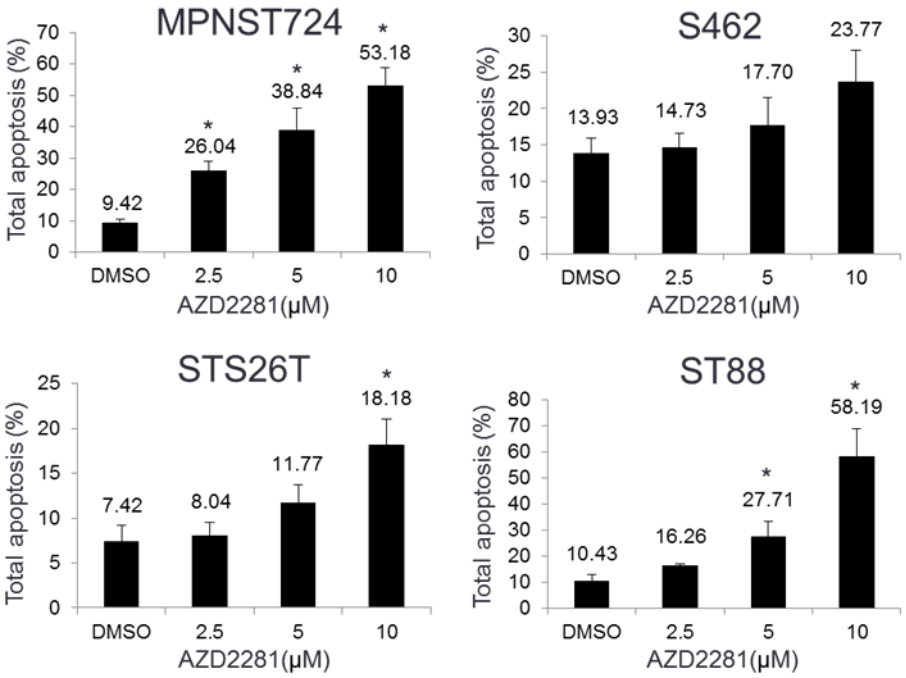

Figure 20. AZD2281 induces apoptosis in a dose-dependent manner. Annexin V-FITC/PI FACS analysis after 96 hour AZD2281 treatment in MPNST cell lines (n=3). Error bars represent standard error of the mean; (*=p<0.05).

Reprinted with permission from Taylor and Francis: [Cancer Biology and Therapy] (98), copyright 2015.

AZD2281 decreases MPNST local tumor growth

To evaluate the effect of AZD2281 on MPNST local tumor growth, we utilized two subcutaneous xenograft mouse models using the MPNST724 and STS26T cell lines. Mice were treated with daily 50mg/kg AZD2281 (n=8) or vehicle (n=9) (IP). AZD2281 treatment significantly reduced tumor volume and weight compared to the vehicle group (Figure 21 and Figure 22). The effects of AZD2281 treatment were validated by IHC analyses. AZD2281 resulted in a decrease in cell proliferation as measured by Ki67 staining. Furthermore, a decrease in the intensity of PAR staining was observed after AZD2281 treatment, supporting the specificity of the inhibitor for PARP enzymatic activity. Increased cyclin B1 staining suggested an accumulation of cells in the G2/M phase. Furthermore, an increase in tumor cell apoptosis (indicated by TUNEL and CC3 positivity) was found after PARP inhibition. These results support our observations *in vitro*: that MPNST724 cells were slightly more sensitive to PARP inhibition than STS26T cells.

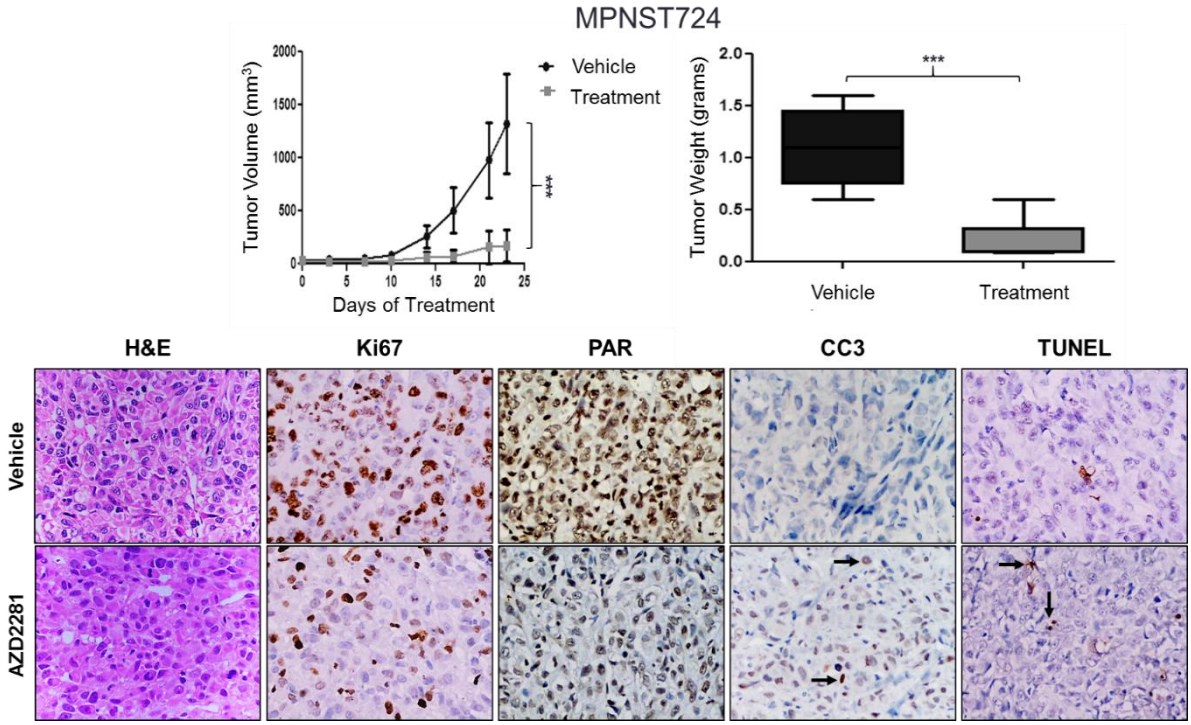

Figure 21. AZD2281 abrogates local tumor growth in a MPNST724 model. Seventeen female hairless SCID mice were injected with $2x10^6$ MPNST724 cells and treated with AZD2281 for 23 days. Treatment groups included vehicle (10% HPCD, 10% DMSO, and PBS) (n=9) and 50mg/kg/day AZD2281 (n=8). Tumor volume and weight were assessed. Tumor samples were stained for Ki67, PAR, cyclin B1, CC3, and TUNEL. Original photos were captured at 400X magnification. Error bars represent standard deviation; *** = $p<0.001$.

Reprinted with permission from Taylor and Francis: [Cancer Biology and Therapy] (98), copyright 2015.

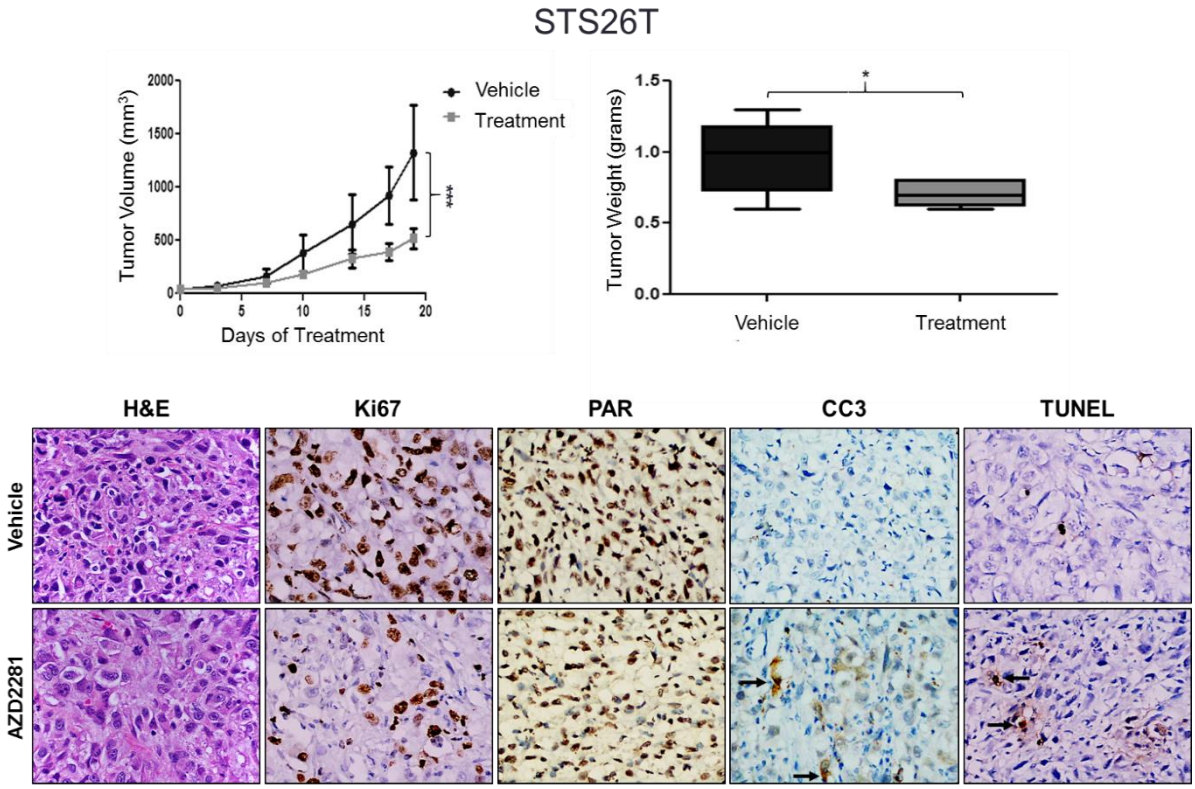

Figure 22. AZD2281 abrogates local tumor growth in a STS26T model. Sixteen female hairless SCID mice were injected with $2x10^6$ STS26T cells and treated with AZD2281 for 19 days. Treatment groups included vehicle (10% HPCD, 10% DMSO, and PBS) (n=9) and 50mg/kg/day AZD2281 (n=8). Tumor volume and weight were assessed. Tumor samples were stained for Ki67, PAR, cyclin B1, CC3, and TUNEL. Original photos were captured at 400X magnification. Error bars represent standard deviation; *** = p<0.001.

Reprinted with permission from Taylor and Francis: [Cancer Biology and Therapy] (98), copyright 2015.

PARP inhibition reduces experimental MPNST lung metastases

MPNSTs have a strong propensity to metastasize, primarily to the lung, within two years of initial disease presentation; therefore, we evaluated whether PARP inhibition would affect metastatic growth. (99,100) Because our established mouse models do not spontaneously metastasize, we utilized an experimental lung metastasis model as previously described. (96) After 21 days of treatment the experiment was concluded; at this time all mice in the vehicle group had macroscopic MPNST lung metastases, whereas 3 out of 7 (43%) had macroscopic metastases in the treatment group. However, microscopic lung metastases were detected in all samples, regardless of treatment. No significant difference in lung weight between treatment groups was observed (Figure 23).

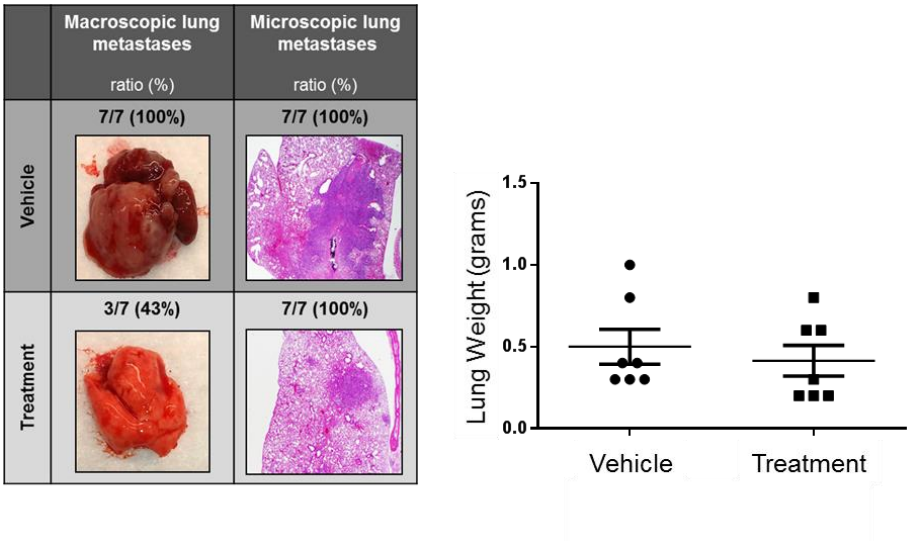

Figure 23. AZD2281 decreases macroscopic metastasis growth but does not affect lung weight. Mice were injected via tail vein with STS26T cells and subsequently treated with vehicle (n=7) or AZD2281 (n=7) for 21 days. Percentage of macroscopic and microscopic lung metastases in vehicle and AZD2281-treated mice. Representative images of gross lung and H&E staining. Graph of lung weights in the vehicle and treatment groups, mean and SEM depicted in the scatter plot (p=0.47).

Reprinted with permission from Taylor and Francis: [Cancer Biology and Therapy] (98), copyright 2015.

AZD2281 long-term treatment increases survival

We then evaluated whether AZD2281 treatment affected survival in a metastatic setting. To answer this question, we utilized the experimental lung metastasis model used in the prior section, but sacrificed the animals individually when euthanasia was mandated due to weight loss >20% of baseline, difficulty of breathing, hunched posture, pallor, impaired ambulation, or lethargy. Overall, treatment continued for 60 days at which point 5 out of 7 (71%) mice in the AZD2281 treatment group were alive versus 0 out of 7 (0%) mice in the control group (Figure 4). These results indicated that treatment with AZD2281 significantly increased the survival of mice with metastatic disease.

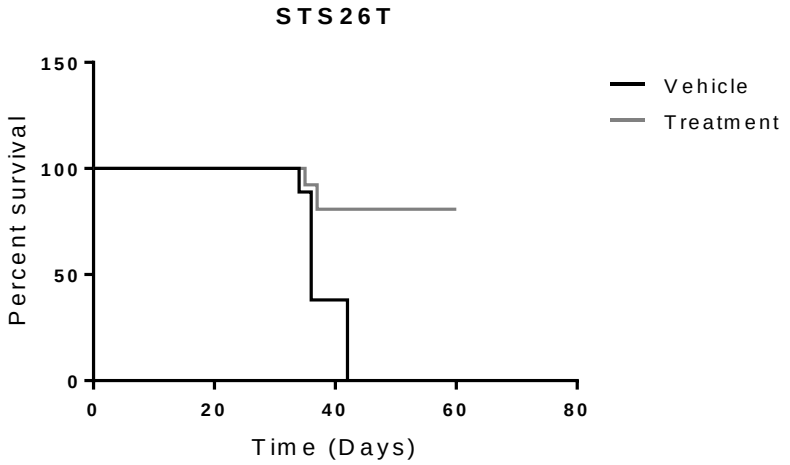

Figure 24. AZD2281 significantly improves survival in an *in vivo* model of metastatic MPNST. Female hairless SCID mice were injected with STS26T cells in the tail vein and treated with AZD2281 for 60 days. Treatment groups included vehicle (10% HPCD, 10% DMSO, and PBS) and 50mg/kg/day AZD2281. (*=p<0.05).

Reprinted with permission from Taylor and Francis: [Cancer Biology and Therapy] (98), copyright 2015.

Chapter 4

Mechanisms of PARP inhibition sensitivity

This chapter is based upon the citation below.

Kivlin, C. M. et al. A Potential Mechanism of Malignant Peripheral Nerve Sheath Tumor Sensitivity to Poly (ADP) Ribose Polymerase Inhibition. In preparation.

Multiple possible mechanisms of cancer cell line sensitivity to AZD2281

A review of the literature from 2005 to 2015 revealed several dysregulated or mutated DNA damage signaling and repair genes that are associated with AZD2281 sensitivity in their respective models (Table 6). This prompted us to evaluate not only the specific DNA repair-related genes dysregulated in MPNST, but also the efficiency of DNA double strand break repair pathways, specifically HR and NHEJ.

Table 6. Mechanisms of sensitivity for AZD2281

Mechanism of Sensitivity	Disease Model	Source
ATM Mutation	Mantle Cell Lymphoma	Williamson CT, et al. MCT. 2010.
ATM Deficiency, p53 Deficiency	Gastric Cancer	Kubota E, et al. Cell Cycle. 2014.
BRCA1 Mutation	Mammary Carcinomas	Rottenberg S, et al. Proc Natl Acad Sci USA. 2008.
BRCA2 Mutation	Invasive Ductal Carcinomas	Evers B, et al. CCR. 2008.
PTEN Mutation	Colorectal Tumors & Endometroid Adenocarcinoma	Mendes-Pereira AM, et al. EMBO Mol Med. 2009.
	Endometroid Carcinoma	Janzen DM, et al. MCT. 2013.
RAD51C Deficiency	Gastric & Breast Cancer	Min A, et al. MCT. 2013.
RAD51D Mutation	Ovarian Cancer	Loveday C, et al. Nat Genet. 2011.
Unknown	Pancreatic Adenocarcinoma	Yang X, et al. Oncol Lett. 2015.

Table 6. Mechanisms of sensitivity for AZD2281. Published mechanisms of sensitivity for AZD2281 from 2005-2015.

MPNST cell lines have DNA repair pathway deficiencies

To interrogate the efficiency of NHEJ and HR in MPNST cell lines, we used the pEGFP-Pem1 plasmid system established by V. Gorbunova. (92,93) The HR plasmid of the pEGFP-Pem1 system is a reporter cassette that consists of two mutated copies of GFP-Pem1. In the first copy the green fluorescent protein (GFP) exon contains a 22 nucleotide deletion, therefore GFP cannot be reconstituted by a NHEJ event, and an insertion of two *I-SceI* recognition sites in inverted orientation. The second copy of GFP-Pem1 lacks the ATG start codon and the second exon of GFP (Figure 25). Upon induction of DSBs by *I-SceI*, a restriction enzyme (RE), the linearized plasmid is transiently transfected into the cells along with the transfection control plasmid pDs-Red2. Intact homologous recombination can then reconstitute an active GFP gene. GFP and RFP expression are reported as a ratio of green (indicating effective HR in the cell) to red (indicating a transfected cell).

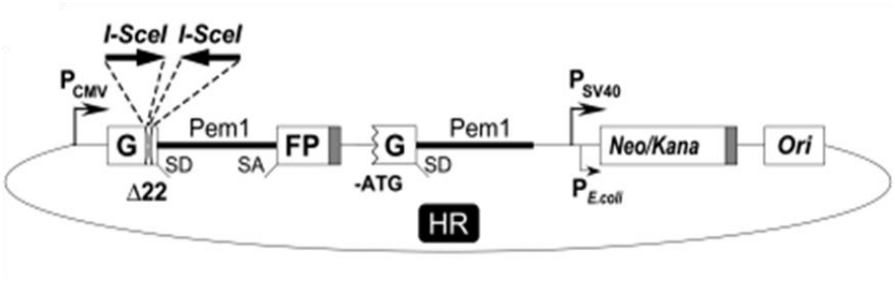

Figure 25. Reporter construct of the HR plasmid of the eGFP-Pem1 system. Reporter plasmid for analysis of HR. The reporter cassette consists of two mutated copies of GFP-Pem1. In the first copy of GFP-Pem1, the first GFP exon contains a deletion of 22 nt and an insertion of two *I-SceI* recognition sites in inverted orientation. The 22 nt deletion ensures that GFP cannot be reconstituted by a NHEJ event. The second copy of GFP-Pem1 lacks the ATG and the second exon of GFP. Upon induction of DSBs by *I-SceI*, gene conversion events reconstitute an active *GFP* gene.

Reprinted with permission from Elsevier: [Neoplasia] (93), Copyright 2009.

The eGFP-Pem1 system also contains a plasmid to measure NHEJ efficiency. GFP is separated by a 2.4 kb Pem1 intron containing an adenoviral exon that is flanked by *HindIII* and *I-SceI* restriction sites. The adenoviral exon inactivates the GFP activity, making the starting substrate GFP negative. Both sides of the adenoviral exon have *HindIII*/*I-SceI* restriction sites. Cleavage with either RE removes the Ad exon and if the cells have intact NHEJ, full length GFP will be expressed. Digestion with *HindIII* generates compatible ends which NHEJ can simply re-ligate; cleavage with *I-SceI* generates incompatible ends which need to be processed by NHEJ nucleases and polymerases before ligation (Figure 26).

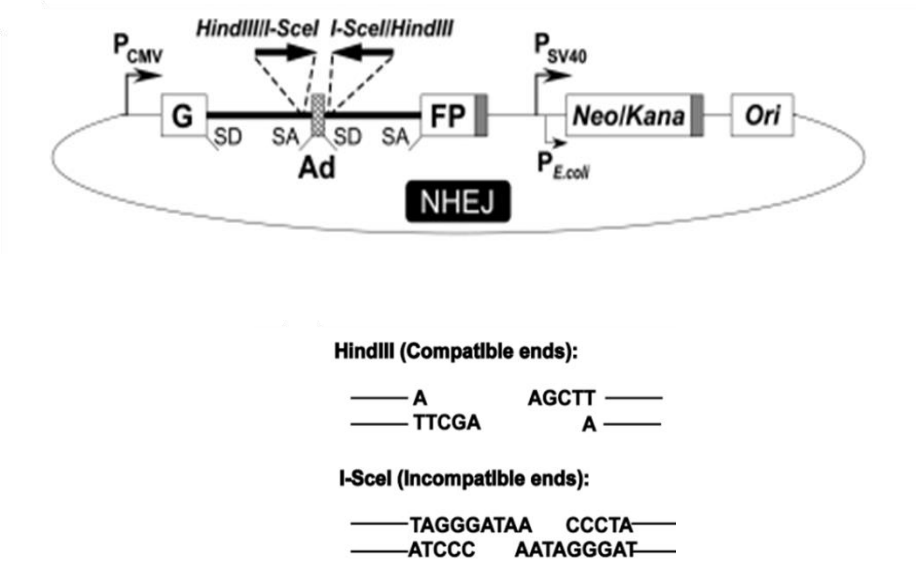

Figure 26. Reporter construct of the NHEJ plasmid of the eGFP-Pem1 system. Reporter plasmid for analysis of NHEJ. The reporter cassette consists of a *GFP* gene under a Human cytomegalovirus (CMV) promoter with an engineered intron from the rat *Pem1* gene, interrupted by an adenoviral exon (Ad). The adenoviral exon is flanked by *I-SceI* recognition sites in inverted orientation for induction of DSBs. In this construct, the GFP gene is inactive; however, upon induction of a DSB and successful NHEJ, the construct becomes GFP+. *SA* indicates splice acceptor; *SA*, splice donor; *shaded squares*, polyadenylation sites. *HindIII* generates compatible ends. *I-SceI* generates incompatible ends.

Reprinted with permission from Elsevier: [Neoplasia] (93), Copyright 2009 and reprinted from Fattah, F. et al. Ku regulates the non-homologous end joining pathway choice of DNA double-strand break repair in human somatic cells. PLoS genetics ***6****, e1000855, doi:10.1371/journal.pgen.1000855 (2010).*

We used T47D breast adenocarcinoma cells as a positive control for the NHEJ and HR plasmids. MDA-MB-231 and MDA-MB-436 breast adenocarcinoma cell lines were used as a positive and negative control for the HR plasmid, respectively. There was no striking difference in the NHEJ efficiency of all MPNST cell lines compared to the T47D control; with S462 having the greatest NHEJ efficiency. However, MPNST cell lines had HR levels similar to the MDA-MB-436 cell line, known to be HR deficient due to a *BRCA1* mutation (101), and substantially lower levels than the HR-intact MDA-MB-231 and T47D cell lines (Figure 27). This indicates that MPNST cells lines have deficient HR which could contribute to their PARP inhibitor sensitivity. Furthermore, the activity of NHEJ in MPNST could also contribute to PARP inhibitor sensitivity by increasing the amount of inherent chromosomal instability in these cells.

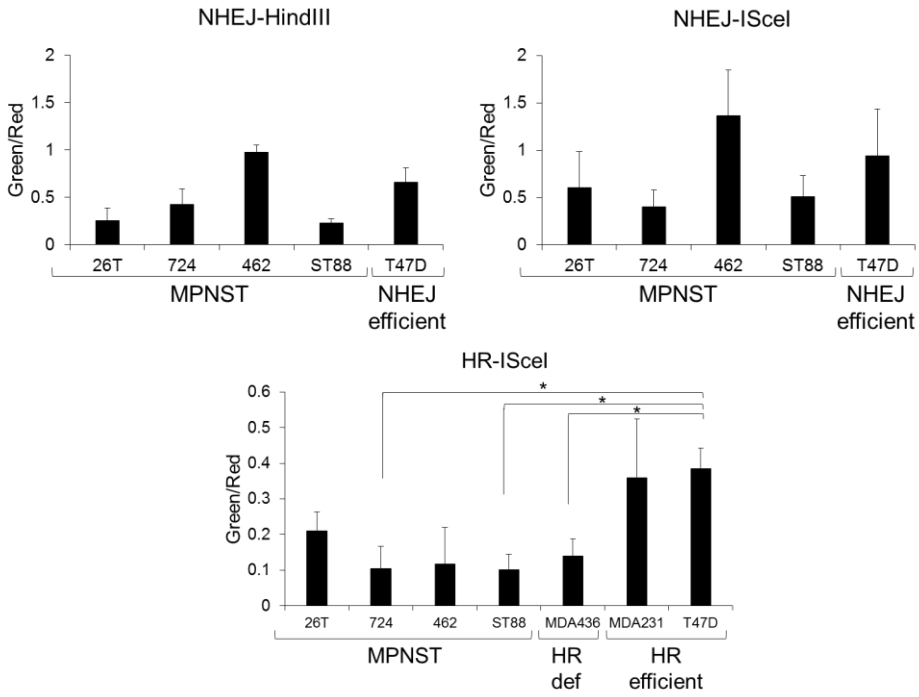

Figure 27. MPNST cell lines have deficient HR repair. Cells were transfected with the NHEJ or HR eGFP-Pem1 plasmid and incubated for 72 hours. Green fluorescence indicates intact NHEJ or HR, and red fluorescence represents transfection efficiency. Fluorescence was assessed by flow cytometry. Error bars represent SEM (n=2). (*=p<0.05).

PARP inhibition enhances NHEJ activity which results in increased chromosomal instability.

Patel et al. showed that in homologous recombination deficient ovarian cancer cell lines, PARP1 acted as a negative regulator of NHEJ activity. (86) Although NHEJ is an efficient method of double strand DNA repair, because it does not utilize a template strand for repair, it is an inherently error- prone mechanism. They suggest that in HR deficient cell lines that have been treated with a PARP inhibitor, despite the accumulation of unresolved DNA DSBs that develop, which are highly toxic to the cell, the main cause of cell death is the enhanced genomic instability due to increased activity of NHEJ. They further show this by blocking NHEJ with a DNA-PKcs inhibitor, which reversed the NHEJ activity and genomic instability and lethality of PARPi even in HR deficient cells. Therefore, treatment with a PARP inhibitor causes increased activity of NHEJ and consequently increased chromosomal instability due to the errors induced by NHEJ. This instability can stall the replication fork and eventually lead to collapse of the replication fork and cell death. To determine if PARP inhibition increases NHEJ activity in MPNST, we treated cells with AZD2281 for 72 hours and performed an immunoblot for DNA-PKcs Ser2056. In contrast to Patel et al. which showed no endogenous activation of DNA-PKcs, MPNST cell lines had a strong baseline expression of DNA-PKcs Ser2056. We observed stable expression of phosphorylated DNA-PKcs with increasing doses of AZD2281 treatment, indicating no change in DNA-PKcs activity (Figure 28). Furthermore, 72 hour treatment with increasing doses of the DNA-PKcs inhibitor, NU7026, decreased phosphorylated DNA-PKcs (Ser2056) in a dose dependent manner, showing the efficacy of this inhibitor.

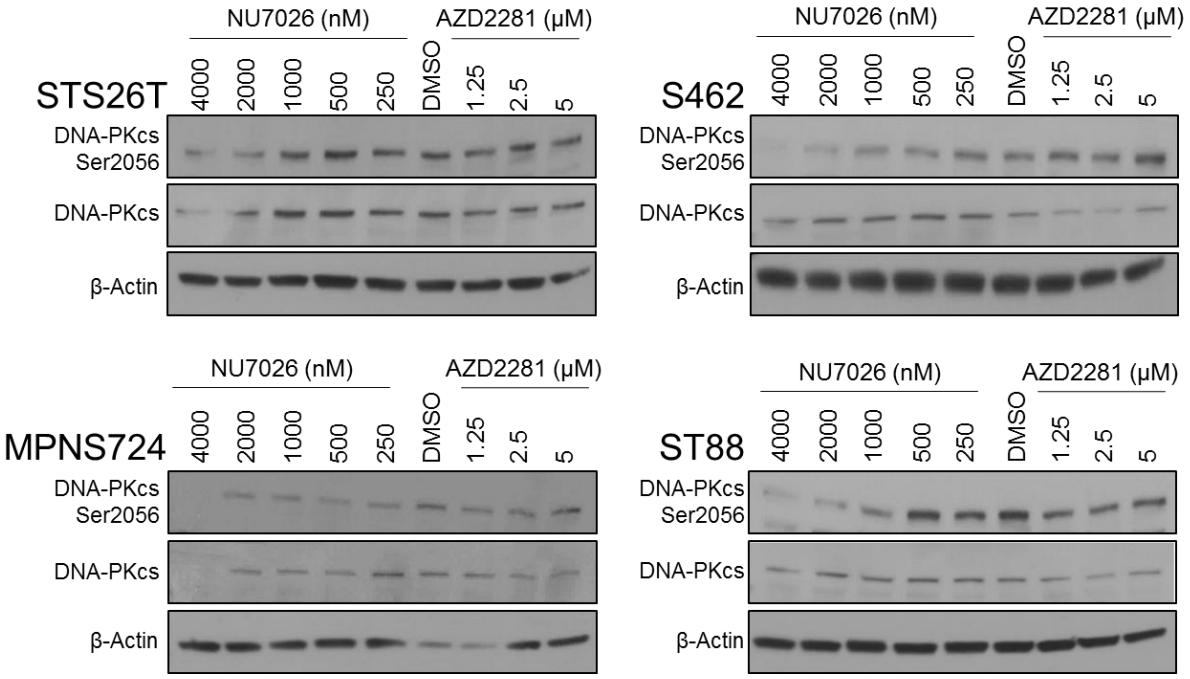

Figure 28. NU7026 decreases DNA-PKcs activity. Cells were treated with DMSO, 1.25-5μM AZD2281 and 250-4000nM NU7026 for 72 hours then immunoblotted for DNA-PKcs (Ser2056) and total DNA-PKcs.

We then wanted to determine if treatment with a NU7026 could decrease the NHEJ activity enhanced by PARP inhibition. Therefore, we treated MPNST cell lines with 2.5 μM AZD2281, 500 or 1000nM NU7026, or a combination with two different doses of NU7026 (500- low combination or 1000nM- high combination) for 72 hours and performed an immunoblot for DNA-PKcs Ser2056. We observed stable phosphorylated DNK-PKcs expression with AZD2281 treatment alone, with a slight decrease in expression when the two inhibitors were combined, especially at the higher combined dose. (Figure 29). This substantiates a slight role for AZD2281 in the increase of NHEJ activity.

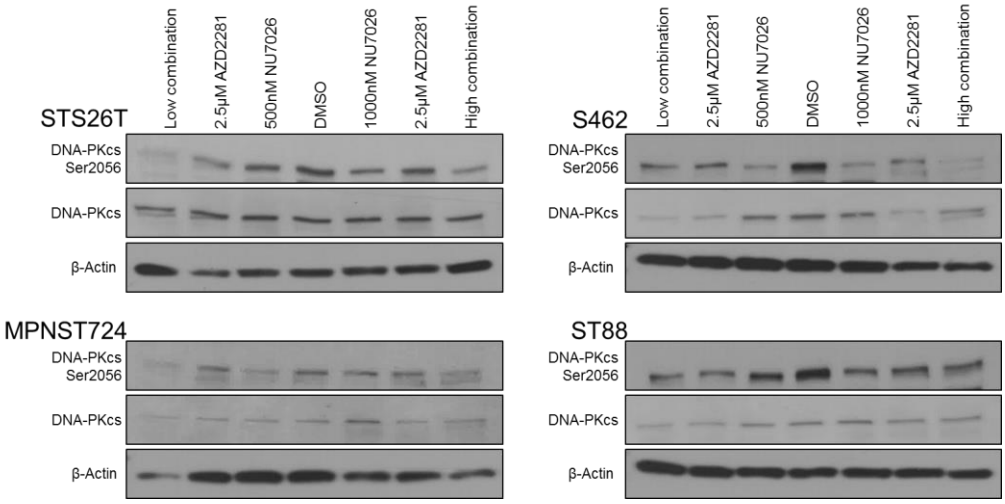

Figure 29. Combination treatment decreases DNA-PKcs activity. Cells were treated with DMSO, 2.5μM AZD2281, 500nM NU7026, or combination for 72 hours then immunoblotted for DNA-PKcs (Ser2056) and total DNA-PKcs.

To further determine the effect of PARP inhibition on MPNST chromosomal instability, we treated MPNST cell lines with AZD2281 and NU7026, alone and in combination, and performed a chromosomal analysis via metaphase spread. These cells were scored for chromosomal breaks, fragments, fusions, and radial structures, all markers of genomic instability. In the untreated control we determined the base line level of genomic instability in each MPNST cell lines. Treatment with AZD2281 alone caused a substantial increase the observed chromosomal breaks, indicating increased genomic instability. Treatment with NU7026 only marginally increased the level of genomic instability from base line. However, dual treatment showed a varied cell line-specific effect in the number of chromosomal breaks compared to the AZD2281 treatment group, with S462 showing the greatest decrease in NHEJ after combination treatment (Figure 30). This could indicate that the damage induced by PARP inhibition in MPNST cell lines that leads to cell death is partly due to NHEJ activity which causes chromosomal instability and that altered dosing could further enhance the effect

of combination treatment.

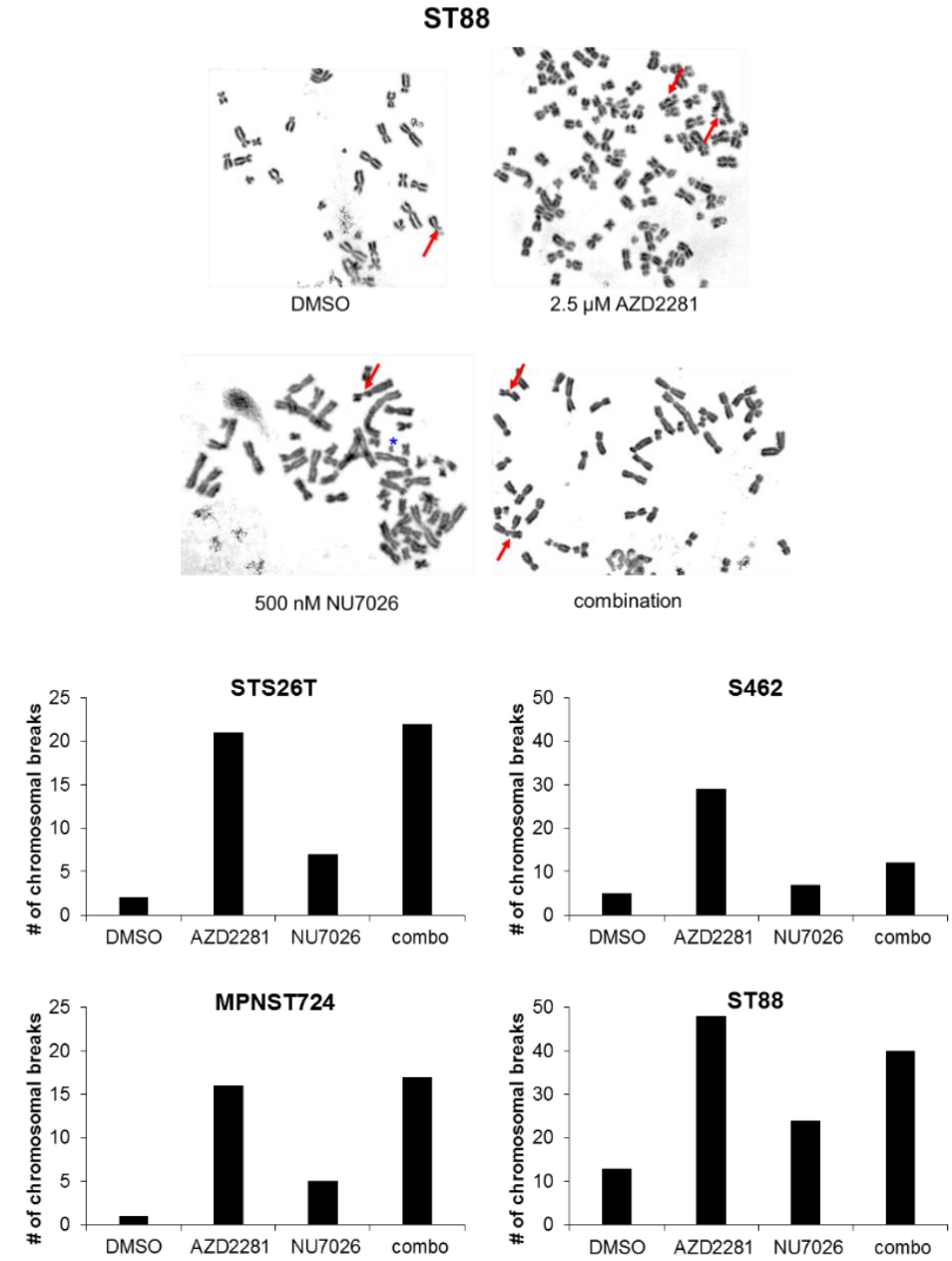

Figure 30. PARP inhibition increases chromosome breaks which is mitigated by combination treatment. Cells were treated with DMSO, 2.5μM AZD2281, 500nM NU7026, or combination for 72 hours then analyzed for chromosomal aberrations, including chromosomal breaks (red arrow), fusions (green x), fragments (blue asterisk), and radial

structures, via metaphase spread. Representative images and graphs of total chromosomal breaks are shown.

Several DNA repair-related genes are dysregulated in MPNST cell lines relative to NSCs

Due to the overwhelming evidence in the literature that cells are sensitive to PARP inhibition when there is a deficiency in a DNA repair gene, we assessed the expression level of DNA repair-related genes in MPNST cell lines compared to NSCs using RNA sequencing (RNAseq). (102) As a deficiency in HR or other DNA repair gene defects combined with a PARP inhibitor is strongly associated with synthetic lethality, we chose to focus on downregulated DNA repair-related genes. The top five downregulated genes, based on $\log_2$ fold change in at least two out of the four MPNST cell lines assessed, are shown in Table 7. Relative to NSCs, *ERCC6*, essential for the transcription coupled repair sub-pathway of NER, is the most downregulated DNA repair-related gene. Likewise, the fifth most downregulated gene, *ERCC5*, is an endonuclease essential for the common pathway of NER. The other top downregulated genes are involved in HR during meiosis (MutS Homolog 4 (*MSH4)* and DNA Meiotic Recombinase 1 (*DMC1)*), as well as regulation of the circadian clock (Period Circadian Clock 1 (*PER1)*). These results indicate multiple dysregulated DNA repair pathways in MPNST cell lines that could contribute to the observed PARP inhibitor sensitivity.

Table 7. Relative decreased expression of DNA repair-related genes in MPNST cell lines

	STS26T		MPNST724		S462		ST88	
	Fold change	Adjusted *p* value	Fold change	Adjusted *p* value	Fold change	Adjusted *p* value	Fold change	Adjusted *p* value
ERCC6	NC*	NC	-2.653	7.48E-09	-2.4870	7.29E-08	-2.583	2.87E-08
MSH4	-1.830	0.089	-1.879	0.092	NC	NC	-1.653	0.114
PER1	-2.722	3.25E-08	NC	NC	-1.344	0.013	-3.377	4.32E-12
DMC1	-2.566	3.16E-07	NC	NC	NC	NC	-1.849	2.63E-04
ERCC5	NC	NC	-1.463	0.018	NC	NC	-1.345	0.031

** NC = No change*

Table 7. Downregulated DNA repair-related genes in MPNST cell lines. RNA sequencing

results for DNA repair-related genes in MPNST cell lines versus an NSC control. No change (NC) indicates no significant differential expression.

ERCC6 has decreased transcript and protein expression in MPNST cell lines

To validate the RNAseq results that indicate a substantial decrease in *ERCC6* expression, we performed qRT-PCR for our MPNST cell panel. There is decreased transcript expression of *ERCC6* detected in MPNST cell lines versus a NSC control (Figure 31).

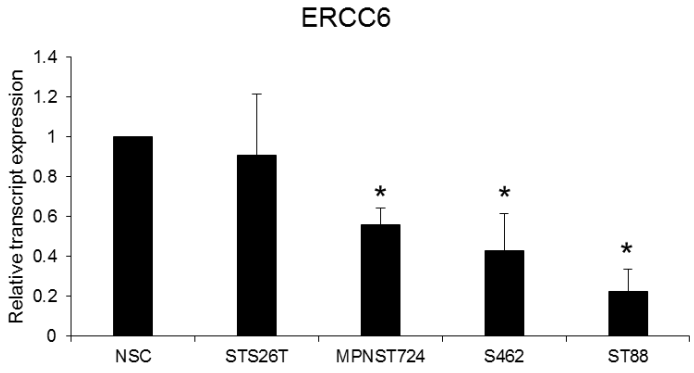

Figure 31. *ERCC6* transcript levels are lower in MPNST cell lines. A panel of MPNST cell lines were assessed by qRT-PCR for *ERCC6* expression versus a NSC control. Error bars represent SEM (n=3). (*=p<0.05).

To further confirm our results, we performed immunoblot analysis for CSB, the protein encoded by *ERCC6*, using an NSC and MPNST cell panel. Full-length CSB is approximately 168 kDa, while the CSB-PGBD3 fusion protein (first five exons of CSB and the piggyBac transposable element derived 3) is 140kDa. This fusion protein has not been shown to have a direct role in DNA repair; however, there could be an indirect effect through incorporation of the fusion protein instead of the full-length CSB which could limit effective repair of the DNA. (103) Fold change (FC) is determine by densitometry and is relative to each sample's β-actin and adjusted to the NSC9674 sample present on both immunoblots. This revealed an average relative CSB expression of 2.5 in the NSC group versus 0.4 in the MPNST group, showing that NSCs have an overall greater expression of CSB as well as overall higher AZD2281 EC50 values (Figure 32). Interrogation by Spearman's rank correlation revealed a positive correlation between FC and AZD2281 EC50 ($r = 0.645$; $p = 0.0368$), indicating a potential link between CSB expression and sensitivity of MPNST cell lines to AZD2281.

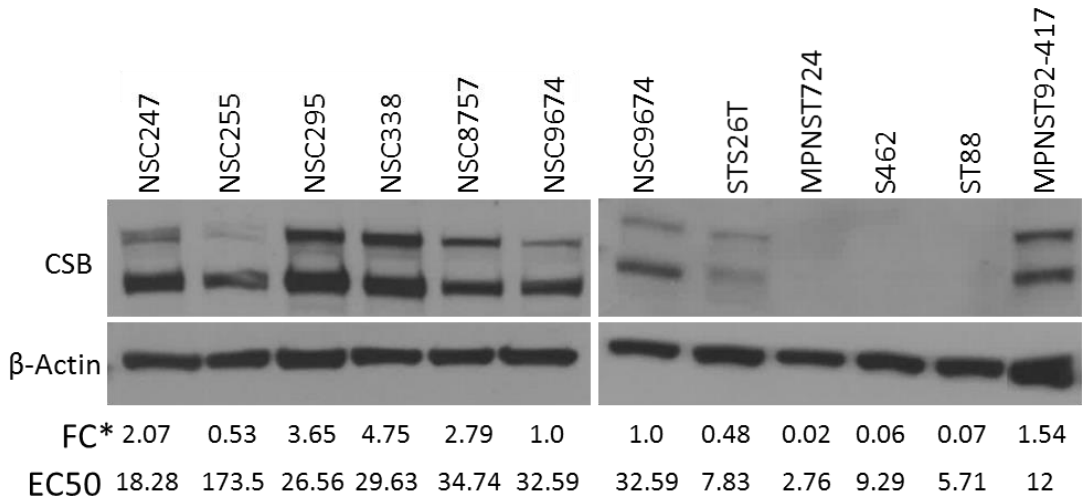

Figure 32. ERCC6 has decreased protein expression in MPNST cell lines. Immunoblot of CSB in a panel of NSC and MPNST cell lines. Fold change (FC) was determine by densitometry and is relative to each sample's actin and adjusted to the NSC9674 sample; (*=$p<0.05$). Spearman's correlation was used to determine if CSB fold change correlated to AZD2281 EC50; ($r = 0.645$; *=$p<0.05$).

Alteration of CSB expression influences cancer cell line sensitivity to AZD2281

Based on the correlation of CSB expression to AZD2281 EC50, we stably overexpressed CSB in MPNST cell lines in order to determine if there is an effect on sensitivity to PARP inhibition. MPNST cell lines were transduced with a CSB lentiviral vector in two separate transduction pools. Immunoblot confirmation of full length CSB overexpression was performed in each cell line. After a 7 day treatment with AZD2281, cell proliferation was measured by MTS assay (Figure 33). In S462 and ST88 cells, overexpression of CSB caused an increase in the AZD2281 EC50 values Overall this shows a more prominent role for CSB in the sensitivity of these MPNST cells to PARP inhibition. However, in STS26T and MPNST724 cells, the overexpression of CSB has a minimal effect on the cell sensitivity to PARP inhibition. This suggests that although CSB expression affects MPNST sensitivity to AZD2281, there may be other players involved in the tumor cell response to treatment.

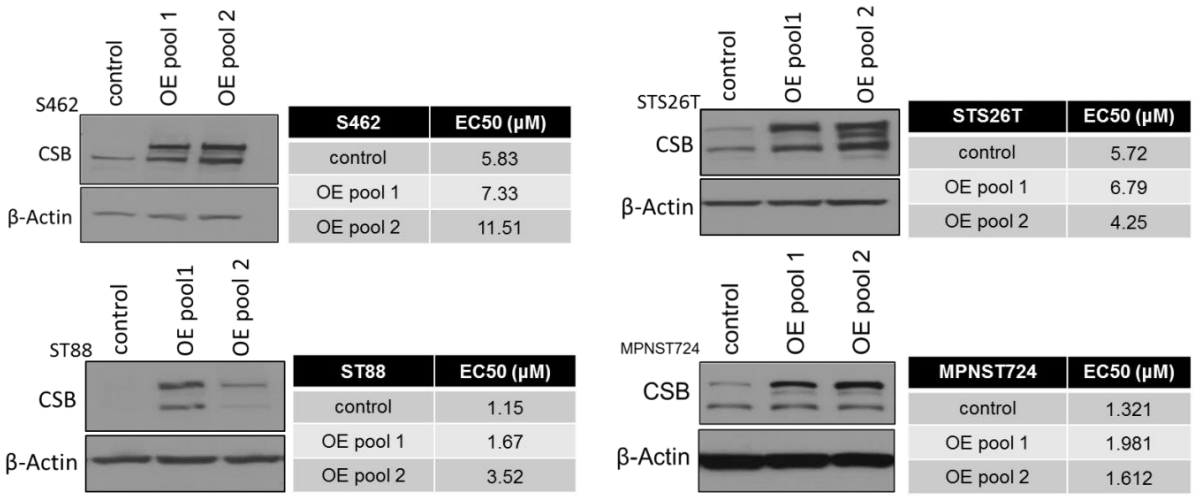

Figure 33. CSB overexpression causes a subset of MPNST cell lines to be less sensitive to PARP inhibition. Immunoblots of CSB show increased expression of CSB after transduction of the lentiviral vector; n=3.

As a proof of principle that CSB expression affects PARP inhibitor (PARPi) sensitivity, we stably knocked down CSB via shRNA in the MDA-MB-231 cell line, known to be relatively resistant to PARP inhibition (Figure 34). (104) Knockdown of CSB caused a 3-6 fold decrease in the EC50 of AZD2281, further substantiating a role for CSB in PARPi sensitivity.

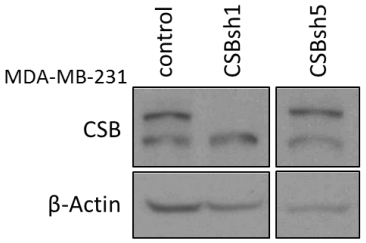

MDA-MB-231	EC50 (μM)
control	10.44
CSBsh1	1.63
CSBsh5	3.35

Figure 34. CSB knockdown causes MDA-MB-231 cells to be more sensitive to AZD2281. Immunoblots of CSB show decreased expression of CSB after transduction of the CSB shRNA; n=3.

CSB does not affect the efficiency of CPD repair

To examine the functional effect of CSB expression, we used an ELISA (Cell Biolabs) recognizing cyclobutane pyrimidine dimers (CPDs), one of the main types of DNA damage induced by UV and repaired by the NER pathway. After treatment with 256J/m2/min of ultraviolet B (UVB), we harvested the cells from 0-24 hours, a time frame in which the majority of CPDs should be repaired, and assessed the level of CPDs (Figure 35). (105) While we expected overexpression of CSB to increase the efficiency of CPD repair compared to the non-targeting cells, we did not see a significant difference in the level of CPDs in the S462 or MPNST724 cell lines. Along the same lines, we also anticipated that the knockdown of CSB in the MDA-MB-231 cell line would decrease CPD repair efficiency compared to the non-targeting cells, but in general, observed no drastic change.

To ensure that any decreased CPD levels seen in our ELISA was due to repair of the damage and not conversion to a double strand DNA break, we also evaluated the expression of gamma-H2AX in the UV treated cells from 0-24 hours. However, the expression pattern of gamma-H2AX was similar in each cell line regardless of CSB expression.

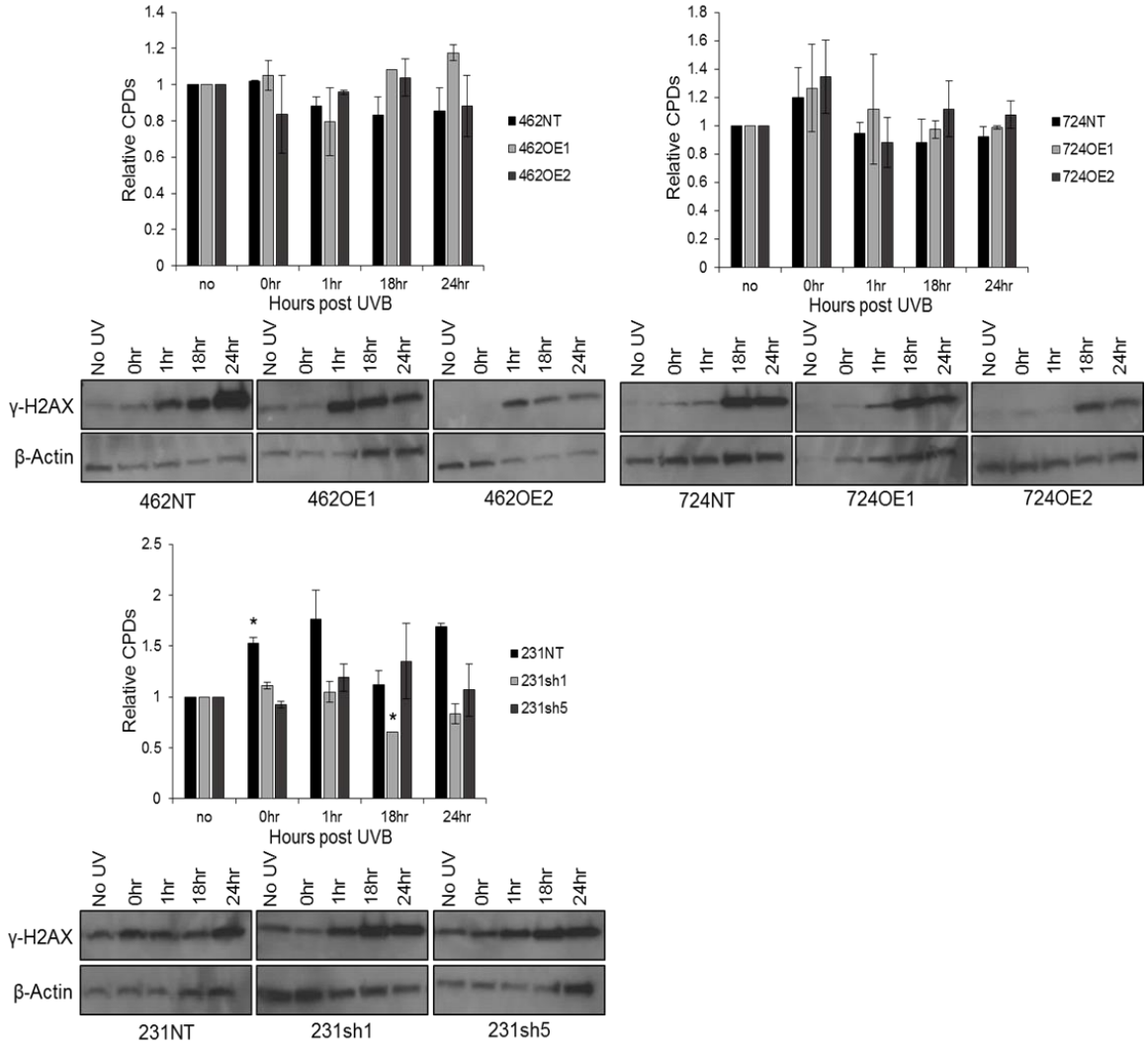

Figure 35. Alteration of CSB expression does not affect the efficiency of CPD repair. Cells were treated with 256J/m2/min UVB then harvested from 0-24 hours and used for CPD ELISA and gamma-H2AX immunoblot. Error bars represent standard error of the mean (n=2); (*=p<0.05).

Chapter 5

Discussion, Conclusions, and Future Directions

MPNST is an aggressive subtype of STS for which surgical resection has been the standard of care for decades and continues to be the most effective treatment. Standard chemotherapy and radiotherapy have shown modest therapeutic benefit, restricted mostly to local control and disease stabilization. MPNSTs have a complex karyotype indicating a high baseline level of genomic instability and a potential DNA repair defect. Despite identification of chromosomal aberrations and specific recurring genetic alterations which could be targeted for therapeutic gain, several clinical trials have been conducted in MPNST and other sarcoma subtype patients with minimal observed responses. (7,19-22,106-108) The aggressive nature of the disease is depicted in the dismal five-year survival rate of only 35-60%. Therefore, a novel targeted therapy is necessary to improve MPNST patient outcome.

PARP inhibitors have been shown to be efficacious in two settings: by exploiting a genetic defect in the cells through synthetic lethality, especially a *BRCA1/2* mutation or 'BRCAness', and as a chemosensitizer to a conventional chemotherapy or radiotherapy. (46) AZD2281, a well-established PARP inhibitor, has been used in multiple preclinical studies including those in breast and lung cancer, and glioma models. (49,109,110) Furthermore, this inhibitor is now in Phase III clinical trials.

To determine the utility of PARP inhibition in MPNST, we first evaluated the expression of PARP1 and PARP2 in neurofibroma and MPNST human tumor samples using a clinically annotated TMA. Overall, we found that all MPNST samples had a high level of PARP1 and PARP2 expression. PARP1 expression has been shown to be elevated in multiple malignancies including breast, ovarian, uterine, and lung; however, PARP2 has less variable expression patterns between normal and tumor tissue. (111,112) The increased level of PARP expression, as well as its ubiquitous expression pattern, supports the potential use of

PARPis in MPNST; however, the applicability of PARP staining to determine MPNST progression is limited. PARP2 was homogenously expressed in our MPNST TMA and therefore was not further evaluated. However, moderate to high PARP1 expression was shown to correlate with a worse patient prognosis, although no statistical significance was reached. This is similar to reports concerning breast cancer patients in which PARP1 overexpression correlated with reduced disease-specific survival. (113,114) This suggests that MPNST patients with a high level of PARP1 expression would not only be a candidate for PARP inhibition treatment, but also warrant a more aggressive treatment plan or closer monitoring due to the more aggressive disease phenotype observed with increased PARP1 staining. While these findings are intriguing, further evaluation is necessary to determine any clinical use of PARP staining in MPNST. Future studies should also consider larger MPNST populations to provide more statistical power, and include clinicopathologic factors (such as age, tumor location, tumor size, etc.) to correlate to PARP expression to find more/any associations.

In this study, we evaluated the efficacy of the PARP inhibitor, AZD2281, in MPNST. We show that AZD2281 has a strong anti-MPNST effect as a single agent *in vitro*. Specifically, AZD2281 treatment decreased cell proliferation, at similar or lower concentrations than those used in models with established sensitizing genetic aberrations, and at comparable or shorter time points. (53,115,116) Furthermore, we observed that AZD2281 caused a substantial dose-dependent cell cycle arrest at 24 hours and significantly enhanced apoptosis at 96 hours. This effect on the cell cycle and viability has been similarly observed after PARP inhibitor treatment in *BRCA2* deficient esophageal squamous carcinoma cells and *BRCA1/2* deficient breast cancer cell lines, among others. (41,117) All MPNST cell lines tested have EC50 values in the micromolar range, and no sensitivity predilection between sporadic and NF1-associated cell lines was observed.

To further determine whether PARP inhibition would be a useful therapeutic option, we

established the level of PARP1, PARP2, and PAR expression in a panel of MPNST cell lines using Western blotting. Increased PARP1, PARP2, and PAR expression was observed in MPNST cell lines compared to NSCs indicating PARP is a viable therapeutic target in MPNST. Of the MPNST cell line panel, MPNST724 cells had the lowest PAR expression. We further determined PARP activity using the modified PARP activity assay and observed uniform increased endogenous PARP activity in our MPNST cell lines compared to NSCs. Perhaps the discrepancy in the level of MPNST724 PARP activity between the immunoblot and the PARP activity assay is due to the cell-free nature of the PARP activity assay indicating true endogenous activation of PARP in MPNST724 cells is not as substantial. Furthermore, inhibition of PARP via AZD2281 pretreatment, decreased PARP activity in a dose-dependent manner in all MPNST cell lines, with MPNST724 cells showing the lowest response, further indicating its lower overall PARP activity level compared to the other MPNST cell lines. Interestingly, it has been suggested that increased PARP expression correlates with increased sensitivity to PARP inhibition. (118) In the setting of MPNST, MPNST724 cells displayed the greatest sensitivity to AZD2281 with an EC50 of 2.76μM. However, these cells also have the lowest level of PAR expression and response of PARP activity to AZD2281 treatment. This indicates that while increased PARP activity may not always correlate with increased sensitivity to PARP inhibition.

Based on these promising *in vitro* results, we evaluated AZD2281 in several *in vivo* models of MPNST. To assess the effect of PARP inhibition on local tumor growth, we treated MPNST724 and STS26T subcutaneous xenograft mouse models starting at an average volume of 50mm^3. While other studies with xenograft mouse models begin treatment when tumors reach approximately 200mm^3, due to the rapid growth rate of untreated MPNST xenografts, we began treatment at a smaller volume in order to treat the mice for a meaningful amount of time before a tumor volume mandating euthanasia was reached. (49,96) Furthermore, MPNST patients, particularly those with NF1, can present with tumors greater

than 5cm at the time of diagnosis, therefore experimental treatment of a more established mass can better recapitulate this clinical presentation. (7) Three-week treatment of mice with AZD2281 resulted in a significant decrease in tumor growth compared to the untreated group and, interestingly, MPNST724 cells were more responsive to treatment than the STS26T. Although no disease regression was observed, PARP inhibition seemed to slow the progression of tumor growth. A previous report in a BRCA wild-type ovarian cancer xenograft also showed decreased progression of disease with AZD2281 treatment rather than disease regression. (119) The IHC analysis of subcutaneous tumors from both cell lines revealed a decrease in cell proliferation, as determined by lower Ki67 expression; specific targeting of PARP enzymatic activity as evidenced by decreased PAR staining; a possible G2/M phase cell cycle arrest indicated by increased cyclin B1 staining; and increased CC3 and TUNEL indicating induced apoptosis with AZD2281 treatment. These results show the potential benefits of PARP inhibition treatment for local MPNST disease. An orthotopic model of MPNST has been described in which tumor cells are injected into the sciatic nerve that more faithfully recapitulates the human disease and local tumor growth; however, this model has not been reproducibly established at our institution. (120) Future endeavors should explore this and other orthotopic models available to expand the potential utility of AZD2281 *in vivo*.

Despite the high metastatic potential of MPNST which contributes to the aggressive nature of the disease, mouse models of MPNST do not incur spontaneous metastases. Therefore, to pursue the effect of PARP inhibition on metastasis *in vivo,* we used an experimental metastasis tail vein injection model using STS26T cells. We observed a decrease in the development of macroscopic lung metastases after PARP inhibition. All mice, regardless of treatment, had microscopic lung metastases suggesting that AZD2281 treatment slowed the growth of lung metastases but did not cause disease regression. Based on the observed effect of PARP inhibition on local MPNST growth in our mouse models, this was expected. In our experimental lung metastasis model, treatment begins three weeks after

the tail vein injection in order for micrometastases to be present. In this way, we are measuring the ability of MPNST cells to establish and proliferate in the lung versus a true metastatic cascade. Still, up to 50% of MPNST patients, especially those with NF1, can present with metastatic disease at the time of initial diagnosis, therefore this mouse model may be relevant to this clinical setting. (7)

The experimental metastasis model was also used to evaluate survival to determine how AZD2281 might benefit MPNST patients with disseminated disease. We treated the animals with AZD2281 following the tail vein injection and sacrificed individual mice only when signs of disease were present. Approximately 70% (5/7) of animals that received AZD2281 treatment survived with lung metastases, compared to 0% (0/7) in the control group. These results highlight the use of PARP inhibition as a potential MPNST therapeutic strategy to manage metastatic lung growths, which could expand the potential application of PARP inhibitor treatment. There are several current clinical trials evaluating the effect of PARP inhibitor treatment in metastatic disease, including advanced solid tumors and triple negative breast cancer; metastatic MPNST patients could therefore be incorporated in this type of trial. Furthermore, approximately 20-54% of patients with malignancies, most notably osteosarcoma, melanoma, and Ewing's sarcoma, will develop lung metastases. (121) Therefore, PARP inhibitor treatment could be evaluated in these tumors, especially those with a characterized DNA repair defect, for potential benefit, not only for the primary lesion, but progressive disease to the lung.

Based on the exciting inhibitory activity of single agent AZD2281 in MPNST, we wanted to determine what genetic mutations or dysregulations led to sensitivity to this drug. Several mechanisms of sensitivity to AZD2281 have been reported in a variety of disease models; specifically, mutations in *ATM, BRCA1* and *BRCA2, PTEN, RAD51C, and RAD51D*. (49,116,122-127) All of these genes are involved in the cellular response to DNA damage or the repair of double strand DNA breaks. Furthermore, in keratinocytes, PTEN downregulation

has been shown to impair GGR, a subpathway of nucleotide excision repair, by suppressing the expression of XPC, highlighting the possible links between DNA repair pathways. (128) In addition, X. Yang et al. recently showed the sensitivity of a HR-intact pancreatic adenocarcinoma cell line, JF-305, to AZD2281, indicating potential mechanisms of cellular sensitivity to PARP inhibition beyond HR defects that are yet to be elucidated. (129) To determine a potential mechanism of sensitivity of MPNST to AZD2281, we began by evaluating the level of HR and NHEJ repair in our cell lines.

HR and NHEJ efficiency was determined using the eGPF-Pem1 plasmid system which requires the transient transfection of a transfection control plasmid, pDs-Red2, and either a linearized HR plasmid or linearized NHEJ plasmid. Our results indicate HR repair levels of MPNST cell lines are similar MDA-MB-436 cells which have a known HR deficiency. In addition, the NHEJ activity of the MPNST cell lines were similar to the control T47D cells with proficient NHEJ repair. Therefore, although no specific mutations or dysregulations in HR genes have been reported in MPNST, there is decreased HR activity that could contribute to the observed MPNST sensitivity to AZD2281. In addition, the increased activity of NHEJ could further enhance MPNST sensitivity to PARP inhibition by augmenting chromosomal instability.

It has been shown that treatment of HR-deficient cells with a PARP inhibitor, can increase the activity of NHEJ, and due to its error-prone nature, increase the level of genomic instability of the cells. (86) To determine if NHEJ has increased activity in MPNST cell lines after PARP inhibition, we first treated our cells with AZD2281. We observed stable activation of DNA-PKcs, a critical member of NHEJ repair, via immunoblot expression of DNA-PKcs Ser2056, and also increased chromosomal aberrations via metaphase spread analysis. Ser2056 of DNA-PKcs is an autophosphorylation site that is required for the full activation of DNA-PKcs and acts to limit end resection in the cell and therefore promote NHEJ over HR. (130-132) To determine if the increased chromosomal damage after AZD2281 treatment was

due to increased NHEJ activity, we treated our cells with two combinations of AZD2281 and NU7026. Dual treatment decreased the amount of phosphorylated DNA-PKcs expression, especially with the highest dose combination, but altered the amount of observed chromosomal breaks in a cell line-specific manner. The S462 cell line had the highest level of NHEJ as shown by the eGFP-Pem1 plasmid system, therefore perhaps the large observed reduction in chromosomal damage after dual treatment could be due to its enhanced endogenous NHEJ. For this cell line the sensitivity to PARP inhibition could, in part, be due to the increase in NHEJ activity and subsequent genomic instability that results from its error-prone activity. In addition, the increased/ steady level of chromosomal breaks observed in the remaining cell lines after dual treatment could be due to increased chromosomal damage due to inhibition of an additional DNA repair pathway, NHEJ. However, perhaps a more substantial inhibition of chromosomal damage could have been achieved by pretreating the cells with the DNA-PKcs inhibitor, NU7026, prior to AZD2281 treatment.

To further evaluate DNA repair gene expression in MPNST, we performed RNA sequencing of our MPNST cell lines. Due to the sensitivity mechanisms reported, we focused the investigation of our RNAseq results to reported DNA repair-related genes. (102) We expected to see decreased expression of DNA repair genes that would cause synthetic lethality with PARP inhibition, specifically those involved in HR, in our MPNST cell lines compared to a NSC control. However, our results indicate the majority of DNA repair-related genes were overexpressed in MPNST cell lines, including *EXO1, PCNA, RPA3, BRCA1, and UNG,* which were among the top overexpressed DNA repair-related genes in three out of four MPNST cell lines evaluated. This observation corresponds to previous findings that MPNSTs have a higher expression of DNA repair genes compared to plexiform neurofibromas, the precursor benign lesion of NF1-associated MPNST. (133) This could further indicate an increased inherent level of DNA damage in MPNST. However, future experiments will be required to determine the status of these genes beyond expression, such as mutation and

functional status. Several DNA repair-related genes were downregulated in at least 2 out of 4 MPNST cell lines (Table 7). These genes include *ERCC6*, *MSH4*, *PER1*, *DMC1*, and *ERCC5*. *MSH4* and *DMC1* play essential roles in HR during meiosis. (134,135) Because our focus concerns the repair of DNA damage in mitotic cells, no further investigation on the role of these genes in AZD2281 sensitivity was performed. *PER1* is a clock gene essential for circadian rhythm. It has been shown to have decreased expression in human cancers including breast, colon, lung, and endometrial cancer, and decreased expression can reduce activation of the DNA damage response signal after ionizing radiation. (136) However, these results have been inconclusive, with subsequent studies unable to validate an effect of *PER1* on DNA damage response. (137) Finally, *ERCC6* (encoding CSB) and *ERCC5* are critical to DNA damage recognition and repair through the nucleotide excision repair pathway. In the event of CSB dysregulation, repair cannot proceed through the transcription coupled repair (TCR) subpathway of NER and must proceed through the slower GGR subpathway. ERCC5/XPG is an endonuclease in the NER pathway; decreased expression could indicate a loss of DNA repair through the GGR subpathway of NER. Taken together, the decreased expression of these two genes could indicate a loss of NER activity in MPNST.

In a previous study to determine mechanisms of sensitivity, aside from HR defects, that could cause sensitivity to PARP inhibition, C. Lord et al. performed a high throughput siRNA screen using PARP inhibitor-treated breast cancer cells. (69) They found two novel TCR genes, *XAB2* and *DDB1*, which sensitized cells to PARP inhibition. Furthermore, they hypothesized that a defect in the TCR pathway could result in stalled replication forks, eventual collapse of the replication fork, and highly deleterious dsDNA breaks beyond a threshold of viability for the cells. Although *XAB2* and *DDB1* were not specifically differentially expressed in MPNST cell lines, this study suggests a TCR deficiency as a mechanism of sensitivity to AZD2281. Furthermore, N. Batenburg et al. recently showed that complete knockout of CSB decreased the amount of HR and increased the amount of NHEJ compared

to parental hTERT-retinal pigment epithelial cells. (76) This result also correlated to sensitivity to Olaparib and decreased damage response signaling after IR. This indicates that CSB plays a role in facilitating HR repair of DSBs, perhaps by facilitating the recruitment of BRCA1 to sites of DNA damage, and that loss of CSB drives S/G2 phase NHEJ activity, increasing genomic instability and subsequently sensitivity to PARP inhibition. However, it is important to note that this result is shown after complete knockout of CSB, whereas MPNST only shows decreased expression of CSB. Due to the possible importance of TCR in PARP inhibitor sensitivity, the observed decrease in HR activity, and because ERCC6 was the most downregulated DNA repair-related gene found in our MPNST cell panel, we proceeded to determine its potential important in MPNST sensitivity to PARP inhibition.

CSB is a SWI/SNF-like DNA-dependent ATPase, that along with its role in TCR, has been reported to play a role in transcriptional elongation at natural transcription pause sites, resumption of RNA synthesis after DNA damage, as well as chromatin remodeling, and unwinding of the DNA. (62,138,139) Furthermore, a role for CSB in base excision repair has been described. (138) Specifically, CSB stimulates either the direct or indirect incision of 7,8-dihydro-8-oxoguanine (8-oxoG) residues or alters the DNA structure around the lesion for better access of other repair proteins during base excision repair. (138,139) CSB interacts with PARP1 with and without oxidative stress; however, after oxidative stress, these proteins relocate to sites of DNA damage and CSB becomes PARylated. PARylated CSB has decreased DNA-dependent ATPase activity, which is not required for its additional activity in BER, but may affects its ability to change the structure of DNA necessary for TCR. CSB may also act to keep PARP1 in close proximity to the DNA lesion, aiding in quick repair of the DNA. Furthermore, it has been shown that in the event of PARP inhibition treatment, CSB could act in the TCR pathway to repair oxidative DNA damage that remains in the absence of BER. If CSB were non-functional, single strand breaks could be converted to double strand breaks at the replication fork. Fittingly, CSB-deficient human fibroblast cells or CSB-null cells

were shown to be more sensitive to PARP inhibition than those cells complemented with wildtype CSB or express wildtype CSB. (138,139) This supports a role of CSB in TCR and as a backup repair mechanism for oxidative DNA damage after PARP inhibition, and shows that loss of CSB can further sensitize cells to PARP inhibition.

To confirm the downregulation of *ERCC6* shown via RNAseq, we first performed qRT-PCR of our MPNST cell lines and NSCs. Consistent with the RNAseq results, *ERCC6* was downregulated in MPNST cell lines compared to the NSC control. Confirmation of CSB expression in a panel of MPNST cell lines and NSCs indicate an average relative CSB expression 6 times higher in NSC than MPNST cell lines. This corresponds with the decreased level of CSB expression reported in lung cancer and head and neck squamous cell carcinoma patients compared to non-cancer controls. (140,141) Decreased CSB expression, among other deficient NER genes, was also shown to increase the risk of disease in both models. In addition, the AZD2281 EC50 values for MPNST cells treated for 96 hours correlate with the observed CSB expression patterns, as assessed by Spearman's correlation. Based on this result, we wanted to manipulate the expression of CSB and determine any effect on the cell sensitivity to AZD2281 treatment.

We anticipate that CSB overexpression would cause the cells to become less sensitive to drug treatment. Based on the AZD2281 EC50 results, CSB overexpression had an effect on the AZD2281 sensitivity of S462 and ST88 cell lines but no substantial effect on STS26T or MPNST724 cells. These results could indicate that STS26T and MPNST724 cell lines have additional defects in the NER pathway downstream of CSB, beyond the decreased expression of *ERCC5* shown in our RNAseq data, so that while overexpression of CSB has a mild effect on AZD2281 sensitivity, increase of CSB expression alone is not enough to overcome other genetic dysregulation. In a previous study by J. Newman et al., re-expression of wild type CSB in CSB-null, hTERT-immortilized human fibroblasts, caused differential expression of approximately 150 genes. (139) A subset of the approximately 50 upregulated

genes after CSB re-expression had a role in DNA repair and drug resistance which could possibly explain the observed resistance to AZD2281 seen after CSB overexpression in MPNST. However, M. Caputo et al. report the opposite expression pattern for CSB, with increased expression of CSB in bladder, cervical, prostate, and breast cancer cell types compared to normal controls. They hypothesized that CSB plays an anti-apoptotic role in these cancer cells by re-equilibrating the cell response upon induction of stress, toward cell proliferation and survival by counteracting p53 activity. (142) Subsequent inhibition of CSB mRNA expression in these cancer models, reduced cell proliferation and increased the sensitivity to conventional chemotherapies. ST88 is the only MPNST cell line assessed with wild-type p53 expression, therefore the increased resistance to AZD2281 observed after increased CSB expression could be due to increased cell robustness through the interaction of CSB and p53. In addition, while it is intriguing, we feel the apparent dichotomy of sensitivity between NF1-associated cell lines and sporadic cell lines to AZD2281 is out of the scope of this thesis. However, future research should be conducted into how the loss of NF1 in S462 and ST88 cells could contribute to the resistance of these cells to AZD2281 once CSB is overexpressed.

As a proof of principle, we also knocked down the expression of CSB in MDA-MB-231 cells. This cell line is shown to be relatively resistant to PARP inhibition, therefore we except if CSB has any role in the sensitivity of cells to AZD2281, that its decreased expression would cause the cells to become sensitive to treatment. We observed a substantial decrease in the AZD2281 EC50 of MDA-MB-231 cells with CSB knockdown compared to the control cells. This indicates that manipulation of CSB alone is enough to induce PARP inhibitor sensitivity in this cell line. In accordance with these results, we wanted to elucidate if manipulation of CSB expression would affect the ability of the cells to repair induced UV damage, specifically CPDs, by the NER pathway, the most defined role for CSB.

To assess the effect of CSB overexpression on MPNST cell response to UV damage,

we treated the cells with 256J/m^2/min UVB and harvested samples 0-24 hours post UV. We used the treated DNA for an ELISA to measure the amount of resolved CPDs over time. We expected if CSB overexpression could make the cells less sensitive to PARP inhibition, potentially by restoring TCR repair of DNA damage, that CSBOE cell lines would be more proficient in CPD repair than control cell lines. In addition, to confirm that CPDs were resolved and not converted in double strand DNA breaks, we also performed immunoblots of gamma-H2AX, a marker of DNA double strand breaks, at corresponding time points to the ELISA. Our results show no change in CPD resolution or gamma-H2AX accumulation after UV damage, regardless of CSB expression level. As previously discussed, CSB has a role in chromatin remodeling that allows access to the DNA and a role in RNA polymerase II transcription, potentially supporting transcription as well as DNA repair. (62,138,139) Therefore, while we expected CSB overexpression or knockdown to effect the efficiency of repair of CPD damage, the observed effect of CSB expression on AZD2281 sensitivity could be due to a role of CSB outside of NER. In addition, the MTS assays performed that show a correlation between CSB expression and AZD2281 sensitivity in a subset of MPNST cell lines was performed over 7 days; the CPD ELISA was performed over 24 hours. Therefore, the effect of CSB expression of AZD2281 sensitivity could have a temporal aspect that was not considered in the CPD ELISA.

Conclusions and Future Directions

MPNST is an aggressive malignancy for which effective targeted therapies are urgently needed to improve therapeutic options and overall patient survival. In this study, we demonstrate that PARP inhibition, specifically AZD2281, exerts a strong anti-MPNST effect *in vitro* and *in vivo* as a single agent. This effect could be due to deficient DNA repair mechanisms, including deficient HR and over-activity of NHEJ, resulting in enhanced genomic instability, and possibly by decreased expression of CSB. Our study provides evidence that PARP inhibition, specifically with AZD2281, could hold therapeutic benefit for

MPNST patients and warrants a clinical trial. However, patients often develop resistance to single agent treatment, therefore future studies should be aimed at determining a synergistic drug combination with AZD2281 that could increase efficacy while decreasing effective doses and off-target effects. Furthermore, additional PARP inhibitors with a similar mechanism of action as AZD2281 are available, further work to evaluate these drugs for greater anti-MPNST effects should be done in order to expand potential clinical trial applications. Importantly, the effect of long term treatment of an inhibitor of DNA repair, such as AZD2281, should be assessed to determine the potential consequence of secondary tumorigenesis.

Future investigations are also necessary to determine the specific genetic mutations or modifications in the HR, NHEJ, and NER pathways that contribute to their dysregulation. In addition, interrogation of the mechanism of CSB loss could help to expand the potential patient population that could benefit from PARP inhibition treatment. As previously mentioned, CSB has multiple roles in the cell beyond DNA repair, including chromatin remodeling, telomere maintenance, and transcription-associated DNA recombination. (76) Determining which roles CSB plays in MPNST will be crucial in elucidating the importance of decreased CSB expression observed in MPNST cell lines. Furthermore, our data suggests that CSB overexpression in NF1-associated MPNST cells lines has more of an effect on the resistance to AZD2281 than in the sporadic cell lines. Examination of this phenomenon could further elucidate the link between CSB expression and PARP inhibitor sensitivity.

There are several roadblocks to furthering the field of MPNST research including the limited bioresources available. The creation of human tumor cell lines in order to expand research data sets would greatly enhance scientific investigation in this field. In addition, NF1-associated cell lines do not grow in mouse models, severely limiting the amount of research that can be done in this MPNST subtype. Better mouse models for MPNST, in

particular NF1-associated MPNST, should be a goal for future research. Furthermore, as MPNST cell lines do not spontaneously metastasize in mice, metastatic MPNST research is lacking. Due to the aggressive nature of MPNST and the propensity for these tumors to metastasize, a mouse model that could better follow the natural order of the disease should be a priority for future studies and is imperative to more fully understand the biology of this destructive and lethal malignancy.

Chapter 6

Appendix- Copyright permission to use figures

Permission for Figure 1. Soft tissue sarcoma subtypes

License Number	3778241011197
License date	Dec 29, 2015
Publisher	Springer New York
Licensed Content Title	Management of Soft Tissue Sarcoma
Licensed Content Author	Brennan, Murray F. ; Antonescu, Cristina R. ; Maki, Robert G.
ISBN	9781461450047
Publication Type	e-Book

Permission for Figure 2. Clinical manifestations of neurofibromatosis type I (NF1)

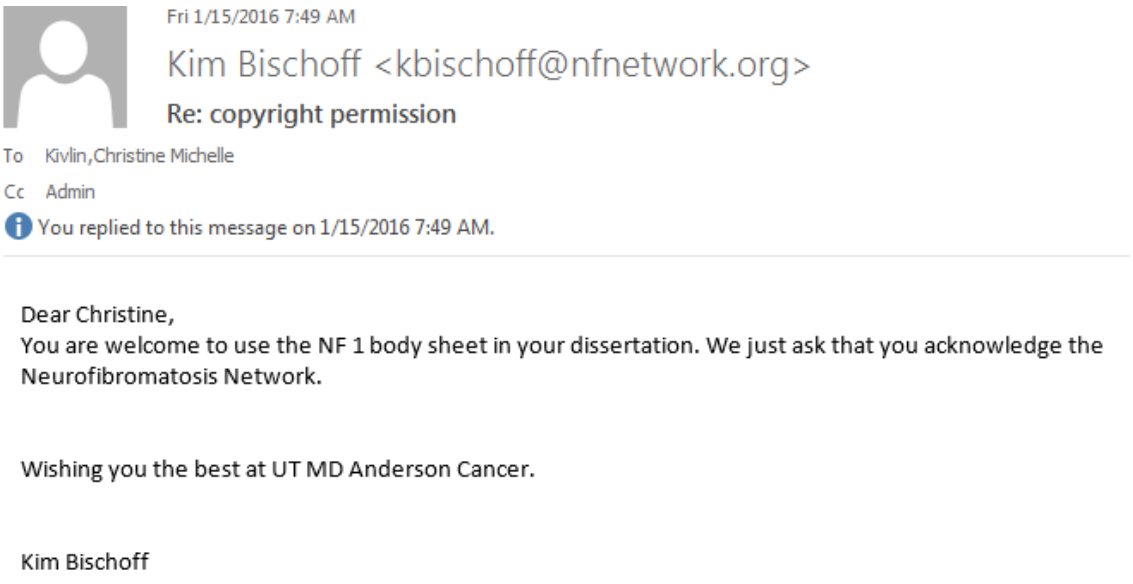

Fri 1/15/2016 7:49 AM

Kim Bischoff <kbischoff@nfnetwork.org>

Re: copyright permission

To Kivlin,Christine Michelle

Cc Admin

You replied to this message on 1/15/2016 7:49 AM.

Dear Christine,
You are welcome to use the NF 1 body sheet in your dissertation. We just ask that you acknowledge the Neurofibromatosis Network.

Wishing you the best at UT MD Anderson Cancer.

Kim Bischoff

Permission for Figure 3. Neurofibromatosis type I molecular pathogenesis

License Number	3778250818163
License date	Dec 29, 2015
Licensed Content Publisher	Cambridge University Press
Licensed Content Publication	Expert Reviews in Molecular Medicine
Licensed Content Title	Malignant peripheral nerve sheath tumour (MPNST): the clinical implications of cellular signalling pathways
Licensed Content Author	Daniela Katz, Alexander Lazar and Dina Lev
Licensed Content Date	Oct 19, 2009
Licensed Content Volume Number	11

Permission for Figure 5. Poly (ADP) ribose polymerase function

License Number	3778841235824
License date	Dec 30, 2015
Licensed Content Publisher	John Wiley and Sons
Licensed Content Publication	BioEssays
Licensed Content Title	Physiology and pathophysiology of poly(ADP-ribosyl)ation *
Licensed Content Author	Alexander Bürkle
Licensed Content Date	Aug 27, 2001
Pages	12

Permission for Figure 6. Effect of Poly (ADP) Ribose Polymerase function and inhibition on DNA repair

Permission for Figure 7. Nucleotide excision repair

License Number	3778841315888
License date	Dec 30, 2015
Licensed content publisher	Nature Publishing Group
Licensed content publication	Nature Reviews Genetics
Licensed content title	Disorders of nucleotide excision repair: the genetic and molecular basis of heterogeneity
Licensed content author	James E. Cleaver, Ernest T. Lam and Ingrid Revet
Licensed content date	Nov 1, 2009
Volume number	10
Issue number	11

Permission for Figure 8. Homologous recombination (HR)

License Number	3778840645871
License date	Dec 30, 2015
Licensed content publisher	Nature Publishing Group
Licensed content publication	Nature Structural and Molecular Biology
Licensed content title	Cooperation of breast cancer proteins PALB2 and piccolo BRCA2 in stimulating homologous recombination
Licensed content author	Rémi Buisson, Anne-Marie Dion-Côté, Yan Coulombe, Hélène Launay, Hong Cai, Alicja Z Stasiak
Licensed content date	Sep 26, 2010
Volume number	17
Issue number	10

Permission for Figure 9. Non-homologous end joining (NHEJ)

License Number	3802570950747
License date	Feb 05, 2016
Licensed content publisher	Nature Publishing Group
Licensed content publication	Nature
Licensed content title	Chromatin dynamics and the preservation of genetic information
Licensed content author	Jessica A. Downs,Michel C. NussenzweigandAndré Nussenzweig

Licensed content date	Jun 21, 2007
Volume number	447
Issue number	7147

Permission for Figure 10. Role of HR and NHEJ in PARP inhibition

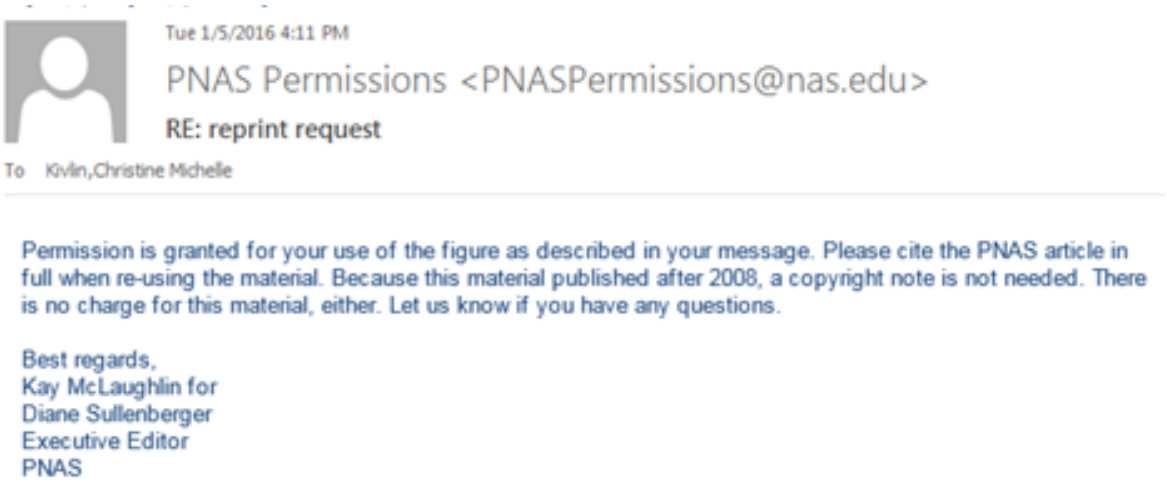

Tue 1/5/2016 4:11 PM

PNAS Permissions <PNASPermissions@nas.edu>

RE: reprint request

To Kivlin,Christine Michelle

Permission is granted for your use of the figure as described in your message. Please cite the PNAS article in full when re-using the material. Because this material published after 2008, a copyright note is not needed. There is no charge for this material, either. Let us know if you have any questions.

Best regards,
Kay McLaughlin for
Diane Sullenberger
Executive Editor
PNAS

Permission for Figures 11, 12, 14-19, and 20-24 and Tables 1-4

Taylor & Francis
Taylor & Francis Group

Journal Reprints

Title: Poly (ADP) ribose polymerase inhibition: A potential treatment of malignant peripheral nerve sheath tumor

Author: Christine M. Kivlin, Kelsey L. Watson, Ghadah A. Al Sannaa, et al

Publication: Cancer Biology & Therapy

Publisher: Taylor & Francis

Date: Dec 9, 2015

Copyright © 2015 Taylor & Francis

LOGIN

If you're a copyright.com user, you can login to RightsLink using your copyright.com credentials. Already a RightsLink user or want to learn more?

Thesis/Dissertation Reuse Request

Taylor & Francis is pleased to offer reuses of its content for a thesis or dissertation free of charge contingent on resubmission of permission request if work is published.

Permission for Figure 25. Reporter construct of the HR plasmid of the eGFP-Pem1 system

License number	3782671002318

License date	Jan 05, 2016
Licensed content publisher	Elsevier
Licensed content publication	Neoplasia
Licensed content title	DNA Repair by Homologous Recombination, But Not by Nonhomologous End Joining, Is Elevated in Breast Cancer Cells
Licensed content author	Zhiyong Mao,Ying Jiang,Xiang Liu,Andrei Seluanov,Vera Gorbunova
Licensed content date	July 2009
Licensed content volume number	11
Licensed content issue number	7

Permission for Figure 26. Reporter construct of the NHEJ plasmid of the eGFP-Pem1 system

License number	3782671002318
License date	Jan 05, 2016
Licensed content publisher	Elsevier
Licensed content publication	Neoplasia
Licensed content title	DNA Repair by Homologous Recombination, But Not by Nonhomologous End Joining, Is Elevated in Breast Cancer Cells

Licensed content author	Zhiyong Mao,Ying Jiang,Xiang Liu,Andrei Seluanov,Vera Gorbunova
Licensed content date	July 2009

Chapter 7

References

1 Society, A. C. Cancer Facts & Figures 2015. . *Atlanta: American Cancer Society* (2015).

2 Morrison, B. A. Soft tissue sarcomas of the extremities. *Proc (Bayl Univ Med Cent)* **16**, 285-290 (2003).

3 Brennan, M. F., Antonescu, C. R. & Maki, R. G. *Management of soft tissue sarcoma*. (Springer, 2013).

4 Lahat, G., Lazar, A. & Lev, D. Sarcoma epidemiology and etiology: Potential environmental and genetic factors. *Surgical Clinics of North America* **88**, 451-+, doi:10.1016/j.suc.2008.03.006 (2008).

5 Jain, S., Xu, R., Prieto, V. G. & Lee, P. Molecular classification of soft tissue sarcomas and its clinical applications. *Int J Clin Exp Pathol* **3**, 416-428 (2010).

6 Husain, N. & Verma, N. Curent concepts in pathology of soft tissue sarcoma. *Indian J Surg Oncol* **2**, 302-308, doi:10.1007/s13193-012-0134-6 (2011).

7 Farid, M., Demicco, E. G., Garcia, R., Ahn, L., Merola, P. R., Cioffi, A. & Maki, R. G. Malignant peripheral nerve sheath tumors. *Oncologist* **19**, 193-201, doi:10.1634/theoncologist.2013-0328 (2014).

8 Gupta, G. & Maniker, A. Malignant peripheral nerve sheath tumors. *Neurosurg Focus* **22**, E12 (2007).

9 Friedman, J. M. Epidemiology of neurofibromatosis type 1. *Am J Med Genet* **89**, 1-6 (1999).

10 Williams, V. C., Lucas, J., Babcock, M. A., Gutmann, D. H., Korf, B. & Maria, B. L. Neurofibromatosis type 1 revisited. *Pediatrics* **123**, 124-133, doi:10.1542/peds.2007-3204 (2009).

11 Pasmant, E., Vidaud, M., Vidaud, D. & Wolkenstein, P. Neurofibromatosis type 1: from genotype to phenotype. *J Med Genet* **49**, 483-489, doi:10.1136/jmedgenet-2012-100978 (2012).

12 Sabbagh, A., Pasmant, E., Imbard, A., Luscan, A., Soares, M., Blanche, H., Laurendeau, I., Ferkal, S., Vidaud, M., Pinson, S., Bellanne-Chantelot, C., Vidaud, D., Parfait, B. & Wolkenstein, P. NF1 molecular characterization and neurofibromatosis type I genotype-phenotype correlation: the French experience. *Hum Mutat* **34**, 1510-1518, doi:10.1002/humu.22392 (2013).

13 Katz, D., Lazar, A. & Lev, D. Malignant peripheral nerve sheath tumour (MPNST): the clinical implications of cellular signalling pathways. *Expert Rev Mol Med* **11**, e30, doi:10.1017/S1462399409001227 (2009).

14 Upadhyaya, M. & Cooper, D. N. 1 online resource. (Springer,, Berlin ; New York, 2012).

15 Ratner, N. & Miller, S. J. A RASopathy gene commonly mutated in cancer: the neurofibromatosis type 1 tumour suppressor. *Nat Rev Cancer* **15**, 290-301, doi:10.1038/nrc3911 (2015).

16 Widemann, B. C., Reinke, D. K., Helman, L. J., Ludwig, J. A., Schuetze, S., Staddon, A. P., Milhem, M. M., Rushing, D. A., Moertel, C. L., Goldman, S., Livingston, M. B., Wagner, L. M., Rodler, E. T., Dombi, E., Perry, A., Annunziata, C. M., Long, L., Viskochil, D., Steinberg, S. M. & Baker, L. H. SARC006: Phase II trial of chemotherapy in sporadic and neurofibromatosis type 1 (NF1)-associated high-grade malignant peripheral nerve sheath tumors (MPNSTs). *Journal of Clinical Oncology* **31** (2013).

17 Dunn, G. P., Spiliopoulos, K., Plotkin, S. R., Hornicek, F. J., Harmon, D. C., Delaney, T. F. & Williams, Z. Role of resection of malignant peripheral nerve sheath tumors in patients with neurofibromatosis type 1. *J Neurosurg* **118**, 142-148, doi:10.3171/2012.9.JNS101610 (2013).

18 Yang, J. C., Chang, A. E., Baker, A. R., Sindelar, W. F., Danforth, D. N., Topalian, S. L., DeLaney, T., Glatstein, E., Steinberg, S. M., Merino, M. J. & Rosenberg, S. A. Randomized prospective study of the benefit of adjuvant radiation therapy in the treatment of soft tissue sarcomas of the extremity. *Journal of Clinical Oncology* **16**, 197-203 (1998).

19 Jhanwar, S. C., Chen, Q., Li, F. P., Brennan, M. F. & Woodruff, J. M. Cytogenetic analysis of soft tissue sarcomas. Recurrent chromosome abnormalities in malignant peripheral nerve sheath tumors (MPNST). *Cancer Genet Cytogenet* **78**, 138-144 (1994).

20 Mertens, F., Dal Cin, P., De Wever, I., Fletcher, C. D., Mandahl, N., Mitelman, F., Rosai, J., Rydholm, A., Sciot, R., Tallini, G., van Den Berghe, H., Vanni, R. & Willen, H. Cytogenetic characterization of peripheral nerve sheath tumours: a report of the CHAMP study group. *J Pathol* **190**, 31-38, doi:10.1002/(SICI)1096-9896(200001)190:1<31::AID-PATH505>3.0.CO;2-# (2000).

21 Rahrmann, E. P., Watson, A. L., Keng, V. W., Choi, K., Moriarity, B. S., Beckmann, D. A., Wolf, N. K., Sarver, A., Collins, M. H., Moertel, C. L., Wallace, M. R., Gel, B., Serra, E., Ratner, N. & Largaespada, D. A. Forward genetic screen for malignant peripheral nerve sheath tumor formation identifies new genes and pathways driving tumorigenesis. *Nat Genet* **45**, 756-766, doi:10.1038/ng.2641 (2013).

22 Bradford, D. & Kim, A. Current treatment options for malignant peripheral nerve sheath tumors. *Curr Treat Options Oncol* **16**, 328, doi:10.1007/s11864-015-0328-6 (2015).

23 Zou, C., Smith, K. D., Liu, J., Lahat, G., Myers, S., Wang, W. L., Zhang, W., McCutcheon, I. E., Slopis, J. M., Lazar, A. J., Pollock, R. E. & Lev, D. Clinical, pathological, and molecular variables predictive of malignant peripheral nerve sheath tumor outcome. *Ann Surg* **249**, 1014-1022, doi:10.1097/SLA.0b013e3181a77e9a (2009).

24 Watson, K. L., Al Sannaa, G. A., Kivlin, C. M., Ingram, D. R., Landers, S. M., Roland, C. L., Cormier, J. N., Hunt, K. K., Feig, B. W., Guadagnolo, B. A., Bishop, A. J., Wang, W.-L., Slopis, J. M., McCutcheon, I. E., Lazar, A. J. & Torres, K. E. Patterns of recurrence and survival in sporadic, neurofibromatosis type 1-associated, and radiation-associated malignant peripheral nerve sheath tumors (MPNSTs). *Journal of Neurosurgery, In Press.* (2016).

25 Rouleau, M., Patel, A., Hendzel, M. J., Kaufmann, S. H. & Poirier, G. G. PARP inhibition: PARP1 and beyond. *Nat Rev Cancer* **10**, 293-301, doi:10.1038/nrc2812 (2010).

26 Schreiber, V., Dantzer, F., Ame, J. C. & de Murcia, G. Poly(ADP-ribose): novel functions for an old molecule. *Nat Rev Mol Cell Biol* **7**, 517-528, doi:10.1038/nrm1963 (2006).

27 Ame, J. C., Spenlehauer, C. & de Murcia, G. The PARP superfamily. *Bioessays* **26**, 882-893, doi:10.1002/bies.20085 (2004).

28 Burkle, A. Physiology and pathophysiology of poly(ADP-ribosyl)ation. *Bioessays* **23**, 795-806, doi:10.1002/bies.1115 (2001).

29 Sousa, F. G., Matuo, R., Soares, D. G., Escargueil, A. E., Henriques, J. A., Larsen, A. K. & Saffi, J. PARPs and the DNA damage response. *Carcinogenesis* **33**, 1433-1440, doi:10.1093/carcin/bgs132 (2012).

30 Ba, X. & Garg, N. J. Signaling mechanism of poly(ADP-ribose) polymerase-1 (PARP-1) in inflammatory diseases. *Am J Pathol* **178**, 946-955, doi:10.1016/j.ajpath.2010.12.004 (2011).

31 Kim, M. Y., Zhang, T. & Kraus, W. L. Poly(ADP-ribosyl)ation by PARP-1: 'PAR-laying' NAD+ into a nuclear signal. *Genes Dev* **19**, 1951-1967, doi:10.1101/gad.1331805 (2005).

32 Wang, X. & Weaver, D. T. The ups and downs of DNA repair biomarkers for PARP inhibitor therapies. *Am J Cancer Res* **1**, 301-327 (2011).

33 Bai, P. Biology of Poly(ADP-Ribose) Polymerases: The Factotums of Cell Maintenance. *Mol Cell* **58**, 947-958, doi:10.1016/j.molcel.2015.01.034 (2015).

34 Krokan, H. E. & Bjoras, M. Base excision repair. *Cold Spring Harb Perspect Biol* **5**, a012583, doi:10.1101/cshperspect.a012583 (2013).

35 Kim, Y. J. & Wilson, D. M., 3rd. Overview of base excision repair biochemistry. *Curr Mol Pharmacol* **5**, 3-13 (2012).

36 Sattler, U., Frit, P., Salles, B. & Calsou, P. Long-patch DNA repair synthesis during base excision repair in mammalian cells. *EMBO Rep* **4**, 363-367, doi:10.1038/sj.embor.embor796 (2003).

37 Robertson, A. B., Klungland, A., Rognes, T. & Leiros, I. DNA repair in mammalian cells: Base excision repair: the long and short of it. *Cell Mol Life Sci* **66**, 981-993, doi:10.1007/s00018-009-8736-z (2009).

38 Gagne, J. P., Isabelle, M., Lo, K. S., Bourassa, S., Hendzel, M. J., Dawson, V. L., Dawson, T. M. & Poirier, G. G. Proteome-wide identification of poly(ADP-ribose) binding proteins and poly(ADP-ribose)-associated protein complexes. *Nucleic Acids Res* **36**, 6959-6976, doi:10.1093/nar/gkn771 (2008).

39 Underhill, C., Toulmonde, M. & Bonnefoi, H. A review of PARP inhibitors: from bench to bedside. *Annals of Oncology* **22**, 268-279, doi:10.1093/annonc/mdq322 (2011).

40 Zaremba, T. & Curtin, N. J. PARP inhibitor development for systemic cancer targeting. *Anticancer Agents Med Chem* **7**, 515-523 (2007).

41 Farmer, H., McCabe, N., Lord, C. J., Tutt, A. N., Johnson, D. A., Richardson, T. B., Santarosa, M., Dillon, K. J., Hickson, I., Knights, C., Martin, N. M., Jackson, S. P., Smith, G. C. & Ashworth, A. Targeting the DNA repair defect in BRCA mutant cells as a therapeutic strategy. *Nature* **434**, 917-921, doi:10.1038/nature03445 (2005).

42 Bryant, H. E., Schultz, N., Thomas, H. D., Parker, K. M., Flower, D., Lopez, E., Kyle, S., Meuth, M., Curtin, N. J. & Helleday, T. Specific killing of BRCA2-deficient tumours with

inhibitors of poly(ADP-ribose) polymerase. *Nature* **434**, 913-917, doi:10.1038/nature03443 (2005).

43 Hartwell, L. H., Szankasi, P., Roberts, C. J., Murray, A. W. & Friend, S. H. Integrating genetic approaches into the discovery of anticancer drugs. *Science* **278**, 1064-1068 (1997).

44 Dedes, K. J., Wilkerson, P. M., Wetterskog, D., Weigelt, B., Ashworth, A. & Reis-Filho, J. S. Synthetic lethality of PARP inhibition in cancers lacking BRCA1 and BRCA2 mutations. *Cell Cycle* **10**, 1192-1199 (2011).

45 Plummer, E. R. Inhibition of poly(ADP-ribose) polymerase in cancer. *Curr Opin Pharmacol* **6**, 364-368, doi:10.1016/j.coph.2006.02.004 (2006).

46 McCabe, N., Turner, N. C., Lord, C. J., Kluzek, K., Bialkowska, A., Swift, S., Giavara, S., O'Connor, M. J., Tutt, A. N., Zdzienicka, M. Z., Smith, G. C. & Ashworth, A. Deficiency in the repair of DNA damage by homologous recombination and sensitivity to poly(ADP-ribose) polymerase inhibition. *Cancer Res* **66**, 8109-8115, doi:10.1158/0008-5472.CAN-06-0140 (2006).

47 Meindl, A., Ditsch, N., Kast, K., Rhiem, K. & Schmutzler, R. K. Hereditary breast and ovarian cancer: new genes, new treatments, new concepts. *Dtsch Arztebl Int* **108**, 323-330, doi:10.3238/arztebl.2011.0323 (2011).

48 Minami, D., Takigawa, N., Takeda, H., Takata, M., Ochi, N., Ichihara, E., Hisamoto, A., Hotta, K., Tanimoto, M. & Kiura, K. Synergistic effect of olaparib with combination of cisplatin on PTEN-deficient lung cancer cells. *Mol Cancer Res* **11**, 140-148, doi:10.1158/1541-7786.MCR-12-0401 (2013).

49 Rottenberg, S., Jaspers, J. E., Kersbergen, A., van der Burg, E., Nygren, A. O., Zander, S. A., Derksen, P. W., de Bruin, M., Zevenhoven, J., Lau, A., Boulter, R., Cranston, A., O'Connor, M. J., Martin, N. M., Borst, P. & Jonkers, J. High sensitivity of BRCA1-deficient mammary tumors to the PARP inhibitor AZD2281 alone and in combination

with platinum drugs. *Proc Natl Acad Sci U S A* **105**, 17079-17084, doi:10.1073/pnas.0806092105 (2008).

50 Burgess, M. & Puhalla, S. BRCA 1/2-Mutation Related and Sporadic Breast and Ovarian Cancers: More Alike than Different. *Front Oncol* **4**, 19, doi:10.3389/fonc.2014.00019 (2014).

51 Lord, C. J., Tutt, A. N. & Ashworth, A. Synthetic lethality and cancer therapy: lessons learned from the development of PARP inhibitors. *Annu Rev Med* **66**, 455-470, doi:10.1146/annurev-med-050913-022545 (2015).

52 Lord, C. J. & Ashworth, A. Mechanisms of resistance to therapies targeting BRCA-mutant cancers. *Nat Med* **19**, 1381-1388, doi:10.1038/nm.3369 (2013).

53 Weston, V. J., Oldreive, C. E., Skowronska, A., Oscier, D. G., Pratt, G., Dyer, M. J., Smith, G., Powell, J. E., Rudzki, Z., Kearns, P., Moss, P. A., Taylor, A. M. & Stankovic, T. The PARP inhibitor olaparib induces significant killing of ATM-deficient lymphoid tumor cells in vitro and in vivo. *Blood* **116**, 4578-4587, doi:10.1182/blood-2010-01-265769 (2010).

54 Brenner, J. C., Feng, F. Y., Han, S., Patel, S., Goyal, S. V., Bou-Maroun, L. M., Liu, M., Lonigro, R., Prensner, J. R., Tomlins, S. A. & Chinnaiyan, A. M. PARP-1 inhibition as a targeted strategy to treat Ewing's sarcoma. *Cancer Res* **72**, 1608-1613, doi:10.1158/0008-5472.CAN-11-3648 (2012).

55 Gunz, D., Hess, M. T. & Naegeli, H. Recognition of DNA adducts by human nucleotide excision repair. Evidence for a thermodynamic probing mechanism. *J Biol Chem* **271**, 25089-25098 (1996).

56 Reardon, J. T. & Sancar, A. Nucleotide excision repair. *Prog Nucleic Acid Res Mol Biol* **79**, 183-235, doi:10.1016/S0079-6603(04)79004-2 (2005).

57 Nickoloff, J. A. & Hoekstra, M. F. *DNA damage and repair*. (Humana Press, 1998).

58 Kelley, M. R. *DNA repair in cancer therapy : molecular targets and clinical applications*. 1st edn, (Elsevier/Academic Press, 2012).

59 Friedberg, E. C. How nucleotide excision repair protects against cancer. *Nat Rev Cancer* **1**, 22-33, doi:10.1038/35094000 (2001).

60 Laine, J. P. & Egly, J. M. When transcription and repair meet: a complex system. *Trends Genet* **22**, 430-436, doi:10.1016/j.tig.2006.06.006 (2006).

61 Marteijn, J. A., Lans, H., Vermeulen, W. & Hoeijmakers, J. H. Understanding nucleotide excision repair and its roles in cancer and ageing. *Nat Rev Mol Cell Biol* **15**, 465-481, doi:10.1038/nrm3822 (2014).

62 Fousteri, M. & Mullenders, L. H. Transcription-coupled nucleotide excision repair in mammalian cells: molecular mechanisms and biological effects. *Cell Res* **18**, 73-84, doi:10.1038/cr.2008.6 (2008).

63 Hoeijmakers, J. H. Genome maintenance mechanisms for preventing cancer. *Nature* **411**, 366-374, doi:10.1038/35077232 (2001).

64 Petruseva, I. O., Evdokimov, A. N. & Lavrik, O. I. Molecular mechanism of global genome nucleotide excision repair. *Acta Naturae* **6**, 23-34 (2014).

65 Wood, R. D. Nucleotide excision repair in mammalian cells. *J Biol Chem* **272**, 23465-23468 (1997).

66 Cleaver, J. E., Lam, E. T. & Revet, I. Disorders of nucleotide excision repair: the genetic and molecular basis of heterogeneity. *Nat Rev Genet* **10**, 756-768, doi:10.1038/nrg2663 (2009).

67 Staszewski, O., Nikolova, T. & Kaina, B. Kinetics of gamma-H2AX focus formation upon treatment of cells with UV light and alkylating agents. *Environ Mol Mutagen* **49**, 734-740, doi:10.1002/em.20430 (2008).

68 Hanasoge, S. & Ljungman, M. H2AX phosphorylation after UV irradiation is triggered by DNA repair intermediates and is mediated by the ATR kinase. *Carcinogenesis* **28**, 2298-2304, doi:10.1093/carcin/bgm157 (2007).

69 Lord, C. J., McDonald, S., Swift, S., Turner, N. C. & Ashworth, A. A high-throughput RNA interference screen for DNA repair determinants of PARP inhibitor sensitivity. *DNA Repair (Amst)* **7**, 2010-2019, doi:10.1016/j.dnarep.2008.08.014 (2008).

70 Jackson, S. P. Sensing and repairing DNA double-strand breaks. *Carcinogenesis* **23**, 687-696 (2002).

71 Lieber, M. R. The mechanism of double-strand DNA break repair by the nonhomologous DNA end-joining pathway. *Annu Rev Biochem* **79**, 181-211, doi:10.1146/annurev.biochem.052308.093131 (2010).

72 Li, X. & Heyer, W. D. Homologous recombination in DNA repair and DNA damage tolerance. *Cell Res* **18**, 99-113, doi:10.1038/cr.2008.1 (2008).

73 Brandsma, I. & Gent, D. C. Pathway choice in DNA double strand break repair: observations of a balancing act. *Genome Integr* **3**, 9, doi:10.1186/2041-9414-3-9 (2012).

74 Chapman, J. R., Taylor, M. R. & Boulton, S. J. Playing the end game: DNA double-strand break repair pathway choice. *Mol Cell* **47**, 497-510, doi:10.1016/j.molcel.2012.07.029 (2012).

75 Symington, L. S. & Gautier, J. Double-strand break end resection and repair pathway choice. *Annu Rev Genet* **45**, 247-271, doi:10.1146/annurev-genet-110410-132435 (2011).

76 Batenburg, N. L., Thompson, E. L., Hendrickson, E. A. & Zhu, X. D. Cockayne syndrome group B protein regulates DNA double-strand break repair and checkpoint activation. *EMBO J* **34**, 1399-1416, doi:10.15252/embj.201490041 (2015).

77 Buisson, R., Dion-Cote, A. M., Coulombe, Y., Launay, H., Cai, H., Stasiak, A. Z., Stasiak, A., Xia, B. & Masson, J. Y. Cooperation of breast cancer proteins PALB2 and piccolo BRCA2 in stimulating homologous recombination. *Nat Struct Mol Biol* **17**, 1247-1254, doi:10.1038/nsmb.1915 (2010).

78 Beck, C., Robert, I., Reina-San-Martin, B., Schreiber, V. & Dantzer, F. Poly(ADP-ribose) polymerases in double-strand break repair: focus on PARP1, PARP2 and PARP3. *Exp Cell Res* **329**, 18-25, doi:10.1016/j.yexcr.2014.07.003 (2014).

79 Hartlerode, A. J. & Scully, R. Mechanisms of double-strand break repair in somatic mammalian cells. *Biochem J* **423**, 157-168, doi:10.1042/BJ20090942 (2009).

80 Banerjee, S., Kaye, S. B. & Ashworth, A. Making the best of PARP inhibitors in ovarian cancer. *Nat Rev Clin Oncol* **7**, 508-519, doi:10.1038/nrclinonc.2010.116 (2010).

81 Davis, A. J. & Chen, D. J. DNA double strand break repair via non-homologous end-joining. *Transl Cancer Res* **2**, 130-143, doi:10.3978/j.issn.2218-676X.2013.04.02 (2013).

82 Lieber, M. R. The mechanism of human nonhomologous DNA end joining. *J Biol Chem* **283**, 1-5, doi:10.1074/jbc.R700039200 (2008).

83 Dueva, R. & Iliakis, G. Alternative pathways of non-homologous end joining (NHEJ) in genomic instability and cancer. *Translational Cancer Research* **2**, 163-177 (2013).

84 Kelley, M. R. 1 online resource (xi, 362 p.) (Humana Press, Totowa, N.J., 2012).

85 Downs, J. A. Chromatin structure and DNA double-strand break responses in cancer progression and therapy. *Oncogene* **26**, 7765-7772, doi:10.1038/sj.onc.1210874 (2007).

86 Patel, A. G., Sarkaria, J. N. & Kaufmann, S. H. Nonhomologous end joining drives poly(ADP-ribose) polymerase (PARP) inhibitor lethality in homologous recombination-deficient cells. *Proc Natl Acad Sci U S A* **108**, 3406-3411, doi:10.1073/pnas.1013715108 (2011).

87 Fang, Y., Elahi, A., Denley, R. C., Rao, P. H., Brennan, M. F. & Jhanwar, S. C. Molecular characterization of permanent cell lines from primary, metastatic and recurrent malignant peripheral nerve sheath tumors (MPNST) with underlying neurofibromatosis-1. *Anticancer Res* **29**, 1255-1262 (2009).

88 Upadhyaya, M. Genetic basis of tumorigenesis in NF1 malignant peripheral nerve sheath tumors. *Front Biosci (Landmark Ed)* **16**, 937-951 (2011).

89 Lazar, A. J., Das, P., Tuvin, D., Korchin, B., Zhu, Q., Jin, Z., Warneke, C. L., Zhang, P. S., Hernandez, V., Lopez-Terrada, D., Pisters, P. W., Pollock, R. E. & Lev, D. Angiogenesis-promoting gene patterns in alveolar soft part sarcoma. *Clin Cancer Res* **13**, 7314-7321, doi:10.1158/1078-0432.CCR-07-0174 (2007).

90 Torres, K. E., Zhu, Q. S., Bill, K., Lopez, G., Ghadimi, M. P., Xie, X., Young, E. D., Liu, J., Nguyen, T., Bolshakov, S., Belousov, R., Wang, S., Lahat, G., Hernandez, B., Lazar, A. J. & Lev, D. Activated MET is a molecular prognosticator and potential therapeutic target for malignant peripheral nerve sheath tumors. *Clin Cancer Res* **17**, 3943-3955, doi:10.1158/1078-0432.CCR-11-0193 (2011).

91 Jin, Z., Lahat, G., Korchin, B., Nguyen, T., Zhu, Q. S., Wang, X., Lazar, A. J., Trent, J., Pollock, R. E. & Lev, D. Midkine enhances soft-tissue sarcoma growth: a possible novel therapeutic target. *Clin Cancer Res* **14**, 5033-5042, doi:10.1158/1078-0432.CCR-08-0092 (2008).

92 Mao, Z., Bozzella, M., Seluanov, A. & Gorbunova, V. DNA repair by nonhomologous end joining and homologous recombination during cell cycle in human cells. *Cell Cycle* **7**, 2902-2906 (2008).

93 Mao, Z., Jiang, Y., Liu, X., Seluanov, A. & Gorbunova, V. DNA repair by homologous recombination, but not by nonhomologous end joining, is elevated in breast cancer cells. *Neoplasia* **11**, 683-691 (2009).

94 Kim, T. H., Ullrich, S. E., Ananthaswamy, H. N., Zimmerman, S. & Kripke, M. L. Suppression of delayed and contact hypersensitivity responses in mice have different UV dose responses. *Photochem Photobiol* **68**, 738-744 (1998).

95 Lopez, G., Liu, J., Ren, W., Wei, W., Wang, S., Lahat, G., Zhu, Q. S., Bornmann, W. G., McConkey, D. J., Pollock, R. E. & Lev, D. C. Combining PCI-24781, a novel histone deacetylase inhibitor, with chemotherapy for the treatment of soft tissue sarcoma. *Clin Cancer Res* **15**, 3472-3483, doi:10.1158/1078-0432.CCR-08-2714 (2009).

96 Lopez, G., Torres, K., Liu, J., Hernandez, B., Young, E., Belousov, R., Bolshakov, S., Lazar, A. J., Slopis, J. M., McCutcheon, I. E., McConkey, D. & Lev, D. Autophagic survival in resistance to histone deacetylase inhibitors: novel strategies to treat malignant peripheral nerve sheath tumors. *Cancer Res* **71**, 185-196, doi:10.1158/0008-5472.CAN-10-2799 (2011).

97 Ren, W., Korchin, B., Lahat, G., Wei, C., Bolshakov, S., Nguyen, T., Merritt, W., Dicker, A., Lazar, A., Sood, A., Pollock, R. E. & Lev, D. Combined vascular endothelial growth factor receptor/epidermal growth factor receptor blockade with chemotherapy for treatment of local, uterine, and metastatic soft tissue sarcoma. *Clin Cancer Res* **14**, 5466-5475, doi:10.1158/1078-0432.CCR-08-0562 (2008).

98 Kivlin, C. M., Watson, K. L., Al Sannaa, G. A., Belousov, R., Ingram, D. R., Huang, K. L., May, C. D., Bolshakov, S., Landers, S. M., Kalam, A. A., Slopis, J. M., McCutcheon, I. E., Pollock, R. E., Lev, D., Lazar, A. J. & Torres, K. E. Poly (ADP) Ribose Polymerase Inhibition: A Potential Treatment of Malignant Peripheral Nerve Sheath Tumor. *Cancer Biol Ther*, 0, doi:10.1080/15384047.2015.1108486 (2015).

99 Goertz, O., Langer, S., Uthoff, D., Ring, A., Stricker, I., Tannapfel, A. & Steinau, H. U. Diagnosis, treatment and survival of 65 patients with malignant peripheral nerve sheath tumors. *Anticancer Res* **34**, 777-783 (2014).

100 Anghileri, M., Miceli, R., Fiore, M., Mariani, L., Ferrari, A., Mussi, C., Lozza, L., Collini, P., Olmi, P., Casali, P. G., Pilotti, S. & Gronchi, A. Malignant peripheral nerve sheath tumors: prognostic factors and survival in a series of patients treated at a single institution. *Cancer* **107**, 1065-1074, doi:10.1002/cncr.22098 (2006).

101 Elstrodt, F., Hollestelle, A., Nagel, J. H., Gorin, M., Wasielewski, M., van den Ouweland, A., Merajver, S. D., Ethier, S. P. & Schutte, M. BRCA1 mutation analysis of 41 human breast cancer cell lines reveals three new deleterious mutants. *Cancer Res* **66**, 41-45, doi:10.1158/0008-5472.CAN-05-2853 (2006).

102 Wood, R. D., Mitchell, M., Sgouros, J. & Lindahl, T. Human DNA repair genes. *Science* **291**, 1284-1289, doi:10.1126/science.1056154 (2001).

103 Bailey, A. D., Gray, L. T., Pavelitz, T., Newman, J. C., Horibata, K., Tanaka, K. & Weiner, A. M. The conserved Cockayne syndrome B-piggyBac fusion protein (CSB-PGBD3) affects DNA repair and induces both interferon-like and innate antiviral responses in CSB-null cells. *DNA Repair (Amst)* **11**, 488-501, doi:10.1016/j.dnarep.2012.02.004 (2012).

104 Drew, Y., Mulligan, E. A., Vong, W. T., Thomas, H. D., Kahn, S., Kyle, S., Mukhopadhyay, A., Los, G., Hostomsky, Z., Plummer, E. R., Edmondson, R. J. & Curtin, N. J. Therapeutic potential of poly(ADP-ribose) polymerase inhibitor AG014699 in human cancers with mutated or methylated BRCA1 or BRCA2. *J Natl Cancer Inst* **103**, 334-346, doi:10.1093/jnci/djq509 (2011).

105 Horspool, W. M. & Lenci, F. *CRC handbook of organic photochemistry and photobiology*. 2nd edn, (CRC Press, 2004).

106 Maki, R. G., D'Adamo, D. R., Keohan, M. L., Saulle, M., Schuetze, S. M., Undevia, S. D., Livingston, M. B., Cooney, M. M., Hensley, M. L., Mita, M. M., Takimoto, C. H., Kraft, A. S., Elias, A. D., Brockstein, B., Blachere, N. E., Edgar, M. A., Schwartz, L. H., Qin, L. X., Antonescu, C. R. & Schwartz, G. K. Phase II study of sorafenib in patients with

metastatic or recurrent sarcomas. *Journal of Clinical Oncology* **27**, 3133-3140, doi:10.1200/JCO.2008.20.4495 (2009).

107 Kim, A., Dombi, E., Tepas, K., Fox, E., Martin, S., Wolters, P., Balis, F. M., Jayaprakash, N., Turkbey, B., Muradyan, N., Choyke, P. L., Reddy, A., Korf, B. & Widemann, B. C. Phase I trial and pharmacokinetic study of sorafenib in children with neurofibromatosis type I and plexiform neurofibromas. *Pediatr Blood Cancer* **60**, 396-401, doi:10.1002/pbc.24281 (2013).

108 Robertson, K. A., Nalepa, G., Yang, F. C., Bowers, D. C., Ho, C. Y., Hutchins, G. D., Croop, J. M., Vik, T. A., Denne, S. C., Parada, L. F., Hingtgen, C. M., Walsh, L. E., Yu, M., Pradhan, K. R., Edwards-Brown, M. K., Cohen, M. D., Fletcher, J. W., Travers, J. B., Staser, K. W., Lee, M. W., Sherman, M. R., Davis, C. J., Miller, L. C., Ingram, D. A. & Clapp, D. W. Imatinib mesylate for plexiform neurofibromas in patients with neurofibromatosis type 1: a phase 2 trial. *Lancet Oncol* **13**, 1218-1224, doi:10.1016/S1470-2045(12)70414-X (2012).

109 Dungey, F. A., Loser, D. A. & Chalmers, A. J. Replication-dependent radiosensitization of human glioma cells by inhibition of poly(ADP-Ribose) polymerase: mechanisms and therapeutic potential. *Int J Radiat Oncol Biol Phys* **72**, 1188-1197, doi:10.1016/j.ijrobp.2008.07.031 (2008).

110 Byers, L. A., Wang, J., Nilsson, M. B., Fujimoto, J., Saintigny, P., Yordy, J., Giri, U., Peyton, M., Fan, Y. H., Diao, L., Masrorpour, F., Shen, L., Liu, W., Duchemann, B., Tumula, P., Bhardwaj, V., Welsh, J., Weber, S., Glisson, B. S., Kalhor, N., Wistuba, II, Girard, L., Lippman, S. M., Mills, G. B., Coombes, K. R., Weinstein, J. N., Minna, J. D. & Heymach, J. V. Proteomic profiling identifies dysregulated pathways in small cell lung cancer and novel therapeutic targets including PARP1. *Cancer Discov* **2**, 798-811, doi:10.1158/2159-8290.CD-12-0112 (2012).

111 Ossovskaya, V., Koo, I. C., Kaldjian, E. P., Alvares, C. & Sherman, B. M. Upregulation of Poly (ADP-Ribose) Polymerase-1 (PARP1) in Triple-Negative Breast Cancer and Other Primary Human Tumor Types. *Genes Cancer* **1**, 812-821, doi:10.1177/1947601910383418 (2010).

112 Bieche, I., Pennaneach, V., Driouch, K., Vacher, S., Zaremba, T., Susini, A., Lidereau, R. & Hall, J. Variations in the mRNA expression of poly(ADP-ribose) polymerases, poly(ADP-ribose) glycohydrolase and ADP-ribosylhydrolase 3 in breast tumors and impact on clinical outcome. *Int J Cancer* **133**, 2791-2800, doi:10.1002/ijc.28304 (2013).

113 Goswami, J., Goyal, S., Wu, H., Moran, M. S. & Haffty, B. G. Poly(ADP-ribose) polymerase-1 (PARP-1) expression in patients treated with breast-conserving surgery and radiation therapy (BCS plus RT). *Journal of Clinical Oncology* **28** (2010).

114 Gennari A, S. M., Varesco L, et al. Prognostic significance of BRCA1, PARP1 and PARP2 in sporadic breast cancer. *Journal of Clinical Oncology* **27s:e22114** (2009).

115 Menear, K. A., Adcock, C., Boulter, R., Cockcroft, X. L., Copsey, L., Cranston, A., Dillon, K. J., Drzewiecki, J., Garman, S., Gomez, S., Javaid, H., Kerrigan, F., Knights, C., Lau, A., Loh, V. M., Jr., Matthews, I. T., Moore, S., O'Connor, M. J., Smith, G. C. & Martin, N. M. 4-[3-(4-cyclopropanecarbonylpiperazine-1-carbonyl)-4-fluorobenzyl]-2H-phthalazin- 1-one: a novel bioavailable inhibitor of poly(ADP-ribose) polymerase-1. *J Med Chem* **51**, 6581-6591, doi:10.1021/jm8001263 (2008).

116 Williamson, C. T., Muzik, H., Turhan, A. G., Zamo, A., O'Connor, M. J., Bebb, D. G. & Lees-Miller, S. P. ATM deficiency sensitizes mantle cell lymphoma cells to poly(ADP-ribose) polymerase-1 inhibitors. *Mol Cancer Ther* **9**, 347-357, doi:10.1158/1535-7163.MCT-09-0872 (2010).

117 Nasuno, T., Mimaki, S., Okamoto, M., Esumi, H. & Tsuchihara, K. Effect of a poly(ADP-ribose) polymerase-1 inhibitor against esophageal squamous cell carcinoma cell lines. *Cancer Sci* **105**, 202-210, doi:10.1111/cas.12322 (2014).

118 Turner, N. C. & Ashworth, A. Biomarkers of PARP inhibitor sensitivity. *Breast Cancer Res Treat* **127**, 283-286, doi:10.1007/s10549-011-1375-8 (2011).

119 Sui, H., Shi, C., Yan, Z. & Li, H. Combination of erlotinib and a PARP inhibitor inhibits growth of A2780 tumor xenografts due to increased autophagy. *Drug Des Devel Ther* **9**, 3183-3190, doi:10.2147/DDDT.S82035 (2015).

120 Turk, A. N., Byer, S. J., Zinn, K. R. & Carroll, S. L. Orthotopic xenografting of human luciferase-tagged malignant peripheral nerve sheath tumor cells for in vivo testing of candidate therapeutic agents. *J Vis Exp*, doi:10.3791/2558 (2011).

121 Seo, J. B., Im, J. G., Goo, J. M., Chung, M. J. & Kim, M. Y. Atypical pulmonary metastases: spectrum of radiologic findings. *Radiographics* **21**, 403-417, doi:10.1148/radiographics.21.2.g01mr17403 (2001).

122 Kubota, E., Williamson, C. T., Ye, R., Elegbede, A., Peterson, L., Lees-Miller, S. P. & Bebb, D. G. Low ATM protein expression and depletion of p53 correlates with olaparib sensitivity in gastric cancer cell lines. *Cell Cycle* **13**, 2129-2137, doi:10.4161/cc.29212 (2014).

123 Evers, B., Drost, R., Schut, E., de Bruin, M., van der Burg, E., Derksen, P. W., Holstege, H., Liu, X., van Drunen, E., Beverloo, H. B., Smith, G. C., Martin, N. M., Lau, A., O'Connor, M. J. & Jonkers, J. Selective inhibition of BRCA2-deficient mammary tumor cell growth by AZD2281 and cisplatin. *Clin Cancer Res* **14**, 3916-3925, doi:10.1158/1078-0432.CCR-07-4953 (2008).

124 Mendes-Pereira, A. M., Martin, S. A., Brough, R., McCarthy, A., Taylor, J. R., Kim, J. S., Waldman, T., Lord, C. J. & Ashworth, A. Synthetic lethal targeting of PTEN mutant cells with PARP inhibitors. *EMBO Mol Med* **1**, 315-322, doi:10.1002/emmm.200900041 (2009).

125 Janzen, D. M., Paik, D. Y., Rosales, M. A., Yep, B., Cheng, D., Witte, O. N., Kayadibi, H., Ryan, C. M., Jung, M. E., Faull, K. & Memarzadeh, S. Low levels of circulating

estrogen sensitize PTEN-null endometrial tumors to PARP inhibition in vivo. *Mol Cancer Ther* **12**, 2917-2928, doi:10.1158/1535-7163.MCT-13-0572 (2013).

126 Min, A., Im, S. A., Yoon, Y. K., Song, S. H., Nam, H. J., Hur, H. S., Kim, H. P., Lee, K. H., Han, S. W., Oh, D. Y., Kim, T. Y., O'Connor, M. J., Kim, W. H. & Bang, Y. J. RAD51C-deficient cancer cells are highly sensitive to the PARP inhibitor olaparib. *Mol Cancer Ther* **12**, 865-877, doi:10.1158/1535-7163.MCT-12-0950 (2013).

127 Loveday, C., Turnbull, C., Ramsay, E., Hughes, D., Ruark, E., Frankum, J. R., Bowden, G., Kalmyrzaev, B., Warren-Perry, M., Snape, K., Adlard, J. W., Barwell, J., Berg, J., Brady, A. F., Brewer, C., Brice, G., Chapman, C., Cook, J., Davidson, R., Donaldson, A., Douglas, F., Greenhalgh, L., Henderson, A., Izatt, L., Kumar, A., Lalloo, F., Miedzybrodzka, Z., Morrison, P. J., Paterson, J., Porteous, M., Rogers, M. T., Shanley, S., Walker, L., Breast Cancer Susceptibility, C., Eccles, D., Evans, D. G., Renwick, A., Seal, S., Lord, C. J., Ashworth, A., Reis-Filho, J. S., Antoniou, A. C. & Rahman, N. Germline mutations in RAD51D confer susceptibility to ovarian cancer. *Nat Genet* **43**, 879-882, doi:10.1038/ng.893 (2011).

128 Ming, M. & He, Y. Y. PTEN in DNA damage repair. *Cancer Lett* **319**, 125-129, doi:10.1016/j.canlet.2012.01.003 (2012).

129 Yang, X., Ndawula, C., Jr., Zhou, H., Gong, X. & Jin, J. JF-305, a pancreatic cancer cell line is highly sensitive to the PARP inhibitor olaparib. *Oncol Lett* **9**, 757-761, doi:10.3892/ol.2014.2762 (2015).

130 Chen, B. P., Uematsu, N., Kobayashi, J., Lerenthal, Y., Krempler, A., Yajima, H., Lobrich, M., Shiloh, Y. & Chen, D. J. Ataxia telangiectasia mutated (ATM) is essential for DNA-PKcs phosphorylations at the Thr-2609 cluster upon DNA double strand break. *J Biol Chem* **282**, 6582-6587, doi:10.1074/jbc.M611605200 (2007).

131 Cui, X., Yu, Y., Gupta, S., Cho, Y. M., Lees-Miller, S. P. & Meek, K. Autophosphorylation of DNA-dependent protein kinase regulates DNA end processing and may also alter

double-strand break repair pathway choice. *Mol Cell Biol* **25**, 10842-10852, doi:10.1128/MCB.25.24.10842-10852.2005 (2005).

132 Douglas, P., Cui, X., Block, W. D., Yu, Y., Gupta, S., Ding, Q., Ye, R., Morrice, N., Lees-Miller, S. P. & Meek, K. The DNA-dependent protein kinase catalytic subunit is phosphorylated in vivo on threonine 3950, a highly conserved amino acid in the protein kinase domain. *Mol Cell Biol* **27**, 1581-1591, doi:10.1128/MCB.01962-06 (2007).

133 Peacock, J. D., Cherba, D., Kampfschulte, K., Smith, M. K., Monks, N. R., Webb, C. P. & Steensma, M. Molecular-guided therapy predictions reveal drug resistance phenotypes and treatment alternatives in malignant peripheral nerve sheath tumors. *J Transl Med* **11**, 213, doi:10.1186/1479-5876-11-213 (2013).

134 Santucci-Darmanin, S., Walpita, D., Lespinasse, F., Desnuelle, C., Ashley, T. & Paquis-Flucklinger, V. MSH4 acts in conjunction with MLH1 during mammalian meiosis. *FASEB J* **14**, 1539-1547 (2000).

135 Bugreev, D. V., Pezza, R. J., Mazina, O. M., Voloshin, O. N., Camerini-Otero, R. D. & Mazin, A. V. The resistance of DMC1 D-loops to dissociation may account for the DMC1 requirement in meiosis. *Nat Struct Mol Biol* **18**, 56-60, doi:10.1038/nsmb.1946 (2011).

136 Gery, S., Komatsu, N., Baldjyan, L., Yu, A., Koo, D. & Koeffler, H. P. The circadian gene per1 plays an important role in cell growth and DNA damage control in human cancer cells. *Mol Cell* **22**, 375-382, doi:10.1016/j.molcel.2006.03.038 (2006).

137 Gaddameedhi, S., Reardon, J. T., Ye, R., Ozturk, N. & Sancar, A. Effect of circadian clock mutations on DNA damage response in mammalian cells. *Cell Cycle* **11**, 3481-3491, doi:10.4161/cc.21771 (2012).

138 Thorslund, T., von Kobbe, C., Harrigan, J. A., Indig, F. E., Christiansen, M., Stevnsner, T. & Bohr, V. A. Cooperation of the Cockayne syndrome group B protein and poly(ADP-ribose) polymerase 1 in the response to oxidative stress. *Mol Cell Biol* **25**, 7625-7636, doi:10.1128/MCB.25.17.7625-7636.2005 (2005).

139 Newman, J. C., Bailey, A. D. & Weiner, A. M. Cockayne syndrome group B protein (CSB) plays a general role in chromatin maintenance and remodeling. *Proc Natl Acad Sci U S A* **103**, 9613-9618, doi:10.1073/pnas.0510909103 (2006).

140 Cheng, L., Spitz, M. R., Hong, W. K. & Wei, Q. Reduced expression levels of nucleotide excision repair genes in lung cancer: a case-control analysis. *Carcinogenesis* **21**, 1527-1530 (2000).

141 Cheng, L., Sturgis, E. M., Eicher, S. A., Spitz, M. R. & Wei, Q. Expression of nucleotide excision repair genes and the risk for squamous cell carcinoma of the head and neck. *Cancer* **94**, 393-397, doi:10.1002/cncr.10231 (2002).

142 Caputo, M., Frontini, M., Velez-Cruz, R., Nicolai, S., Prantera, G. & Proietti-De-Santis, L. The CSB repair factor is overexpressed in cancer cells, increases apoptotic resistance, and promotes tumor growth. *DNA Repair (Amst)* **12**, 293-299, doi:10.1016/j.dnarep.2013.01.008 (2013).

Vitae

Christine Michelle Kivlin was born in New Braunfels, Texas on June 30, 1987, the daughter of Shirley Abel Kivlin and Michael Louis Kivlin. After completing her work at New Braunfels High School, New Braunfels, Texas in 2005, she entered The University of Texas at Austin in Austin, Texas. She received the degree of Bachelor of Science with a major in biology from The University of Texas at Austin in December, 2008. For the next year, she worked as a Research Volunteer in the Section of Integrative Biology at The University of Texas at Austin, and as a Laboratory Technician in the Institute of Cell and Molecular Biology at The University of Texas at Austin. In September of 2010 she entered The University of Texas Graduate School of Biomedical Sciences at Houston.

Permanent address:

13802 Bryan Street

Alvin, Texas 77511